University of Alberta

Flocculation of silica particles in a model oil solution: Effect of adsorbed asphaltene

by

Atoosa Zahabi

A thesis submitted to the Faculty of Graduate Studies and Research
in partial fulfillment of the requirements for the degree of

Doctor of Philosophy
in
Chemical Engineering
Department of Chemical and Materials Engineering

Fall 2011
Edmonton, Alberta

To my mother for her precious love.

To my younger brother, Arshia, for his endless support.

And to my father. Although he left me soon, but what he taught me was enough for my whole life.

Abstract

The removal of solid particulates from crude oils and hydrocarbon streams is a common challenge in refining. Finding a method for efficient removal of the suspended solids in the oil streams is the main objective of this work. Paraffinic and aqueous treatment and the combination of these two methods were studied in details to determine the efficiency of each method for removal of solid particles from the oil streams. In this study, we investigate the role of adsorbed and precipitated asphaltenes in flocculation and sedimentation of particles from a model oil. Silica particles (1 μm) were suspended in a reacted pitch material (5 wt%) dissolved in toluene to give a model oil (O). In toluene solution, the silica suspension was stabilized by the asphaltenes in the pitch. The onset of asphaltene precipitation was determined to occur at S/O = 0.43 by weight (pentane/oil). At S/O < 0.33, the removal efficiency of silica particles from the oil phase by sedimentation for one hour was poor. Above this ratio, however, the concentration of silica remaining in the supernatant decreased. There was no significant difference in removal efficiency whether the silica particles were hydrophilic or hydrophobic. We did a similar study for removal of other types of solid particles such as clays (~ 1 μm) which was also successful above S/O = 0.36. Treating the model oil with small amounts of water did not lead to destabilization of the silica suspension in short times. However, paraffinic treatment of the model oil solution in the presence of emulsified water destabilized the silica suspensions at lower S/O (S/O = 0.25) compared to solutions without water (S/O = 0.33) after one hour.

The results obtained from destabilization of silica suspensions showed that asphaltene adsorbs on surfaces even below the visible onset of precipitation. Fourier transform infrared (FTIR) spectroscopy in the region of 2800 - 3000 cm^{-1} and quartz crystal microbalance (QCM) showed measurable asphaltene adsorption on the surface of the silica before the onset of asphaltene precipitation; however, the amount of adsorption increased significantly beyond this point. QCM measurements on gold and on silica surfaces showed the same trend with S/O. Adsorption was more pronounced on the gold surface than on the silica particles, especially after the onset of asphaltene precipitation.

It was interesting to study the interaction forces between the coated silica particles with asphaltene in oil solutions to have a better understanding of the flocculation mechanism of the silica particles. Therefore, the interaction between asphaltene adsorbed on the gold surface with a gold probe tip was studied by using atomic force microscopy (AFM) in organic solvent (mixture of toluene – pentane). Asphaltenes adhered to the gold surface at various ratios of oil – pentane solution; similar ratios used in the destabilization of silica particles in the model oil. The results from AFM show adsorption of materials with different heights, structures and rupture strengths on the gold substrate. Heterogeneous adsorption of asphaltene aggregates (materials with different heights) were observed on gold surface for various S/O especially above the onset of asphaltene precipitation (S/O>0.43).

Acknowledgement

My deepest gratitude to my supervisors, Dr. Murray Gray and Dr. Tadek Dabros, for giving me the opportunity to work with them. I appreciate their valuable guidance and hints and their supports during this research work.

I acknowledge Dr. Jan Czarnecki for his comments and ideas and for sharing his experience for paraffinic treatment of the oil solution.

Thanks to Derek Chao and multi phase team in canmetENERGY laboratories, Devon. I also would like to thank Dhraj Dgoutam for helping me doing part of the experiments for the QCM and aqueous treatment for removal of the solid particles. My special thanks to Loredana Dorobantu for sharing her experience in AFM with me.

My special thanks to Lily Laser for her energetic and kind supports and her help during these years.

The financial support of the project from Panel of Energy Research and Development (PERD) of the Canadian government is acknowledged.

And my deepest love and gratitude goes to my family and my friends. Being far from my family was the hardest part during this period of my life. I appreciate their love and support. Thanks to my brothers especially Arshia for believing in me and reminding me that nothing is greater than human hope and will. I want to thank my lovely friends who helped me to go through sad and happy moments while doing this research work.

Table of contents

List of tables

List of figures

Nomenclature

Abbreviations

AFM	Atomic Force Microscopy
API	American Petroleum Institute
C5	Precipitated asphaltene with pentane
C6	Precipitated asphaltene with hexane
C7	Precipitated asphaltene with Heptane
CMC	Critical Micelle Concentration
DOSY	^{1}H diffusion ordered Spectroscopy
EST	Eni Slurry Technology
FTA	First Ten Angstroms
FTC	Flow Through Cell
FTIR	Fourier Transform Infra Red
H/C	Hydrogen/Carbon
ID	Internal Diameter
IPA	Isopropyl alcohol
LB	Langmuir Blodgett
LDI	Laser Desorption Ionization
MW	Molecular Weight
M-WLC	Modified Worm Like Chain model
NMR	Nuclear Magnetic Resonance
O	Model oil solution
Pentol	Pentane –Toluene
PFT	Paraffinic Froth Treatment
QCM	Quartz Crystal Microbalance
QCM-D	Quartz Crystal Microbalance with measuring dissipation
RPM	Round per Minute
R-QCM	Quartz Crystal Microbalance with measuring resistance
S	Solvent
SANS	Small Angle X-ray Scattering
SAXS	Small Angle Neutron Scattering

SARA	Saturates-Aromatics-Resins-Asphaltenes
SRU	Solvent Recovery Unit
S/O	Solvent (pentane)/Oil solution
VDW	van der Waals
VPO	Vapor Pressure Osmometry
Wt%	Weight %
XPS	X-ray Photo-electron Spectroscopy

Symbols

U	Hindered settling rate
φ	Volume fraction of the flocs in suspension
u_0	Free settling rate of the flocs
g	Gravitational constant
ρ_E	Effective density of the flocs
ρ	Density
d	Diameter of the flocs
η	Viscosity
ε	Porosity
φ_p	Volume fraction of the primary particles in suspension
Δf	Change in frequency
C_f	Sensitivity factor for the quartz crystal
Δm	Change in mass
v_q	Shear wave velocity of the quartz
μ_q	Shear modulus of the quartz
ΔR	Change in resistance
ΔD	Change in dissipation
x	Distance
t	Time
τ	Variable of time
n	Concentration of solutes

D	Diffusion coefficient
M	Mass
k_B	Boltzmann constant
K	Kelvin
T	Temperature
C	Capacitance
L	Inductor
t'	$t-t_{immersion\ of\ the\ quartz\ in\ the\ solution}$
F	Force
a	Radii of a sphere
h	Distance
A_H	Hamaker constant
$\overline{\lambda}$	London retardation wavelength
κ	Debye-Huckel parameter
ψ	Electric potential
k	Spring constant
D	Cantilever deflection

Subscripts

E	Effective density of the flocs
m	medium
P	Primary particles
S	Solvent
L	Liquid
q	Quartz

1 Introduction

1.1 Solid particles: Problem for the oil industry

One of the recurring problems that the refining industry is facing is the contamination of crude oils by fine solid particles. Such particles, with sizes less than 10 μm, can arise from a variety of upstream and refinery operations. The removal of these particles using centrifugation or filtration is expensive and ineffective at a large scale. These problems are particularly acute for heavy oils and bitumens, where high viscosity makes physical separations more difficult.

The solid particles that remain in the heaviest fractions of crude oil after distillation can cause severe problems in downstream refinery units, including plugging of packed-bed reactors and introduction of undesirable reactions.

1.2 Types of contaminants in bitumen, heavy oil and petroleum residues

The fine solid particles of concern in the bitumen, heavy oil and petroleum vacuum residues are from different sources. Below is a brief review of the sources

of these contaminants, their composition and the problems caused by each type of material.

1.2.1 Water and mineral solids in bitumen from naphtha froth treatment

Bitumen, recovered as froth from the hot-water processing of oil sands, contains roughly 30 wt% water and 10 wt% fine solids. Dilution of the bitumen with naphtha enables removal of a large fraction of these contaminants by centrifugation or gravity separation in inclined-plate settlers. Yet, the residual water content is about 4 wt% and fine mineral particles comprise about 0.5 wt% of the bitumen. This residual water is in form of micrometer water - in - oil emulsion, which is extremely stable. The emulsion is stabilized by bitumen natural surfactant, such as resins and asphaltene, as well as mineral solids adsorbed at the oil - water interface. These mineral solids have bitumen components adsorbed on their surfaces, so they have intermediate contact angles giving stable accumulation at the oil - water interface.

1.2.2 Emulsified water and salts in heavy oils

Almost all crude oils contain significant amounts of water when produced. The water in petroleum - bearing formations is normally saline; therefore, when emulsified water is found in crude oil it contains dissolved chlorides and other types of salts. The most common salts that exist in crude oils and bitumens are magnesium, calcium and sodium chlorides. The removal of emulsified water is

most difficult with heavy oils due to their high viscosity and small density difference with brines. Dilution with solvent followed by gravity separation or electrostatic coalescence is often used. When the solvent is eventually removed by distillation, the dissolved salts remain as solid particles in the crude oil as solid particles.

The standard refinery practice to remove such salts is called desalting, where fresh water is mixed with the crude oil to mix with brine droplets. The resulting emulsion is allowed to separate in electrostatic coalescers. This operation is not efficient with heavy oils; therefore a significant fraction of the original salts may remain after this washing step [1].

1.2.3 Corrosion due to chloride salts

Chloride salts enter high temperature refining and upgrading processes either as dissolved salts in emulsified water droplets, or as solids remaining after evaporation of the water. The most reactive salts are magnesium chloride, calcium chloride and sodium chloride. The hydrolysis reactions of these salts are accelerated by the presence of naphthenic acids and mineral solids. The hydrochloric acid produces in the hydrolysis of calcium chloride, for instance, causes serious corrosions of steel vessels and piping. The presence of hydrochloric acid and ammonia, ammonium chloride is formed which gives both plugging and corrosion of the equipment [1].

1.2.4 Coke and sediment in processed heavy streams from visbreaking and coking

Visbreaking is a mild thermal cracking process to reduce the viscosity of the residue or crude oil to make transportation and pumping easier. Low residence time is required to avoid coke formation during heating and reaction of the oil. Coke is defined as the insoluble carbonaceous material that forms at high temperatures (>600°C) and as toluene-insoluble material by filtration assays. If coke particles form in the liquid phase or detach from furnace surfaces, then they will contaminate downstream equipment. When the cracked product is cooled, asphlaltenes may also precipitate in the cracked product due to incompatibility with the reacted liquid phase at low temperature. This type of material is often called sediment. Both coke and sediment particles are hydrophobic organic materials.

The delayed coking and fluid-coking processes are designed to produce coke for upgrading the heavy fractions of bitumen and heavy oil. In these processes, the cracked products are recovered as vapor streams, which would be expected to be free of solids. If the separation of the vapor products is inefficient, due to the fouling of the equipment or operation above design throughput, the solids from the heavy liquid phase such as coke or mineral solids are entrained into the vapor products.

1.2.5 Catalyst particles in slurry hydroconversion processes

Catalysts enable series of process technologies in the oil area such as hydroconversion, hydrotreating, hydrocracking, etc. One of the roles of catalysts is in the hydrogenation of aromatics and olefins. Hydrotreating and hydrocracking of petroleum fractions is conducted in packed bed reactors filled with catalyst pellets. The catalysts act as a granular bed filter for removal of fine particles. The catalyst bed is comprised of pellets of diameter 1 - 2 mm. Large particles (>100 μm) sort out at the top of the reactor. Fine particles (<20 μm) enter the catalyst bed and form deposits. The fine particles suspended in the liquid feed can be intercepted by the catalyst pellets leading to an increase in pressure drop and plugging of the catalyst bed inside the reactor [2].

Catalysts are also used in removal of metals such as vanadium and nickel and heteroatoms such as nitrogen, sulfur and oxygen from the vacuum residue fractions. After the reaction is completed, these catalyst particles should be removed to avoid plugging of the downstream operations.

Catalysts are also used in slurry or suspension based processes. There are a variety of slurry based processes such as EST (ENI Slurry Technology), CANMET hydrocracking and Resid Slurry Hydroconversion. The additives to these processes such as iron based additives or molybdenum inhibit coke formation on the wall. However, if coke forms in the process, it deposits on solid particles. These additives remain as unconverted residues in the slurry and need further processing for their removal [3].

1.3 Current methods for solid removal from oil streams

Process filters are commonly used in refineries and upgraders, but the practical limit for filtration using cartridge units to physically strain particles out of the liquid stream is in the range of 40 micrometer. Deep bed filtration is routinely used to remove fine solids with diameters below 1 micrometer from aqueous streams; however, this technology has not been applied to refinery streams. Low efficiency of deep bed filtration in oil area is due to the high stability of the particles suspension in the oil phase. In addition, the particles do not attach efficiently to a solid surface in a packed bed filter at process conditions [4].

The method that is being used currently for efficient removal of fine particles and emulsified water in oil sands industry is using a paraffinic solvent. In this method, the micrometer sized solid particles and water droplets flocculate by means of the precipitated asphaltene and have a higher sedimentation rates compared to the original particles. As practiced in the oil sands industry, about 7% of the bitumen is precipitated to enhance the removal of water and fine solids. The amounts of the solvent and precipitated asphaltene are currently high in froth treatment. Therefore, there is a need to establish an inexpensive, fast and environmental-friendly method for removal of solid particles from the oil streams. While the paraffinic solvent method is interesting, its current industrial application removes too much of the oil stream. Therefore, it is necessary to find the threshold amount of added solvent to the oil streams that has the potentials for

high removal efficiency of solid particles in addition to produce the least amount of wastes and using the least amount of solvents.

1.4 Thesis objectives

The purpose of this research was to find an efficient method for removal of fine and stable particles from the oil phase. The hypothesis was that flocculation of the solids by precipitated asphaltenes present in the oil solution would occur. Subsequent gravity settling should be used to remove the contaminants from the solution. The term flocculation in this work means joining the particles together to form a loosely connected structure by means of some kind of bridging.

A pitch derived from heavy oil was dissolved in toluene to generate a model process stream, with 1 μm silica particles to represent the solid phase. Two methods were used to study the flocculation of solid particles:

a) Paraffinic treatment

b) Paraffinic treatment with the addition of water

For both methods, the same model oil solution was used. The pitch material was high in asphaltenes; therefore, it can be used to simulate heavy process streams in refineries and upgraders. In the first method, by addition of a paraffinic solvent, asphaltene would start precipitating at a certain ratio of added solvent to the oil solution. It is expected that asphaltene would act as a bridge and flocculate the solid particles. The size of the asphaltene-solid flocs would be larger than the original solid particles. Therefore, fast settling of the flocs would be possible.

In the second method, water droplets were used to agglomerate the solid particles. The main purpose of the work was heteroflocculation of micrometer sized solid particles either with asphaltenes or water droplets or the combination of the two materials.

The method that is being developed should have some important characteristics:

- It should be general to be used for removal of micrometer sized particles (less than 10 μm) from bitumen and petroleum vacuum residues and other refinery streams.
- It should be suitable for removal of different types of particles in bitumen, petroleum residues and heavy oils.
- It should generate as little precipitate and waste as possible to avoid environmental disposal problems.
- Finally, it is important to have a high efficiency for removal of solid particles in the least amount of time.

1.5 Thesis outline

In this work, the second chapter gives the background information on petroleum residues and bitumen characteristics. The next chapter is about the materials that have been used in this work. Chapter 4 deals with the removal of the solid particles by solvent addition to drive flocculation. In the fifth chapter, the focus was on removal of solid particles by addition of small amounts of water. Due to interesting results obtained for removal from solvent-diluted suspensions

(chapter 4), we studied the asphaltene adsorption on different surfaces by using FTIR (Fourier Transform Infra Red spectroscopy) and QCM (Quartz Crystal Microbalance) in chapter 6. Chapter 7 presents the results on measurement of forces between asphaltene coated surfaces in the non-aqueous environment by using AFM (Atomic Force Microscopy). The implications and conclusions of this work are presented in chapters 8. Appendices A and B are about the methods that were used to measure the contact angles of silica particles and acoustic spectroscopy of the model oil solution, respectively. Appendix C, gives the plots on force measurements in oil solution at S/O = 0.5 and 0.

1.6 References

[1] Gary, J. H, G. E. Handwerk, 1984, Petroleum Refining: Technology and Economics. Marcel Dekker, New York.

[2] Narayan, R., Coury, J. R., Masliyah, J. H., 1997, "Particle Capture and Plugging in Packed-Bed Reactors," Industrial and Engineering Chemistry Research, 36(11) pp. 4620-4627.

[3] Pruden, B. B., J. M. Deni, G. Muir, 1989, Presented at the 4th UNIT AR/UNDP conf. Heavy Crude Tar Sands, Edmonton, AB

[4] Wang, S., Chung, K. H., Masliyah, J. H., 1999, "Deposition of Fine Particles in Packed Beds at Hydrotreating Conditions: Role of Surface Chemistry," Industrial and Engineering Chemistry Research, 38(12) pp. 4878-4888.

2 Background

2.1 Classification of petroleum

Petroleum (also called crude oil) is a natural mixture of hydrocarbons from very light gases to solids of various molecular weights. Crude oil may also include compounds containing heteroatoms such as oxygen, nitrogen and sulfur, metals (nickel and vanadium) and other elements. They are found beneath the earth's surface and are in liquid phase under pressure. Inorganic sediment and water may also be present in crude oils [1]. Crude oil is classified based on its viscosity and API (American Petroluem Institute) gravity.

2.1.1 Light crude oil

Conventional (light) crude has a low viscosity and density and can flow easily. The amount of heteroatoms and metals in light crudes are low. The API gravity, however, is high (>20) due to a high proportion of light hydrocarbons. Crude oils contain a wide variety of components; therefore, their physical properties vary widely from different reservoirs. The properties of crude oil such

as viscosity, specific gravity and density change for crude oil from different sources. The carbon and hydrogen content, however, remains relatively constant for all crudes (usually between 83 - 87% carbon and 11 - 14% hydrogen by weight). The price of the light crude oil is much higher than the heavy one [1, 2].

2.1.2 Heavy oil

Heavy oils are different from conventional petroleum in that they are much more difficult to recover from the subsurface reservoirs. Classification of the petroleum and heavy oils based on a single property is no longer enough. Several parameters should be employed to define the nature and properties of different types of petroleum.

Heavy oils have a much higher viscosity and lower API gravity (<20) than conventional petroleum. Primary recovery of this type of petroleum usually requires thermal stimulation of the reservoir [2]. The main problem in heavy oil industry is the difficulty in processing the complex and high boiling point components that exist in their structure. In contrast to conventional crude oils, heavy oils are darker in color and may even be black. The classification of petroleum based on their viscosity and API gravity is shown in Figure 2-1.

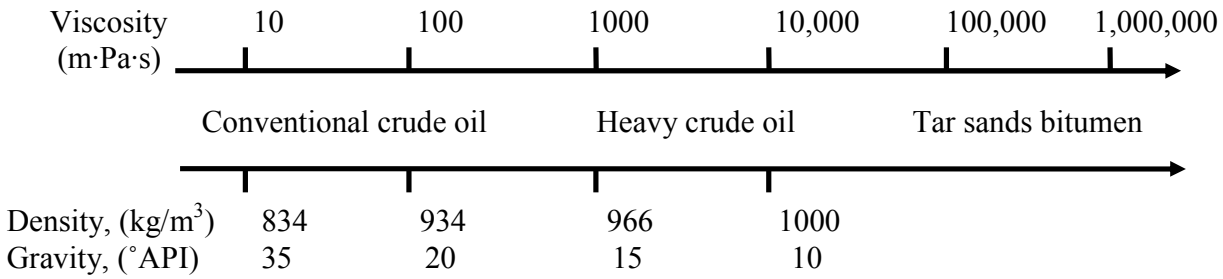

Figure 2-1 Classification of petroleum based on their viscosity and API gravity [2]

2.1.3 Petroleum residues

Residues are the products from the bottom of the distillation tower after all the volatile components have been removed by distillation. These black and viscous solid materials are obtained either by distillation under atmospheric pressure (atmospheric residues) or reduced pressure (vacuum residues). Residues are also defined as nonvolatile components that can be used as asphalt. This fraction includes the most complex constituents of the petroleum with a boiling point higher than 525˚C. The majority of the heteroatoms exist in vacuum residues. When residues are obtained from crude oil via a thermal decomposition process, the product is referred to as pitch [1, 3].

2.1.4 Extra heavy oils and bitumens

Extra heavy oils and bitumens are materials that occur in the solid or near-solid state and are generally incapable of free flow under reservoir conditions. This black material has higher viscosity and lower API gravity compared to

conventional crude oil (Figure 2-1). Bitumen contains high boiling components, mostly higher than 350°C. The amount of heteroatoms and metals such as sulfur, vanadium, nitrogen, and nickel is also higher in bitumen. The hydrogen and carbon content of bitumen would change for different sources but mainly varies between 5 - 12% and 80 - 85%, respectively [1, 3]. The data in table 2-1 gives the elemental composition of Alberta bitumen:

Table 2-1 Elemental composition of Alberta bitumen [2]

Source of Bitumen	Wt% C	Wt % H	Wt % N	Wt % O	Wt % S
Syncrude	83.1	10.6	0.4	1.1	4.8
Suncor	83.9	10.5	0.4	1	4.2
Cold Lake	83.7	10.4	0.1	1.1	4.4

2.2 Bitumen components

Typical bitumen consists of a mixture of hydrocarbons, solid particles and water. The hydrocarbons that exist in bitumen are normally characterized as saturates, aromatics, resins, and asphaltenes, known as SARA contents. Asphaltene, the most complex component of the bitumen, precipitates upon addition of a paraffinic solvent. The deasphalted fraction of bitumen, aromatics, resins and saturates, is called maltenes [5]. Below more details about the bitumen components is presented.

2.2.1 Solid particles

In petroleum upgrading, the solid particles existing in the oil phase are from different sources such as:

- Naturally remaining aluminosilicates and clay crystallites in oilsands streams. Clay particles that are mainly kaolinite, illite and a small amount of montmorillonite only appear in the fine fraction (particles with sizes less than 40 μm).
- Solid particles such as metal oxides, catalysts, etc. that are purposefully added to the oil phase during refinery processes.
- Contaminants such as metal sulfides and mineral material that exist in the oil phase.
- Insoluble organics particles such as coke that would form during refinery processes because of phase transition and wax material that crystallize from the solution due to change of temperature.

In the oil sands industry, fine particles are referred to as particles with sizes less than 44 μm [4]. In general small particles in this size range from 44 μm down to a fraction of micrometer are the main solid contaminants of interest in petroleum streams.

2.2.2 Resins

The portion of bitumen that is soluble in pentane or heptane is often referred to as maltenes (malthenes). Part of the maltenes that dissolve in propane is known

as resins. Resins are commonly separated from the maltenes by adsorption on silica gel or clay from a pentane solution. This adsorptive separation procedure is fundamentally different from the adsorption behavior of asphaltenes.

Resin structure was initially claimed to be composed of long paraffinic chains with naphthenic rings interspersed throughout. Condensed aromatic structure of resins and naphthenic ring systems with heteroatoms throughout the molecule have been proposed as well. Resins interact with asphaltenes through their polar ends [2, 4]. Resins are dark, semi solid or solid and very adhesive materials of high molecular weight. Their composition can vary depending on the kind of liquid used in extraction and on the temperature of the liquid system. They become fluid while heated but are often brittle when cold.

The structural investigation on resin fractions is not as extensive as on the asphaltene fractions. The available data on the molecular weight of resins show lower molecular weight than the asphaltenes, circa 1100 g/mol, from the same crude oil. However, they have a higher hydrogen/carbon (H/C) ratio between 1.38 and 1.69 [1, 5].

2.2.3 Aromatics

Aromatic materials contain one or more ring structures similar to benzene. Aromatics are the portion of the bitumen that is separated from the maltenes by a silica/alumina column in n-pentane solution [4].

Aromatics have a yellow to red color at room temperature. They are slightly aliphatic with lightly condensed aromatic rings and a number-average molecular weight of the order 800 g/mol [5, 6].

2.2.4 Saturates

Paraffins, iso-paraffins and cyclo-alkanes with low amount of heteroatoms, are the components of the saturate fraction. Saturates are different from resins, aromatics and asphaltenes as they are the least polar part of the petroleum or bitumen. After separating the aromatics and resins from the maltenes, the rest is saturates that do not readily adsorb on any conventional packing [4].

At room temperature, saturates are colorless or lightly colored liquid. Their H/C ratio is close to 2 and their average molecular weight is around 600 g/mol [6].

2.2.5 Asphaltene

In the last few years, the focus of researche studies on the structure and chemical composition of the asphaltene has increased. Many researches have studied asphaltenes by new techniques and instruments. Here, we give a brief review of asphaltene on the existing literature.

Asphaltene is considered as the heaviest and most polar components of the crude oil. Asphaltene fractions isolated from different sources are remarkably constant in terms of ultimate composition. However, there can be variations in

terms of heteroatom content due to local and regional variations in the plant precursors and mineralogical composition of the geological formations.

Asphaltenes belong to a solubility class present in crude oils which have been studied extensively in recent years to obtain a better understanding of its complex nature. The common characteristics of asphaltenes are insolubility in light aliphatic solvents (n-pentane or n-heptane) and solubility in aromatic solvents (toluene) [4, 7-10].

These molecules contain a high amount of carbon and low hydrogen content. The density of asphaltene is about $1200 \frac{kg}{m^3}$ [4].

A portion of the asphaltenes can play the role of stabilizer at water/oil emulsions [11-13]. This property of asphaltene fraction is due to the amphiphilic characteristic of their molecules or aggregates of molecules [14, 15]. They are lyophobic with respect to low molecular weight paraffin hydrocarbon and lyophilic with respect to resins and aromatics [16]. Not the entire asphaltene fraction is surface active. Asphaltenes can be used to flocculate water droplets and fine solids [17]. Kotlyar *et al.* demonstrated that asphaltene-like materials have the ability to adsorb on aluminosilicate clays that exist in oil sands [18, 19]. This adsorption occurs as a result of the attraction between the polar functional groups of asphaltenes and the hydroxyl groups present in silica [20].

Molecular weight (MW) of the asphaltene molecules gives more information about its characteristics which is difficult to measure due to complex structure of asphaltene fractions. These large molecules often have a low solubility in the liquids used for determining the MW and have the tendency to form aggregates.

This characteristic complicates the determination of asphaltene molecular weight. The existence of resins leads to some discrepancies in molecular weight determination as well.

Several different methods have been applied to determine the molecular mass of asphaltenes and/or their different aggregation states. Guzman *et al.* (2009) [21] estimate the MW of the Colombian vacuum residue asphaltenes by VPO (Vapor Pressure Osmometry) to be around 1700 ± 200 Da. Hortal *et al.* (2006) [22] reported the MW of the Arabian crude oil by LDI (Laser Desorption Ionization) to be 300 - 500 amu. Yarranton *et al.* measured the molar masses of Athabasca C5 and C7-asphaltene with VPO. The molar mass was reported to be 1800 g/mol for concentrations below 0.5 kg/m^3 [23].

There are two configurations for asphaltene molecular structure suggested in the literature:

1) The continental configuration: asphaltenes have large central aromatic region and alkane components are connected like fingers to the central palm.

2) The archipelago model: asphaltene molecules have several smaller aromatic regions linked by bridging alkanes.

These two model compounds for asphaltene are still under study by many scientists to find out the best structure for asphaltene molecules.

2.2.5.1 Asphaltene self-association behavior

The experimental results show that asphaltenes have self-association characteristics, i.e. forming aggregates of colloidal size. Asphaltene self-

association can be assessed through molar mass measurements [24]. This behavior has also been observed using different experimental methods such as scattering techniques [25], fluorescence [26], vapor pressure osmometry (VPO) [23, 27], small-angle X-ray, and neutron scattering (SAXS and SANS) [28-31]. Yet, the size and structure of both asphaltene monomers and aggregates and the mechanism of self-association are debatable. The main challenge to model the asphaltene self-association is the complex mixture of asphaltene. Asphaltene aggregates can not be defined as a single pure component; therefore, it is difficult to predict the amount of precipitation accurately [24, 32].

As discussed above, different structures of asphaltene molecules have been proposed. These structures lead to different points of view of the self-association mechanism of asphaltenes. Teu Fu [33] introduced the asphaltenes as fractal structures in crude oil and the term micelle was used for these aromatic structures. In this view, asphaltene micelles have a critical micelle concentration (CMC) behavior similar to surfactants. Surface tension versus asphaltene concentration in solvents such as pyridine showed CMC behavior. For a long time, it was believed that self-associating behavior of asphaltene is initiated above CMC. Self-association of asphaltenes has been understood to be the first step in the formation of small aggregates. However, considering CMC characteristics for asphaltene molecules has been questioned by many authors. Anderson *et al*. showed that the titration of asphaltenes with toluene does not fit the behavior of a micelle-like system [34]. Yarranton also mentioned that reverse micelle formation has been observed for some asphaltenes. However, for some samples, the change in surface

tension versus the asphaltene concentration is linear and no evidence of CMC was observed [24].

Yen *et al.* [35] proposed a highly condensed aromatic core with small alkyl chains on the periphery for asphaltene molecules. Considering this structure, asphaltenes are likely to form colloidal stacks held together with $\pi - \pi$ bonds. In this model, it is assumed that asphaltenes are in the form of colloids suspended in the oil phase. The resins molecules are assumed to be adsorbed on the surface or the interior part of the asphaltene particles. Under unfavorable solvent conditions (addition of a low polarity, low solubility solvent), these resin molecules are dissolved; thus, exposing the insoluble asphaltene core and leading to flocculation and precipitation [36]. This model can give a simple picture of asphaltene behavior; however, its validation is still questionable [24, 37]. In particular, the stability of asphlatenes in solvents such as toluene completely contradicts the proposition that resins are required to stabilize the asphaltene colloids.

Strausz proposed a smaller aromatic cluster for the asphaltene molecule [38]. In this case the intermolecular forces between the aggregates can be due to $\pi - \pi$, acid-base and/or hydrogen bonds [39-41]. Hydrogen bonding is mainly due to the interaction between the heteroatoms of the functional groups. When asphaltene molecules are packed, van der Waals forces can be important as well [24, 42-44]. In this case, the aggregates may be considered as macromolecules which can be treated as polymers.

Considering asphaltenes as macromolecules which are either dispersed in solution freely or via resins, then a thermodynamic model can be applied for

asphaltene self- association. Precipitation of asphaltene is considered as a phase change in a non-ideal mixture. The asphaltenes and resins are assumed to form weak bonds. The main differences between resins and asphaltenes are their self-association capability; asphaltenes have multiple active sites for interaction with other components in solution. However, resins are assumed to have one active site in their molecular structure. Asphaltenes are considered as propagators in a straight or branch structure behaving similar to polymers. On the other hand, resins with one active site are treated as terminators. Therefore, their self association behavior is totally different. In the presence of enough resins, little or no association of asphaltenes is observed [24].

In thermodynamic models, precipitated asphaltenes can be considered as solid or liquid. Therefore, both the liquid-liquid equilibrium model using Hilderbrand and Scott [45] and the solid-liquid equilibrium using Scatchard and Hilderbrand regular solution theory have been used to model asphaltene precipitation [46].

The input data for the liquid-liquid model is solubility parameter, molar volume and mole fraction of each component. In this model, the solvent that is used is considered as a component and the SARA fraction of bitumen, i.e. saturates, aromatics, asphaltenes, and resins, are considered as pseudo-components. The asphaltenes are assumed to be a continuum of aggregates of mono-dispersed asphaltene monomers with a different molar mass attributed to each fraction. The molar mass is calculated using gamma molar mass distributions [32, 47-49]. When the solvent power decreases, the destabilization of the asphaltenes occurs and the asphaltenes are no longer soluble. The problem with

using such a model is difficulty in characterizing the asphaltenes in terms of the molar mass, molar volume and solubility parameter distributions. The solubility parameter of different components is a key factor in predicting the results in the thermodynamic model which is difficult to calculate for asphaltenes. The onset and amount of asphaltene precipitation predicted by this model was in good correlation with experimental results for asphaltene and bitumen solution in toluene/alkanes [24, 47, 48].

For the solid-liquid model the input parameters are the same as the liquid-liquid model. The uncertainty of the model, similar to the liquid-liquid model, is the amount of molar volume and solubility parameter. However, by using this model the precipitation point and the amount of precipitated asphaltene was predicted and were in good agreement with experimental data for toluene/alkanes mixtures [50].

2.2.5.2 Deposition and adhesion of asphaltenes on solid and metal surfaces

Different mechanisms have been suggested for the deposition of asphaltene aggregates on surfaces. However, the nature of the interaction between the asphaltene and surfaces has not been established yet. There are several steps for asphaltene deposition: precipitation, flocculation, surface contact, and adhesion. Asphaltenes can be adsorbed on surfaces as colloidal aggregates or as individual molecules without precipitation via carboxylic and phenolic weak acidic groups [51].

The adsorption and deposition of asphaltenes on surfaces creates problems for heavy oil recovery and upgrading. Deposition of asphaltenes on mineral surfaces and reservoir rocks changes the wettability of the surface and limits the extraction of heavy oils from reservoirs. Asphaltene adsorption onto the catalyst surfaces deactivates the catalysts [51]. While aggregation is mainly due to solubility aspects of the asphaltenes, the adsorption of these molecules on surfaces gives information about the surface behavior of the asphaltenes [43].

As mentioned earlier, the asphaltene fraction includes polar molecules which have amphiphilic characteristics [16]. Therefore, they can adhere to surfaces via their functional groups containing oxygen, nitrogen and sulphur [52]. Few studies have focused on the type of bonds that asphaltenes form with a surface and the chemical species involved in the surface interaction. Yet, more experimental results are needed to understand the interaction between asphaltene with other surfaces better.

The mechanism of the adsorption also depends on the type of the asphaltenes, the existence of the resins, the solvent that is used, and the morphology of the surface. Asphaltenes from different sources are not similar in the type of the chemical species that exist in their structure. Therefore, the chemical bonds that are formed between the surface and asphaltenes can be different. The resins fraction also includes surface active materials. They can adsorb on the surface and occupy some of the available sites for asphaltene adsorption [53]. The morpholoy of the surface also affects the mechanism of the adsorption [52, 53]. For instance, Alboudwarej *et al.* [53] used three different metal powders and measured the

amount of asphaltene adsorption by using UV-Vis spectroscopy. The results show that the amount of asphaltene adsorption on metal powders were in this range: stainless steel > iron > alumina. They also reported that the amount of resin adsorption to be lower than the asphaltene adsorption on metal surfaces.

The amount of asphaltene adsorption on the surfaces is affected by the degree of the hydrophobicity of the surface as well. Hydrophilic particles seem to adsorb more asphaltene than the hydrophobic ones [54, 55].

Adhesion of the asphaltene aggregates to the surfaces can be due to van der Waals attraction, as well [20]. Van der Waals forces are considered as weak and short range forces. Both Langmuir and multilayer adsorption of asphaltene aggregates on surfaces have been observed [53, 56-58]. More details on the deposition of asphaltene on surfaces would be discussed in chapter 6 and 7.

2.3 Existing options for contaminants removal from bitumen and vacuum residues

2.3.1 Naphtha-based processing

In general, froth contains around 60% bitumen, 30% water and 10% solids by weight. A diluent is added to the froth to decrease the viscosity and enhance the removal of solid particles. Syncrude and Suncor use naphtha as the diluent at a ratio of 0.7:1 and two stages centrifuges to remove the particles. Both gravity settling (incline plate settlers) and centrifuges are commonly utilized in the froth treatment using naphtha. After treating the froth in the scroll centrifuge to remove

the particles, the product would go to a disc centrifuge for further removal of the solid particles. The naphtha should be removed in naphtha recovery units (NRU). The problem with using naphtha as the diluent is that the final product does not have a high quality. The current naphtha treatment plant product contains 0.3 to 1.0 wt% solids and 1 to 5 wt% water [3, 4, 59, 60].

2.3.2 Paraffinic Froth Treatment (PFT)

Using paraffinic solvents can be an alternative froth treatment process for naphtha. In this process, the amount of solids and water can reduce to less than 1 wt%. By using an aliphatic solvent such as hexane or pentane, not only the emulsified water and micrometer sized particles are removed, but also some of the asphaltenic components of the bitumen are separated [3, 61]. This method is now used at Muskeg River Mine, Albian sands Energy.

For bitumen froth treatment process to perform at its highest efficiency some of the controlling parameters of the process should be fixed. These parameters include solvent to bitumen ratio (S/B), asphaltenes rejection level, density, and viscosity of the diluted oil phase [59].

In Shell-Albian froth treatment, by treating the bitumen phase with heptane, part of the asphaltene precipitates. The precipitated asphaltene flocculate the solid particles and water droplets and form water/solids/asphaltenes aggregates that are larger than the original emulsified water droplets and dispersed solids. These larger aggregates have higher settling rates than the original particles due to their larger sizes. Later the diluted bitumen is pumped to a solvent recovery unit

(SRU). In this step of the process, the added solvent is removed in distillation units [4, 61].

2.3.3 ENI Slurry Technology (EST)

In 1990s, Eni [62] started a new concept for full conversion and upgrading of the heavy materials into light products. The Eni Slurry Technology (EST) is a slurry hydroprocessing process combined with using a solvent such as pentane or hexane for deasphalting of the vacuum residues. In this method, the unconverted asphaltene are removed and the particles such as molybdenum sulfide are flocculated; producing a solid-free product. Highly active catalyst is used to maximize the upgrading and later the catalyst is recycled with the asphaltenes. A range of feedstocks such as atmospheric residues, extra heavy crude oils, deasphalted oils, and vacuum residues can be converted to products like light gases, naphtha, gasoil (diesel), and deasphalted oil. Almost complete conversion can be obtained with high selectivity to distillates, optimum hydrogen consumption, low catalyst consumption, and a flexible product slate. In addition, the operation removes the heteroatoms or reduces them to a level manageable in conventional refinery operations. EST can be considered as a hydrocracking process which has an original process scheme for handling the catalysts that allows a high conversion and upgrading performance. The EST process is attractive for heavy feeds, but unlike other methods, it combines the advantages of carbon rejection and the product quality upgraded by hydrogen addition processes.

2.4 Depth filtration

Depth filtration is one of the filtration methods used for separating particles with various sizes and density. This type of filtration has four main filtration layers. Larger suspended particles are removed by the upper layers while smaller particles are removed in the lower layers. When the pressure between the inlet and outlet of the depth filtration system increases by 5 - 10 psi (34 to 68 kPa), the filter should be reconditioned. The reconditioning cycle consists of an upflow backwash followed by a downflow rinse, using water as the rinsing medium. Mainly water is used as the rinsing medium.

The main depth filter in water treatment plant is made of granular and crushed materials in addition to sand, garnet, alumina, magnetite, anthracite, and quartz. Using these materials for refinery purposes can be troublesome for cleaning and would cause problems with fouling. In addition, water can not be used for reconditioning of the filter in refineries. The main advantage of the depth bed filtration to conventional filtration is that larger flow rates can be used in the former filteration methods. For using the depth filtration for the oil industry, care should be taken with the choice of the median and the reconditioning solvent.

The effective method that can be used for removal of fine particles is paraffinic or naphtha treatment. We used the former method for detailed study in this thesis. By increasing the size of the flocs by adding pentane, depth bed filtration can be further used to remove the larger flocs of asphaltene – silica.

2.5 References

[1] Speight, J.G., and Ancheyta, J., 2007, "Hydroprocessing of heavy oils and residua" CRC Press, .

[2] Speight G, J., 1999, "The chemistry and technology of petroleum," Marcel Dekker, New York, .

[3] Gray, M.R., 1994, "Upgrading petroleum residues and heavy oils " New York: M.Dekker, .

[4] Murray R.Gray, and Jacob H.Masliyah, 2007, "Extraction and upgrading of oilsands Bitumen," .

[5] Lesueur, D., 2009, "The Colloidal Structure of Bitumen: Consequences on the Rheology and on the Mechanisms of Bitumen Modification," Advances in Colloid and Interface Science, 145(1-2) pp. 42-82.

[6] Corbett, L. W., 1969, "Composition of Asphalt Based on General Fractionation, using Solvent Deasphaltening, Elution-Adsorption Chromatography, and Densimetric Characterization," 41(4) pp. 576-579.

[7] Rahmani, N. H. G., Dabros, T., and Masliyah, J. H., 2005, "Settling Properties of Asphaltene Aggregates," Energy and Fuels, 19(3) pp. 1099-1108.

[8] Rahmani, N. H. G., Dabros, T., and Masliyah, J. H., 2005, "Fractal Structure of Asphaltene Aggregates," Journal of Colloid and Interface Science, 285(2) pp. 599-608.

[9] Rahmani, N. H. G., Dabros, T., and Masliyah, J. H., 2005, "Online Optical Monitoring of Asphaltene Aggregation," Industrial and Engineering Chemistry Research, 44(1) pp. 75-84.

[10] Yiecheng Long, Tadeusz Dabros, and Hassan Hamza, July 14, 2006, "Selective Solvent Deasphalting for Heavy Oil Emulsion Treatment," pp. 507-544.

[11] Zhang, L. Y., Breen, P., Xu, Z., 2007, "Asphaltene Films at a toluene/water Interface," Energy and Fuels, 21(1) pp. 274-285.

[12] Singh, S., McLean, J. D., and Kilpatrick, P. K., 1999, "Fused Ring Aromatic Solvency in Destabilizing Water-in-Asphaltene-Heptane-Toluene Emulsions," Journal of Dispersion Science and Technology, 20(1) pp. 279-293.

[13] Frdedal, H., Schildberg, Y., Sjoblom, J., 1996, "Crude Oil Emulsions in High Electric Fields as Studied by Dielectric Spectroscopy. Influence of Interaction between Commercial and Indigenous Surfactants," Colloids and Surfaces A: Physicochemical and Engineering Aspects, 106(1) pp. 33-47.

[14] Li, D., Shi, Z., Mei, S., 2006, "Effects of Flocculation Conditions on Aggregates Fractal Structures," Huanjing Kexue/Environmental Science, 27(3) pp. 488-492.

[15] Li, X. , Elliott, J. A. W., McCaffrey, W. C., 2005, "Dynamic Surface Tensions of Athabasca Bitumen Vacuum Residue Including the Effect of Dissolved Air," Journal of Colloid and Interface Science, 287(2) pp. 640-646.

[16] Rahmani, N. H. G., Dabros, T., and Masliyah, J. H., 2004, "Evolution of Asphaltene Floc Size Distribution in Organic Solvents Under Shear," Chemical Engineering Science, 59(3) pp. 685-697.

[17] Skuse, D. R., Tadros, T. F., and Vincent, B., 1986, "Controlled Heteroflocculation of Nonaqueous Silica Dispersions," Colloids and Surfaces, 17(4) pp. 343-360.

[18] Kotlyar, L. S., Sparks, B. D., Woods, J. R., 1999, "Solids Associated with the Asphaltene Fraction of Oil Sands Bitumen," Energy and Fuels, 13(2) pp. 346-350.

[19] Kotlyar, L. S., Sparks, B. D., Woods, J. R., 1998, "Distribution and Types of Solids Associated with Bitumen," Petroleum Science and Technology, 16(1) pp. 1-19.

[20] Abraham, T., Christendat, D., Karan, K., 2002, "Asphaltene - Silica Interactions in Aqueous Solutions: Direct Force Measurements Combined with Electrokinetic Studies," Industrial and Engineering Chemistry Research, 41(9) pp. 2170-2177.

[21] Guzman, A., Bueno, A., and Carbognani, L., 2009, "Molecular Weight Determination of Asphaltenes from Colombian Crudes by Size Exclusion Chromatography (SEC) and Vapor Pressure Osmometry (VPO)," Petroleum Science and Technology, 27(8) pp. 801-816.

[22] Hortal, A. R., Martinez-Haya, B., Lobato, M. D., 2006, "On the Determination of Molecular Weight Distributions of Asphaltenes and their Aggregates in Laser Desorption Ionization Experiments," Journal of Mass Spectrometry, 41(7) pp. 960-968.

[23] Yarranton, H. W., Alboudwarej, H., and Jakher, R., 2000, "Investigation of Asphaltene Association with Vapor Pressure Osmometry and Interfacial Tension

Measurements," Industrial and Engineering Chemistry Research, 39(8) pp. 2916-2924.

[24] Yarranton, H. W., 2005, "Asphaltene Self-Association," Journal of Dispersion Science and Technology, 26(1) pp. 5-8.

[25] Barre, L., Jestin, J., Morisset, A., 2009, "Relation between Nanoscale Structure of Asphaltene Aggregates and their Macroscopic Solution Properties; Relation Entre Nanostructure Des Agregats d'Asphaltene Et Les Proprietes Macroscopiques De Leur Solution," Oil and Gas Science and Technology, 64(5) pp. 617-628.

[26] Da, S. S., Nicodem, D. E., Garden, S. J., 2010, "Study of the Asphaltene Aggregation Structure by Time-Resolved Fluorescence Spectroscopy," Energy and Fuels, 24(2) pp. 1135-1138.

[27] Strausz, O. P., Peng, P., and Murgich, J., 2002, "About the Colloidal Nature of Asphaltenes and the MW of Covalent Monomeric Units," Energy and Fuels, 16(4) pp. 809-822.

[28] Xu, Y., Koga, Y., and Strausz, O. P., 1995, "Characterization of Athabasca Asphaltenes by Small-Angle x-Ray Scattering," Fuel, 74(7) pp. 960-964.

[29] Sheu, E. Y., 2006, "Small Angle Scattering and Asphaltenes," Journal of Physics Condensed Matter, 18(36) pp. S2485-S2498.

[30] Tanaka, R., Hunt, J. E., Winans, R. E., 2003, "Aggregates Structure Analysis of Petroleum Asphaltenes with Small-Angle Neutron Scattering," Energy and Fuels, 17(1) pp. 127-134.

[31] Safieva, J. O., Likhatsky, V. V., Filatov, V. M., 2010, "Composition of asphaltene solvate shell at precipitation onset conditions and estimation of average aggregate sizes in model oils," Anonymous American Chemical Society, 2540 Olentangy River Road, P.O. Box 3337, Columbus, OH 43210-3337, United States, 24, pp. 2266-2274.

[32] Alboudwarej, H., Akbarzadeh, K., Beck, J., 2003, "Regular Solution Model for Asphaltene Precipitation from Bitumens and Solvents," AICHE Journal, 49(11) pp. 2948-2956.

[33] Yen, T. F., 1990, "Macrostructure of petroleum asphalt," Symposium on Chemistry and Characterization of Asphalts, August 26, 1990 - August 31, Anonymous Publ by ACS, Washington, DC, USA, 35, pp. 314-319.

[34] Merino-Garcia, D., and Andersen, S. I., 2005, "Calorimetric Evidence about the Application of the Concept of CMC to Asphaltene Self-Association," Journal of Dispersion Science and Technology, 26(2) pp. 217-225.

[35] Dickie, J. P., and Yen, T. F., 1967, "Macrostructures of Asphaltic Fractions by various Instrumental Methods," Analytical Chemistry, 39(14) pp. 1847-1852.

[36] Pfeiffer, J. P., and Saal, R. N. J., 1940, "Asphaltic Bitumen as Colloid System," Journal of Physical Chemistry, 44pp. 139-149.

[37] Sirota, E. B., 2005, "Physical Structure of Asphaltenes," Energy and Fuels, 19(4) pp. 1290-1296.

[38] Strausz, O. P., Lown, E. M., and Mojelsky, T. W., 1994, "Molecular structure of asphaltene," Proceedings of the Symposia on the Role of Asphaltenes

in Petroleum Exploration, Production and Refining, March 13, 1994 - March 18, Anonymous Publ by ACS, San Diego, CA, USA, 39, pp. 199.

[39] Larsen, J. W., and Li, S., 1995, "Determination of Bitumen Molecular Weight Distributions using 252Cf Plasma Desorption Mass Spectrometry," Energy and Fuels, 9(5) pp. 760-764.

[40] Maruska, H. P., and Rao, B. M. L., 1987, "Role of polar species in the aggregation of asphaltenes" Fuel Science and Technology International, 5(2) pp. 119-168.

[41] Moschopedis, S. E., and Speight, J. G., 1976, "Oxygen Functions in Asphaltenes," Fuel, 55(4) pp. 334-336.

[42] Spiecker, P. M., Gawrys, K. L., and Kilpatrick, P. K., 2003, "Aggregation and Solubility Behavior of Asphaltenes and their Subfractions," Journal of Colloid and Interface Science, 267(1) pp. 178-193.

[43] Cadena-Nava, R., Consultchi, A., and Ruiz-Garcia, J., 2007, "Asphaltene Behavior at Interfaces," Energy and Fuels, 21(4) pp. 2129-2137.

[44] Camacho-Bragado, G., Santiago, P., Marin-Almazo, M., 2002, "Fullerenic Structures Derived from Oil Asphaltenes," Carbon, 40(15) pp. 2761-2766.

[45] Hildebrand, J.H., and Scott, R.L., 1950, "Solubility of nonelectrolytes," Reinhold Pub Corp, NY, NY, United States,.

[46] Cimino, R., S. Correra, E. Sacomani, and C. Carniani, “Thermodynamic Modelling for Prediction of Asphaltene Deposition in Live Oils,” SPE Int. Symp. Oilfield Chemistry, San Antonio (Feb. 1995)

[47] Akbarzadeh, K., Alboudwarej, H., Svrcek, W. Y., 2005, "A Generalized Regular Solution Model for Asphaltene Precipitation from n-Alkane Diluted Heavy Oils and Bitumens," Fluid Phase Equilibria, 232(1-2) pp. 159-170.

[48] Akbarzadeh, K., Ayatollahi, S., Moshfeghian, M., 2004, "Estimation of SARA Fraction Properties with the SRK EOS," Journal of Canadian Petroleum Technology, 43(9) pp. 31-39.

[49] Akbarzadeh, K., Dhillon, A., Svrcek, W. Y., 2004, "Methodology for the Characterization and Modeling of Asphaltene Precipitation from Heavy Oils Diluted with n-Alkanes," Energy and Fuels, 18(5) pp. 1434-1441.

[50] Yarranton, H. W., and Masliyah, J. H., 1996, "Molar Mass Distribution and Solubility Modeling of Asphaltenes," AICHE Journal, 42(12) pp. 3533-3543.

[51] Nassar, N. N., 2010, "Asphaltene Adsorption Onto Alumina Nanoparticles: Kinetics and Thermodynamic Studies," Energy and Fuels, 24(8) pp. 4116-4122.

[52] Dudasova, D., Simon, S., Hemmingsen, P. V., 2008, "Study of Asphaltenes Adsorption Onto Different Minerals and Clays. Part 1. Experimental Adsorption with UV Depletion Detection," Colloids and Surfaces A-Physicochemical and Engineering Aspects, 317(1-3) pp. 1-9.

[53] Alboudwarej, H., Pole, D., Svrcek, W. Y., 2005, "Adsorption of Asphaltenes on Metals," Industrial and Engineering Chemistry Research, 44(15) pp. 5585-5592.

[54] Hannisdal, A., Ese, M., Hemmingsen, P. V., 2006, "Particle-Stabilized Emulsions: Effect of Heavy Crude Oil Components Pre-Adsorbed Onto

Stabilizing Solids," Colloids and Surfaces A: Physicochemical and Engineering Aspects, 276(1-3) pp. 45-58.

[55] Zahabi, A., Gray, M. R., Czarnecki, J., 2010, "Flocculation of silica particles from a model Oil solution: Effect of adsorbed asphaltenes," Anonymous American Chemical Society, 2540 Olentangy River Road, P.O. Box 3337, Columbus, OH 43210-3337, United States, 24, pp. 3616-3623.

[56] Marczewski, A. W., and Szymula, M., 2002, "Adsorption of asphaltenes from toluene on mineral surface," Anonymous Elsevier, 208, pp. 259-266.

[57] Rudrake, A., Karan, K., and Horton, J. H., 2009, "A Combined QCM and XPS Investigation of Asphaltene Adsorption on Metal Surfaces," Journal of Colloid and Interface Science, 332(1) pp. 22-31.

[58] Gaboriau, H., and Saada, A., 2001, "Influence of Heavy Organic Pollutants of Anthropic Origin on PAH Retention by Kaolinite," Chemosphere, 44(7) pp. 1633-1639.

[59] Long, Y., Dabros, T., and Hamza, H., 2004, "Analysis of Solvent-Diluted Bitumen from Oil Sands Froth Treatment using NIR Spectroscopy," Canadian Journal of Chemical Engineering, 82(4) pp. 776-781.

[60] Gray, M. R., Zhang, Z., McCaffrey, W. C., 2003, "Measurement of Adhesive Forces during Coking of Athabasca Vacuum Residue," Industrial and Engineering Chemistry Research, 42(15) pp. 3549-3554.

[61] Long, Y., Dabros, T., and Hamza, H., 2004, "Structure of water/solids/asphaltenes Aggregates and Effect of Mixing Temperature on Settling Rate in Solvent-Diluted Bitumen," Fuel, 83(7) pp. 823-832.

[62] Richard H. Nielson, “Eni slurry hydroprocssing technology for diesel fuel”, PEP Review 99-2, (June 2003)

3 Materials

In this chapter, the materials that were used in the experimentals are introduced. The different methods that were used in the experiments are introduced in the related chapters.

3.1 Silica particles

Spherical silica particles with diameters of approximately 1 μm (Figure 3-1) were purchased from Fiber Optic Center (Massachusetts, USA). The surface area of the particles was around 2–6 m^2/g and their density is 2000 kg/m^3. The silica particles were left in HNO_3 overnight and then washed with water and dried in an oven at 120˚C. The contact angle of these particles measured by the sessile drop method, using FTA 200 instrument (First Ten Angstroms, Virginia, USA), was 20˚±10˚. Therefore, these particles were considered to be hydrophilic. Hydrophobic particles were prepared by dispersing acid-treated particles in 5 V/V dichlorodimethylsilane in toluene for 10 min, then washing with toluene and oven-drying at 120˚C overnight. The contact angle of these particles obtained by

the same method was more than 90˚ (around 120˚), which shows high hydrophobicity.

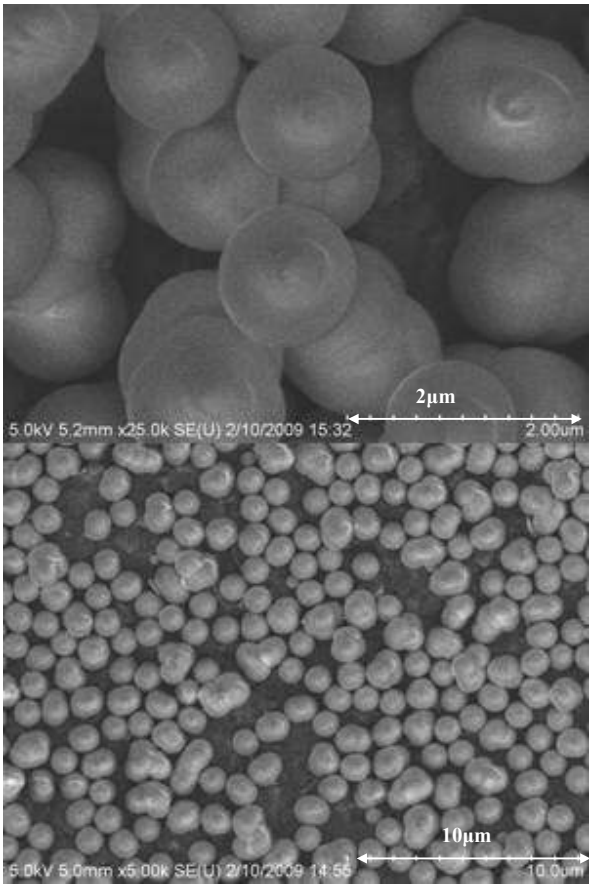

Figure 3-1 Scanning electron microscopy images of silica particles

3.2 Clay particles

The rod shape clay particles (Kaolinite) with approximate sizes around 1 µm were used to represent another source of solids in the model oil solution (Georgia kaoline).

3.3 Pitch material

A sample of thermally cracked vacuum residue material from Cold Lake bitumen having a density of 1116 kg/m^3 (ASTM D2638) was used as a representative source of asphaltenes in upgrader and refinery streams. Table 3-1 shows the analysis of the pitch material, which was used in all the experiments. The main characteristics of the pitch material for the purposes of this study are the high asphaltene and low ash contents.

Table 3-1 Analysis of the pitch material derived from thermal cracking of Cold Lake bitumen

Analysis	Weight %	Method
Carbon	83.14	ASTM D5373
Hydrogen	8.66	
Nitrogen	1.08	
Sulfur	6.65	ASTM D4239
Oxygen	0.64	
Ash	0.26	ASTM D5142
Toluene Insoluble	0.19	ASTM D4072
Saturates	2.20	ASTM D2007
Aromatics	22.5	
Polars	15.8	
Asphaltenes	59.5	

3.4 Solvents

Reagent-grade toluene and n-pentane were purchased from Fisher Scientific and were used as received. Ultrapure water (resistivity $\approx$ 18.2 MΩ cm) was freshly collected from a Millipore Milli-Q system.

4 Removal of solid particles from a model oil solution by paraffinic treatment

4.1 Introduction

As conventional sources of crude oil become depleted, new resources such as the oil sands in Alberta and crude oil in deep-sea reservoirs play an increasingly important role in meeting market demand. These non-conventional petroleum resources require pre-processing to make them suitable as petroleum products. Typical bitumen froth from commercial production contains approximately 30% water, 10% solids and 60% bitumen [1, 2]. The solid particles encountered during petroleum recovery and processing vary in make-up and origin and may include naturally occurring aluminosilicates and clay crystallites originating in oil sand; solid particles such as metal oxides, materials such as catalysts that are intentionally added to the oil phase during refining; contaminants such as metal sulfides that exist in the oil phase; and insoluble organic particles such as coke that can form because of phase transition during refining. Most upgrading processes focus on removal of solid particles and emulsified water. For transportation by pipeline, a diluted bitumen is required to contain less than 0.5

vol% total bottom solids and water [1, 2]. The paraffinic froth treatment (PFT) process (used by Albian Sands Energy) uses a diluent that is rich in n-hexane to precipitate a portion of the asphaltenes in the bitumen, which is then flocculated with emulsified water droplets and fine solids to enable removal of impurities by gravitational settling [3]. Particle growth by flocculation is required in order to achieve efficient particle removal in filtration or settling stages. Here, we use the term flocculation to describe the joining together of primary particles in suspension to form a structure held together by means of some kind of bridging.

Asphaltene molecules are commonly defined on the basis of their solubility; these large molecules are insoluble in paraffinic solvents such as pentane, hexane and heptane, but soluble in aromatic solvents such as toluene and benzene [4-10]. Asphaltene molecules can also act as a stabilizing agent for dispersions and emulsions. Asphaltene coat the solid particles and the suspension of the particles would be stabilized by means of steric repulsion between the particles.

Nellensteyn [11] in 1933 first mentioned the fact that resins are responsible for the stability of asphaltenes in crude oil. Resin molecules have an intermediate polarizability between the asphaltene molecules and the rest of the crude oil, while asphaltene molecules are considered to be the most polarizable part of the crude oil. Resins, therefore, bind to asphaltene molecules and act as a steric dispersant to stabilize the asphaltenes from forming aggregates [12, 13]. This model of resins peptizing asphaltenes was based on observation of Tyndall effect and Brownian movements of particles in oil [14]. Nellensteyn's ideas were then refined by Pfeiffer and Saal [15, 16] resulting in the 'colloidal model' theory.

Contrary to this model, asphaltenes dissolved in toluene form colloidal-size aggregates in the absence of any resins, which according to the Pfeiffer model are essential to keep them in suspension [15]. Despite this obvious deficiency, the model of resins stabilizing asphaltenes in solutions is still used and resin−asphaltene interactions are considered to be the key to understanding crude oil behavior, especially in connection with asphaltene precipitation. There is no complete understanding of the mechanism or mechanisms involved. The limit to growth of asphaltene aggregates may be due to steric repulsion from aliphatic chains attached to their aromatic core [11, 15].

When particles such as silica or clays are dispersed in oil phase, resins and asphaltene molecules likely interact with the hydroxyl groups on solid surfaces [17]. If resins adsorb weakly on the particle surfaces, the van der Waals interactions between the coated particles are weak and the particles are therefore stabilized in the oil phase.

However, upon addition of a nonpolar solvent, such as heptane or pentane, the polyaromatic clusters in the structure of asphaltene molecules bind together by π-π van der Waals interactions and form larger aggregates [12, 13]. Hannisdal *et al*. have shown that the adsorption of asphaltenes on silica is higher compared to resin adsorption on the same surface [18]. Therefore, as asphaltene molecules aggregate under addition of a non-polar solvent, their adsorption on silica particles increases. The asphaltene coatings on the particles and the precipitating asphaltenes likely form bridges between silica particles resulting in formation of

asphaltene – silica flocs. This mechanism may be useful for removing fine solids from a range of refinery streams that contain asphaltene components.

The objective of this chapter was to study in detail the removal of solid particles by flocculation with asphaltene molecules to provide a basis for the development of separation technology. A model oil suspension referred to as model oil (O) was investigated, consisting of 1 μm silica particles suspended in a pitch material dissolved in toluene. Various ratios of n-pentane as solvent (S) were added to precipitate a portion of the asphaltenes and flocculate solid particles by rapid sedimentation, thereby cleaning the liquid. Determination of solid removal at low solvent addition ratios with minimal precipitation of asphaltenes was a key objective.

4.2 Experimental methods

4.2.1 Settling tests

The components of the model oil were pitch material, toluene, and silica particles. To determine the optimal concentration of pitch material in toluene for the model oil, various concentration of pitch material were dissolved in toluene. Each sample was shaken using a horizental shaker for 2 hours and left overnight to make sure that all the pitch materials were dissolved in toluene.

n-pentane with a known ratio (S/O = 1/1 by weight) was added to each oil sample and the whole solution was transferred to the mixing vessel, a glass jar, 104 mm in diameter and 145 mm high, with four baffles. The impeller used for

mixing was a three-bladed, square-pitch, marine-type impeller 67 mm in diameter. A clearance of 30 mm was maintained between the impeller and the bottom of the container during mixing. The oil solution and solvent were stirred at 600 rpm for 10 min.

Upon completion of mixing, the diluted solution was quickly transferred to a 500 mL graduated glass cylinder (370 mm high and 46.5 mm in inner diameter). The observed area of the settler was illuminated using two fiber-optic bundles. The settling experiments were conducted at room temperature. The position of the interface was recorded versus times to determine the settling velocity of asphaltene flocs for various concentrations of pitch material in toluene. The densities and viscosities of each oil solution before and after dilution with n-pentane are listed in Table 4-1.

Table 4-1 Density and viscosity of various concentrations of pitch material in toluene

Wt% of pitch sample in toluene	**Viscosity (mPa·s)**	**Density (kg/m^3)**	**Viscosity of diluted oil solution at S/O = 1 (mPa·s)**	**Density of diluted oil solution at S/O = 1 (kg/m^3)**
3	0.78	870	0.39	728
5	0.81	875	0.4	729
10	1.2	885	0.43	731
25	3.03	917	0.52	738

The densities of the oil samples were determined using a laboratory densitometer (Anton Paar model DMA 4500, Fisher Scientific, Ottawa, Ontario, Canada), and the viscosity was measured using a Viscolab 3000 rheometer

(Cambridge Applied Systems, Medford, MA). Both viscosity and density were measured using the suspension-free supernatant. The supernatant was separated from the rest of the suspension using a centrifuge for 10 min at 3000 rpm (around 1500*g*).

4.2.2 Onset of asphaltene precipitation

The onset of asphaltene precipitation was determined by three different methods.

1) Asphaltene content in the supernatant: Oil samples were prepared by the standard mixing method (section 4.2.1). Upon completion of the settling test, the supernatant was carefully separated from the sediment using a pipet. The solvent in the supernatant was removed by rotary evaporation. The asphaltene content of the remaining solid material was measured based on ASTM D2007. Similar experiments were repeated for various S/O.

2) Volume of the sediment: For more precise determination, solutions with various S/O were prepared. Each solution (10 mL) was mixed for 25 min with a shaker and centrifuged at 3000 rpm (1500*g*) for 30 min after 2 hours. The volumes of sediment at the bottom of the centrifuge tubes were measured.

3) Microscopic observation: Samples with various S/O were prepared. Each sample was mixed for 25 min with a shaker. After 2 hours, the samples were examined using a light microscope (Zeiss Axiotechvario) coupled with a camera (Zeiss model ZVS-3C75DE) to check for the onset of asphaltene precipitation at various S/O. The samples were placed in cells 100 μm deep.

4.2.3 Preparation of model oil suspension

The model oil (O) was obtained by preparing a stock toluene solution of pitch material (5 wt%). The stock sample was left overnight and then centrifuged at 4500 rpm for 20 min. Silica particles (4 wt%) were added to the oil solution and mixed using a shaker for 30 min; the suspension was then blended at 27,000 rpm for 10 min using a homogenizer. Some of the silica particles were lost due to adhesion to the instrument walls. The solvent (n-pentane) was introduced into the oil suspension and the suspension was shaken for 25 min using a shaker and transferred to a graduated cylinder. To study the effect of n-pentane on settling of the silica particles, samples were taken by pipette at different heights in the graduated cylinder after a certain time (65 min) for different S/O values. The ash contents were determined for individual samples using ASTM 5142 to measure the silica content at each height. We used a programmed oven overnight to burn the samples in air. The oven temperature was raised to 800°C over 4 hours, maintained at the target temperature for 2 hours and then cooled down per 4 hours.

4.2.4 Contact angle measurement

For micrometer-size particles, the direct measurement of the contact angle is not possible. One of the indirect methods of measuring the contact angle of such particles is to use a sessile drop on a compressed disk of particles [20]. The three-phase contact angles of silica particles were measured in air and by introducing a

water droplet. Images were taken by means of FTA 200 (First Ten Angstroms, Virginia, USA).

4.3 Results and discussion

4.3.1 Settling curve of asphaltene flocs at various concentrations of pitch material in toluene at S/O = 1

Figure 4-1 presents the experimental settling curves at various concentrations of pitch material in toluene diluted with n-pentane at S/O = 1 by weight at room temperature. This ratio was chosen because it was easier to follow the interface and we could make sure that asphaltene has precipitated. The settling rate was defined as the descending velocity of the interface and was obtained by visual observation of the interface. The data in Figure 4-1 show that the settling of asphaltene flocs in a sample of 25 wt% of pitch material was very low and that, by reducing the amount of pitch material in toluene, the settling rate of the asphaltene flocs was increased. The settling rate of flocculated asphaltenes depends on many factors including the viscosity and density of the medium and the density and diameter of the flocs [8]. A concentration of 5 wt% pitch material in toluene diluted with n-pentane gave a reasonable settling rate and the amount of pitch material was sufficient to stabilize silica particles in this model oil solution. Therefore, a concentration of 5 wt% pitch material in toluene was chosen as the model oil solution and for detailed study.

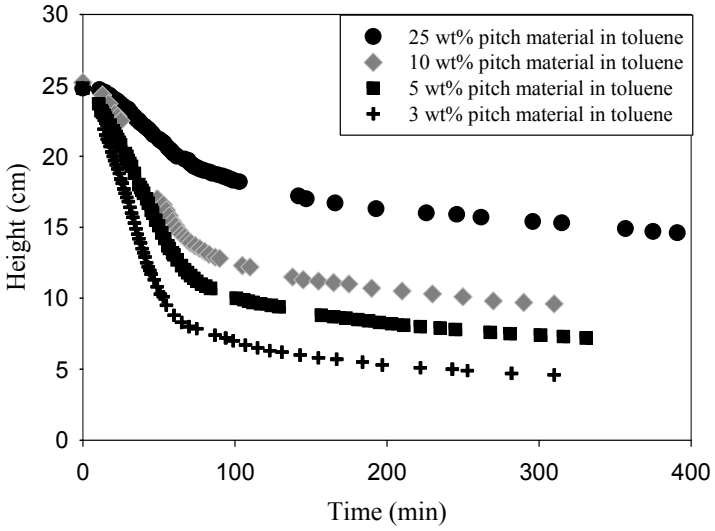

Figure 4-1 Settling curves of oil solution diluted with n-pentane at various concentrations of pitch material in toluene at S/O = 1

4.3.2 Onset of asphaltene precipitation

The onset of asphaltene precipitation was determines for a concentration of 5 wt% of pitch material in toluene. Figure 4-2 shows the asphaltene concentration in the solvent-free supernatant at various S/O. The asphaltene concentration in the solvent-free supernatant was analyzed using n-pentane as precipitant. The initial amount of asphaltene in the original pitch material was around 60 wt%. At higher S/O it is obvious that the asphaltene content in the solvent-free supernatant has decreased due to precipitation. At S/O = 0.5, the asphaltene concentration in the supernatant was close to that in the pitch material (60 wt%), but decreased at higher S/O. Therefore, the onset of asphaltene precipitation occurred around S/O = 0.5 (by weight).

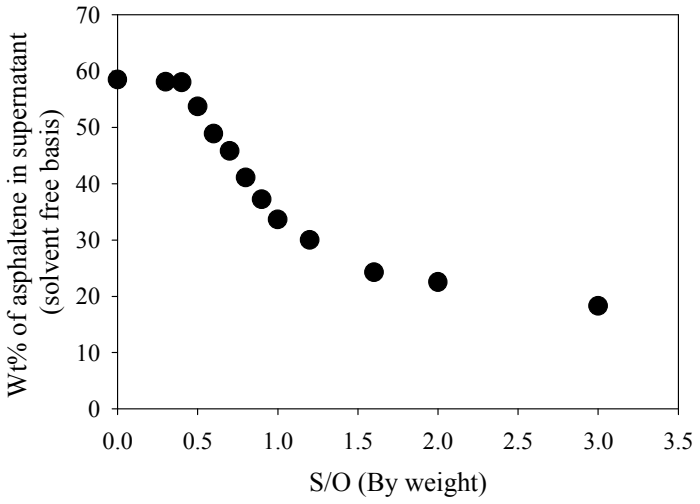

Figure 4-2 Asphaltene concentration in the solvent–free supernatant of model oil diluted with n-pentane as a function of various S/O after 2 hours

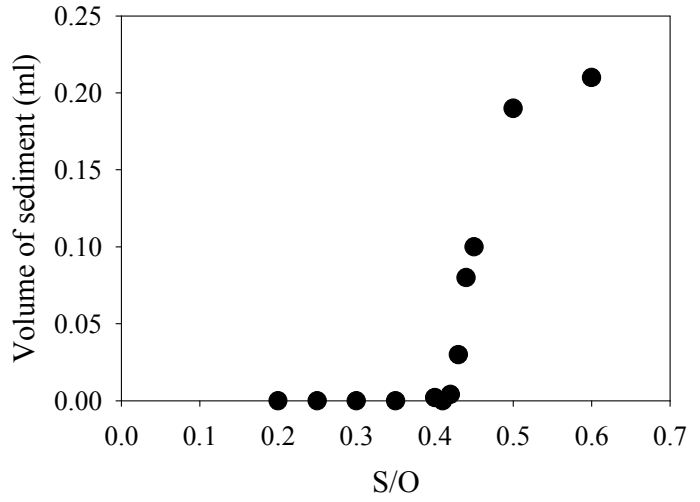

Figure 4-3 Volume of asphaltene sediment at various S/O after 2 hours

In Figure 4-3 the volume of the asphaltene sediment is plotted for various S/O (by weight). At S/O = 0.43 there was small amount of sediment at the bottom of the centrifuge tubes, whereas no solids were observed at S/O lower than 0.43. This method indicated onset of precipitation at S/O of 0.43.

Samples with various S/O (by weight) ranging from 0.35 to 0.5 were observed using a light microscope in a 100-μm cell. Immediately after the addition of n-pentane, only the sample at S/O = 0.5 gave visible flocs. After an hour, more flocs were observed in the sample with S/O = 0.5, and some tiny flocs were formed in sample with S/O = 0.43. After 2 hours (which is the duration of the experiment) the concentration of flocs increased even more at S/O = 0.5 and 0.43; however, no flocs were observed in the samples with S/O lower than 0.43. The microscopic images for the samples at various S/O values after 2 hours are shown in Figure 5. Microscopic observations confirmed the absence of precipitates at S/O < 0.43. The onset of asphaltene precipitation was estimated to occur around S/O = 0.43 based on these methods.

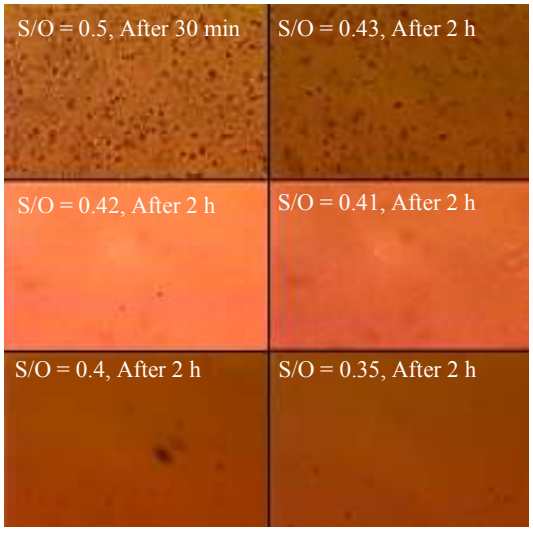

Figure 4-4 Microscopic images of diluted oil solution at various S/O

4.3.3 Settling behavior of silica particles in model oil

The rate of settling of flocculated asphaltenes was determined for a range of silica concentrations at S/O of 0.6. The data in Figure 4-5 show the changing height of the interface between clear supernatant and flocculated asphaltenes and silica as a function of time.

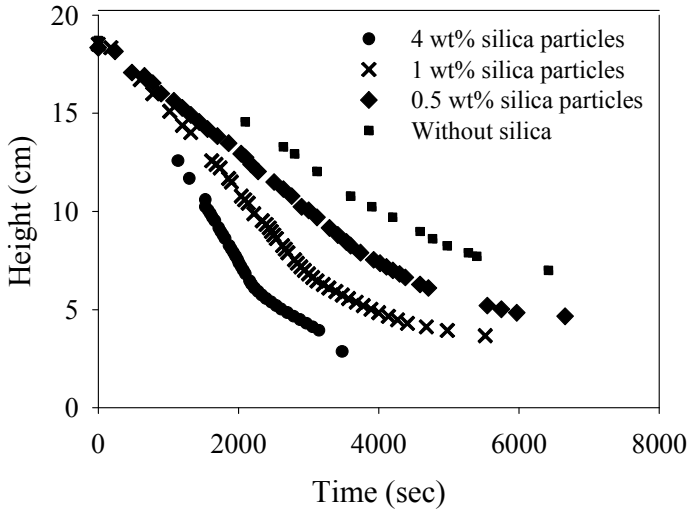

Figure 4-5 Settling rates for various concentrations of silica particles in the oil solution at S/O = 0.6

The initial settling rate increased from 0.0027 to 0.0043 cm/s when the silica content increased from 0 to 4 wt%. Departure from linearity indicates ongoing slow flocculation of asphaltene aggregates and silica particles. These data show that introducing the silica particles in the system increased the settling rate of the flocs by a factor of almost 1.6. At a concentration of silica particles of 0.5 wt% in the oil phase, the settling rate of the flocculated silica particles was very similar to the settling rate of the asphaltene flocs without silica. Therefore, one can conclude that at higher concentrations of silica, the flocculation of the the particles with the

asphaltenes gave denser asphaltene-silica flocs with less porosity that settled more rapidly. Based on the data in Figure 4-5, we selected 4 wt% silica at a settling time of 65 min (3900 s) as the standard set of conditions for more detailed study.

4.3.4 Settling behavior of silica particles at various S/O

The sedimentation experiments (Figure 4-5) suggested that flocculation of the silica particles with asphaltenes followed by 65 min of settling would give a solid free supernatant. The data in Figure 4-6 show the wt% of silica particles (based on ash content) at different height for 4 wt% hydrophilic silica suspended in model oil for various S/O.

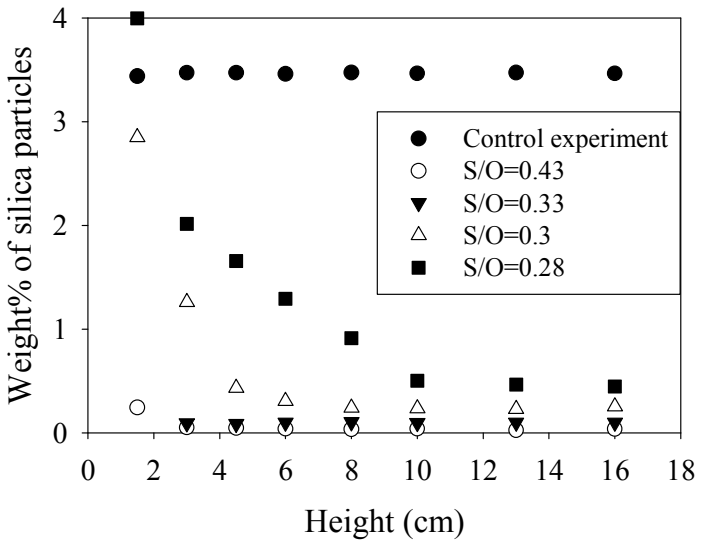

Figure 4-6 Concentration of hydrophilic silica particles at different heights in the suspension after 65 min (4 wt% silica in model oil)

Without addition of pentane, the samples from different heights in the column showed constant ash content (3.5±0.1 wt%), indicating a stable suspension after 65 min. These data show that 11.7±0.8 wt% of the silica particles were lost during the steps of mixing and preparing the suspension, mainly due to adhesion to the walls of the containers.

When solvent was added beyond the flocculation point of the asphaltenes, rapid settling occurred, as illustrated in Figure 4-5, and over 98% of the silica was precipitated, based on ash determinations. Experiments at lower S/O showed very surprising results. Figure 4-7 shows the removal efficiency of silica particles at height = 3 cm from the bottom of the cylinder. Removal efficiency was defined as the amount of remained particles at each height divided by the initial wt% of silica particles at the same height. The results showed that silica particles were removed from the suspension with high efficiency even before the onset of asphaltene precipitation at S/O = 0.43. At ratios of $0.33 < S/O < 0.43$, the addition of n-pentane to the oil suspension efficiently removed the silica particles in 65 min. At S/O = 0.4, for instance, the amount of ash was 0.050±0.005 wt% at the top of the column. Assuming that this ash was mostly silica, we can say that 98.1±0.3% of the silica particles were removed from the clear liquid above the sediment layer. Even at S/O = 0.33, 97.5±0.2% of the silica particles were precipitated and the supernatant was almost clean. In this case the ash content at each height was measured to be around 0.09±0.01 wt%. However, the silica content started increasing with decreasing height at S/O = 0.3 and did not follow the same trend. Therefore, S/O below 0.33 was considered to be the range in

which addition of n-pentane does not clean the model oil, although the solvent does destabilize the suspension.

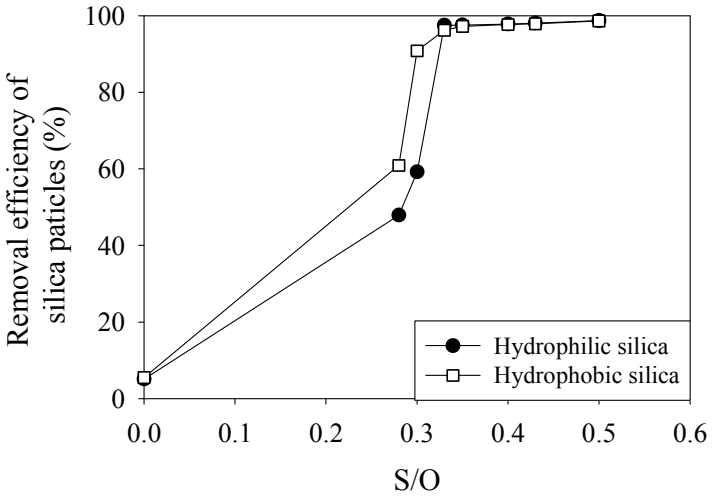

Figure 4-7 Removal efficiency of silica particles at h = 3 cm for various S/O

Results for hydrophobic silica particles are shown in Figure 4-8. These results are similar to those for the experiments with hydrophilic silica, and show that the lowest ratio at which the rapid settling of silica particles occurs is around S/O = 0.3. Comparison of the results for hydrophobic (silanized) and hydrophilic silica particles suggests that both types of particles were equally modified by adsorption of asphaltene molecules at the particle surfaces or attachment of asphaltene agglomerates to the surfaces. The settling rates of hydrophilic and hydrophobic silica particles were also similar. For both types of silica, the suspension was destabilized by the addition of small amounts of solvent, prior to the onset of visible flocculation of asphaltenes.

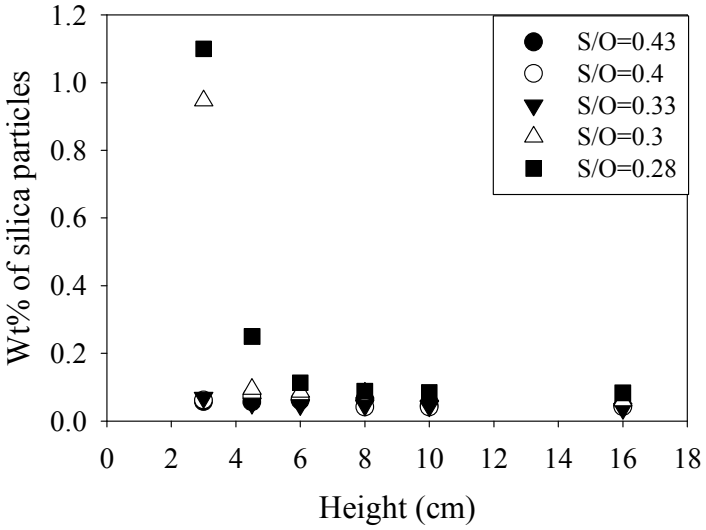

Figure 4-8 Concentration of hydrophobic silica particles at different heights in the suspension after 65 min (4 wt% silica in model oil)

Some authors have mentioned that the low-molecular-weight fraction of the asphaltenes is dissolved in solvents, and its high-molecular-weight fraction is in the form of colloidal suspension in paraffinic oils and in aggregated form in aromatic oils [19]. Even before the first appearance of asphaltene flocs in the oil, a portion of the pitch would be present in the form of asphaltene aggregates. Interaction of small amounts of this asphaltene material with the silica surface could dramatically improve sedimentation by providing bridging between the silica particles. As S/O increases from 0 to 0.33, one would expect more aggregation of asphaltene molecules at size scales below the limit of observation by the light microscope. By the same logic, the structure of adsorbed asphaltene on the silica surface would likely change. At about S/O = 0.33, attractive interactions between the silica particles led to rapid sedimentation of these

particles. Further study is required to understand the mechanism of this process more fully.

The efficiency of adsorbed asphaltene or adsorbed aggregates in promoting flocculation was dependent on the particle concentration. When the concentration of silica was 0.5 wt%, S/O > 0.5 was required to achieve clean supernatant in 65 min. For 1 wt% silica particles in the oil phase, S/O > 0.43 gave more than 90% removal of silica particles from the supernatant in the same time. Clearly, the efficiency of this mechanism for cleaning oils in a given time interval will depend on the size and density of the flocculated material in suspension, as well as the properties of the fluid phase such as viscosity and density.

This phenomenon is also general for asphaltene from different sources that would be used. In PFT (Paraffinic Froth Treatment), destabilizing the oil streams with paraffinic solvents has been established and removal of solid particles were successful [7, 8]. Our work showed that even below the onset of asphaltene precipitation, the removal of solid particles can be achieved with minor amount of precipitates.

4.3.5 Effect of asphaltene coating on contact angle of silica particles

In order to test the hypothesis that the asphaltenes from the pitch would modify the surfaces of both hydrophobic and hydrophilic silica particles, we measured the contact angles of particles treated with pitch. Both hydrophilic and hydrophobic silica particles were exposed to the model oil solution for 2 hours. The particles were then separated from the oil phase and washed with toluene to

remove all the residues that had not adsorbed on the surfaces of the silica particles. The washing was repeated until the supernatant was colorless. The particles were then oven-dried at 100ºC and stored in a dessicator. The contact angles of these particles are given in Table 4-2.

Table 4-2 Effect of asphaltene adsorption on contact angle of silica particles

Type of particles	**Contact angle**	**Contact angle after adsorption of asphaltenes**
Hydrophilic silica	$20^o \pm 10^o$	$115^o \pm 5^o$
Hydrophobic silica	$>90^o$	$123^o \pm 6^o$

From the data in Table 4-2, it is obvious that the contact angle of the silica particles after contact with the model oil was the same, regardless of the initial contact angle. Both types of particles became strongly hydrophobic. These results are consistent with Figure 4-6 and Figure 4-8, which show no difference between the settling behaviors of the two types of particles. The color of the particles also changed from white to light brown, which indicated some adsorption of asphaltene on the surfaces of the silica particles. Hannisdal *et al*.[18] also tested the change in contact angle of different particles, both hydrophilic and hydrophobic, in samples of pure asphaltene, resin and a mixture of asphaltene and resin. The results of their work also showed an increase in contact angle from around 16º for hydrophilic silica particles to 90º due to treatment with asphaltene solution. In the case of hydrophobic particles in asphaltene solution, the contact angle changed from 110º to 115º. Yan *et al*. made similar observations when performing contact angle measurements on clays. The contact angle increased

significantly with an increase in the asphaltene concentration. At lower asphaltene concentrations, the contact angles of the treated clays were smaller than 90º and the clays were hydrophilic. At higher asphaltene concentrations, however, the contact angles were greater than 90º and the clays became hydrophobic [20].

4.3.6 Destabilization of clay particles with paraffinic solvent

To generalize the usage of paraffinic treatment for removal of any types of solid, clay particles with average sizes around 1μm were used to represent the solid particles in the oil solution instead of silica particles. Similar procedure for preparing the silica particles suspension in oil solution was used for the clay particles to obtain the validity of paraffinic approach for removal of clays.

The microscopic images for clay and silica particles are shown in Figure 4-9. Comparing the images show some differences between the structures of these solid particles (Figure 4-9). Silica particles have a spherical shape, whereas the clay particles have plate-like structures.

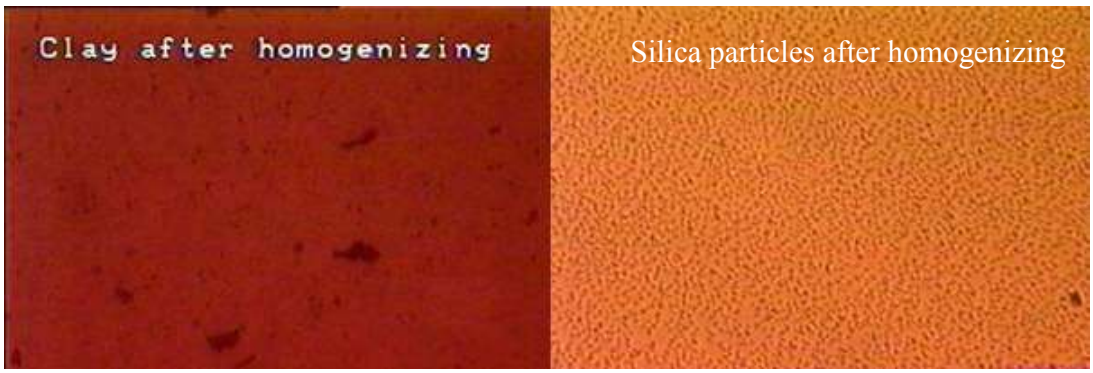

Figure 4-9 Microscopic image of 4 wt% clay and silica particles after homogenizing in the oil solution

The surface chemistry of the silica (Figure 4-10) and clays (Figure 4-11) are also different. Therefore, their behavior in oil solution is expected to be different as well.

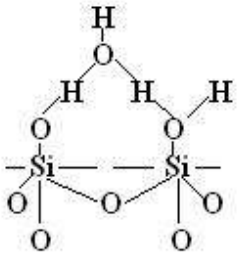

Figure 4-10 Silica surface chemistry

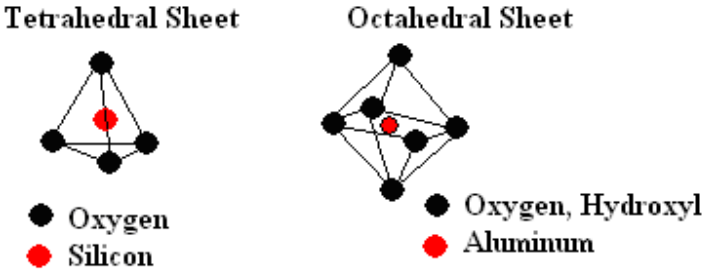

Figure 4-11 Clay surface chemistry

Clay particles are composed of two dimensional arrays of silicon-oxygen tetrahedral and two dimensional arrays of aluminum- or magnesium-oxygen octahedral. Different clays are composed of different arrangement of these sheets in their unit layers. Based on the structure of their unit layers, clay minerals can be divided into different families. Three layered clays such as illite or smectite have unit layers composed of one octahedral sheet located between two tetrahedral sheets of silicon oxygen. Two layered clay particles, such as kaolinite clays have one tetrahedral silicon-oxide sheet attached to a aluminum oxide or

hydroxide octahedral. The position of the metal oxides in the tetrahedral and octahedral sheets gives a hexagonal symmetry to the plate like structure of clay particles [21].

The results for the ash content of the clay particles are shown in Figure 4-12. The results show that for S/O = 0.36 and above that the addition of n-pentane would clean the oil solution from clay particles. However, these results show that the settling behavior of clay particles is different than silica particles which can be due to their different structures.

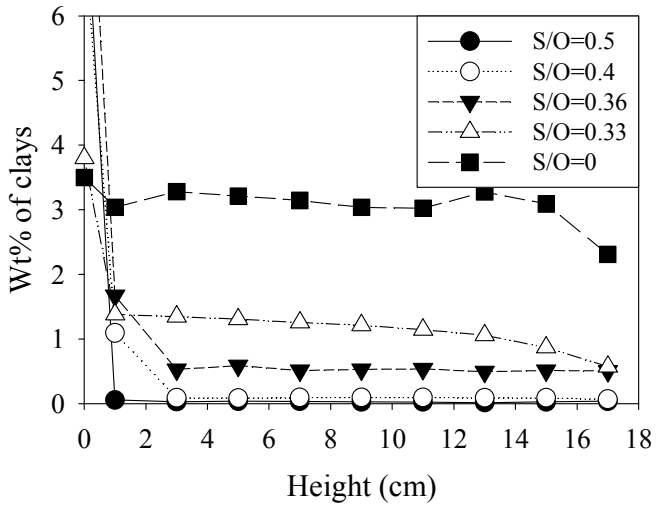

Figure 4-12 Ash content of 4 wt% clays after 65 minutes

Our hypothesis was based on the fact that destabilizing and sedimentation of the silica particles is due to the addition of paraffinic solvent and formation of asphaltene aggregates. To make sure that the sedimentation of the particles is not due to the density and viscosity changes in the solution, the solution was diluted with toluene and cyclopentane. The results are shown in Figure 4-13. It is obvious that toluene and cyclopentane with S/O=0.5 (highest S/O) was not able to

destabilize the system and the concentration of silica particles at different heights remain constant as their original concentration in the model oil.

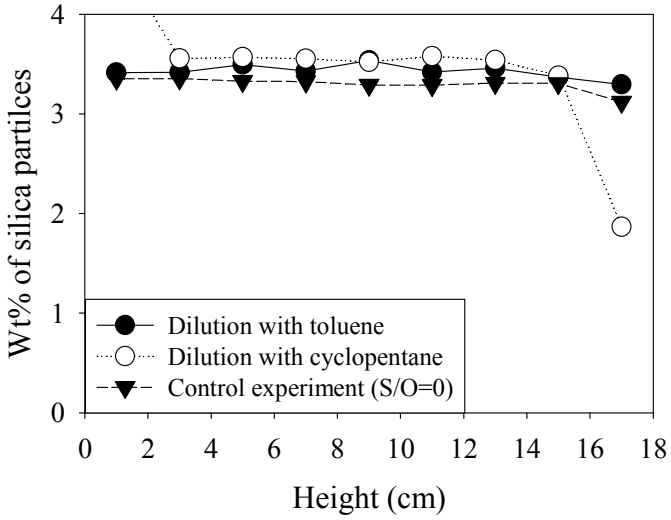

Figure 4-13 Effect of dilution with different solvent on the settling of the silica particles

4.3.7 Porosity and size of asphaltene flocs

The hindered settling rate of the flocculated asphaltenes (before the flocs reach the point of compaction) can be modeled using Kynch's theory (1952) [22] of kinematic sedimentation. The formula for the hindered settling rate, U, can be derived from the Richardson-Zaki approximation [23]:

$$U=u_0(1-\varphi)^n \tag{4-1}$$

where φ is the volume fraction of the flocs, n is a coefficient that can vary from 4 to 22, u_0 is the free settling rate of the flocs. For a solid sphere with low Reynolds number, u_0 can be found from Stokes law:

$$u_0 = \frac{d^2 g (\rho_E - \rho_m)}{18 \eta} \tag{4-2}$$

where g is the gravitational constant, ρ_E is the effective density of the flocs, ρ_m is the density of the medium, d is the diameter of the flocs, and η is the viscosity of the continuous medium. For a floc with porosity ε

$$(\rho_E - \rho_m) = (1-\varepsilon)(\rho_p - \rho_m) \tag{4-3}$$

where ρ_p is the density of the primary particles. Substituting equation (4-3) into equation (4-2) and equation (4-1), one obtains the hindered settling rate of impermeable flocs, U, as

$$U = \frac{g(1-\varepsilon)(\rho_p - \rho_m)d^2}{18\eta}(1-\phi)^n \tag{4-4}$$

If the volume fraction of the primary asphaltene particles in the system is φ_P and the volume fraction occupied by the asphaltene flocs in suspension is φ, the average porosity of the flocs can be calculated as

$$\varepsilon = 1 - \frac{\varphi_p}{\varphi} \tag{4-5}$$

In order to estimate the porosity of the flocs, the settling curves without silica for S/O = 0.6 (Figure 4-5) and S/O = 2 (data are not shown) were obtained. Sample volumes used for estimating the porosity of the aggregates containing the oil phase and n-pentane were 100 mL for both S/O = 0.6 and S/O = 2. The settling rates were calculated as the slopes of the initial part of the settling curves by fitting linear equation to the experimental data before the compaction zone of the sediments was formed. The density of asphaltene aggregates (or primary particles in the flocs) was assumed to be 1200 kg/m^3. The volume fraction of the primary

particles in suspension, φ_p, was calculated from the initial mass of the precipitated asphaltene in the model oil. In order to estimate the volume fraction, φ, the oil solution was diluted with a known amount of n-pentane (0.6 and 2) and left overnight. The volume of the sediment was then measured to give the compacted volume of the flocculated asphaltenes and φ. The porosity of the flocs was then calculated using equation (4-5) (Table 4-3).

The diameter of the flocs was estimated from both the microscopic observations and equation (4-4). According to Long *et al*., for a mixture of n-pentane and n-hexane, constant *n* was estimated to be around 4.27 [23]. The solvent in the present work was n-pentane so we decided to use the same value for *n*. Microscopy showed that the size of the flocs increased with the amount of solvent, from 5 to 30 μm for S/O = 0.6 to over 60 μm for S/O = 2. The diameters of the aggregates calculated from equation (4-4) were in good agreement with the microscopic observation.

The porosity, as estimated from the experimental data, was high and indicates a fluffy structure for the asphaltene flocs. The results in Table 4-3 give much higher porosity of flocs ($\varepsilon = 0.98$) than Long *et al*. [23] who estimated $\varepsilon = 0.404$. A crucial difference was in the concentrations of asphaltenes in the two studies, 5 wt% pitch in toluene (3 wt% asphaltene) in the present work compared to 15 wt% asphaltene in diluted bitumen for Long *et al.* [23]. This difference likely resulted in flocs with higher porosity in the present study, giving a much lower settling rate. The settling rate of the flocs in the referenced study was 0.036 cm/s at 30ºC using pentane plus hexane as the solvent at S/O = 2, compared to 0.0048 cm/s in

the present study, which is one order of magnitude lower. An additional factor was the sources for the asphaltene, which were different for the two studies. Our estimates of low floc density were consistent with Rahmani *et al*. [7] who used 0.12 wt% asphaltenes in toluene and estimated a porosity of over 0.9 for the flocs upon precipitation. On the basis of Rahmani *et al*. [7] and our work, we expect that a low concentration of asphaltenes in the oil would give less compact asphaltene aggregates. The size of the silica-asphaltene flocs was observed with microscopy and they are almost the same size of asphaltene aggregates (5-30 μm). As the size of the flocs has not changed, it shows that the flocs have become more porous in the existence of solid particles.

Table 4-3 Estimated properties of asphaltene flocs without silica particles

Solvent/Oil phase (weight ratio)	0.6	2
Initial settling velocity of the aggregates u_{ip}, (cm/s)	0.003	0.0048
Volume fraction of the primary particles in suspension, φ_p	0.003	0.004
Volume fraction of aggregates in suspension, φ	0.05	0.25
Average porosity of the aggregates, ε	0.95	0.98
Density of the medium, ρ_m, kg/m^3	763	629
Viscosity of the medium, μ, mPa·s	0.48	0.35
Diameter of the aggregates (μm) (4-4)	33	59
Diameter of the aggregates from microscopic images, d (μm)	5–30	Larger than 60

4.4 Summary

A model oil consisting of approximately 1 μm silica particles suspended in a reacted pitch material dissolved in toluene was studied to examine the role of

asphaltene precipitation in enhancing particle removal by asphaltene-silica flocculation and sedimentation. For a concentration of 5 wt% pitch material in toluene, the onset of asphaltene precipitation was determined to occur at S/O = 0.43 by weight.

The concentration of silica particles in the original sample was 4 wt%. This concentration decreased to 0.035 ± 0.01 wt% ash at different heights in the supernatant for S/O = 0.43. This reduction indicates more than 98% removal of the silica particles with the assumption that the ash was mostly silica particles. Even with S/O lower than 0.43, the removal efficiency was high. For instance, for S/O = 0.33 the ash contents of samples at different heights were 0.09 ± 0.01 wt%, which indicates more than 97.5 ± 0.2% removal of silica particles. At ratios lower than 0.33, the silica content in the suspension did not decrease rapidly and removal was not successful. The results for hydrophobic silica particles were similar to those for hydrophilic ones.

Model oil solution with clays (kaolinite) was also prepared to determine the validity of solvent treatment for destabilizing other types of solids. At S/O > 0.36 the concentration of clay particles in the model oil solution decreased to less than 0.06 wt% which shows 98.5% removal of the clay particles.

The most important finding from this study is that efficient flocculation of fine solids can be achieved by means of a very small amount of asphaltene precipitation.

4.5 References

[1] Gu, G., Zhang, L., Xu, Z., 2007, "Novel Bitumen Froth Cleaning Device and Rag Layer Characterization," Energy and Fuels, 21(6) pp. 3462-3468.

[2] Xu, Y., Dabros, T., and Hamza, H., 2007, "Study on the Mechanism of Foaming from Bitumen Froth Treatment Tailings," Journal of Dispersion Science and Technology, 28(3) pp. 413-418.

[3] Romanova, U. G., Yarranton, H. W., Schramm, L. L., 2004, "Investigation of Oil Sands Froth Treatment," Canadian Journal of Chemical Engineering, 82(4) pp. 710-721.

[4] Rahmani, N. H. G., Dabros, T., and Masliyah, J. H., 2005, "Settling Properties of Asphaltene Aggregates," Energy and Fuels, 19(3) pp. 1099-1108.

[5] Rahmani, N. H. G., Dabros, T., and Masliyah, J. H., 2005, "Fractal Structure of Asphaltene Aggregates," Journal of Colloid and Interface Science, 285(2) pp. 599-608.

[6] Rahmani, N. H. G., Dabros, T., and Masliyah, J. H., 2005, "Online Optical Monitoring of Asphaltene Aggregation," Industrial and Engineering Chemistry Research, 44(1) pp. 75-84.

[7] Rahmani, N. H. G., Dabros, T., and Masliyah, J. H., 2004, "Evolution of Asphaltene Floc Size Distribution in Organic Solvents Under Shear," Chemical Engineering Science, 59(3) pp. 685-697.

[8] Long, Y., Dabros, T., and Hamza, H., 2002, "Stability and Settling Characteristics of Solvent-Diluted Bitumen Emulsions," Fuel, 81(15) pp. 1945-1952.

[9] Long, Y., Dabros, T., and Hamza, H., 2004, "Analysis of Solvent-Diluted Bitumen from Oil Sands Froth Treatment using NIR Spectroscopy," Canadian Journal of Chemical Engineering, 82(4) pp. 776-781.

[10] Long, Y., Dabros, T., and Hamza, H., 2004, "Structure of water/solids/asphaltenes Aggregates and Effect of Mixing Temperature on Settling Rate in Solvent-Diluted Bitumen," Fuel, 83(7) pp. 823-832.

[11] Nellensteyn, F. J., 1924, "The Constitution of Asphalt," Institution of Petroleum Technologists -- Journal, 10(43) pp. 311-325.

[12] Gonzalez, G., Neves, G. B. M., Saraiva, S. M., 2003, "Electrokinetic Characterization of Asphaltenes and the Asphaltenes-Resins Interaction," Energy and Fuels, 17(4) pp. 879-886.

[13] Pereira, J. C., Lopez, I., Salas, R., 2007, "Resins: The molecules responsible for the stability/instability phenomena of asphaltenes," Energy & Fuels, Anonymous 21, pp. 1317-1321.

[14] Andreatta, G., Bostrom, N., and Mullins, O. C., 2005, "High-Q Ultrasonic Determination of the Critical Nanoaggregate Concentration of Asphaltenes and the Critical Micelle Concentration of Standard Surfactants," Langmuir, 21(7) pp. 2728-2736.

[15] Pfeiffer, J. P., and Saal, R. N. J., 1940, "Asphaltic Bitumen as Colloid System," Journal of Physical Chemistry, 44pp. 139-149.

[16] Buenrostro-Gonzalez, E., Groenzin, H., Lira-Galeana, C., 2001, "The Overriding Chemical Principles that Define Asphaltenes," Energy and Fuels, 15(4) pp. 972-978.

[17] Abraham, T., Christendat, D., Karan, K., 2002, "Asphaltene - Silica Interactions in Aqueous Solutions: Direct Force Measurements Combined with Electrokinetic Studies," Industrial and Engineering Chemistry Research, 41(9) pp. 2170-2177.

[18] Hannisdal, A., Ese, M., Hemmingsen, P. V., 2006, "Particle-Stabilized Emulsions: Effect of Heavy Crude Oil Components Pre-Adsorbed Onto Stabilizing Solids," Colloids and Surfaces A: Physicochemical and Engineering Aspects, 276(1-3) pp. 45-58.

[19] Solaimany-Nazar, A. R., and Rahimi, H., 2009, "Investigation on Agglomeration-Fragmentation Processes in Colloidal Asphaltene Suspensions," Energy & Fuels, 23(1) pp. 967-974.

[20] Yan, N., and Masliyah, J. H., 1996, "Effect of pH on Adsorption and Desorption of Clay Particles at Oil-Water Interface," Journal of Colloid and Interface Science, 181(1) pp. 20.

[21] Van Olphen, H., 1963, An introduction to clay colloid chemistry, Interscience Publishers, John Wiley and Sons, New York

[22] Kynch, G. J., 1952, "A Theory of Sedimentation," Transactions of the Faraday Society, 48(2) pp. 166-176.

[23] Long, Y., Dabros, T., and Hamza, H., 2004, "Structure of water/solids/asphaltenes Aggregates and Effect of Mixing Temperature on Settling Rate in Solvent-Diluted Bitumen," Fuel, 83(7) pp. 823-832.

5 Removal of solid particles from a model oil solution by aqueous treatment

5.1 Introduction

Finding a method for efficient removal of solid particles suspension from oil streams is the main objective of this work. In chapter 4, removal of silica particles with paraffinic treatment was a successful challenge. The interesting finding of the previous chapter was a possibility of destabilizing the silica particles suspension even below the onset of asphaltene precipitation.

This chapter had two primary focuses: first, we studied the effect of small amounts of added water on accelerating the sedimentation of silica particles from the model oil solution. Our purpose was using water as an agglomeration agent for the silica particles. It was then expected that the emulsified water in the model oil solution agglomerate the silica particles in the model oil solution and the silica-water clusters would sediment. Second, we examined the combined effects of water and the addition of a paraffinic solvent for removal of fine solids. The model oil solution was modified to create stable emulsions of water in oil. Similar

to paraffinic treatment (Chapter 4), these oil emulsions were treated with pentane. It was expected that the addition of pentane would precipitate a portion of asphaltene. The precipitated asphaltene would act as a bridge and heteroflocculation of the silica particles, emulsified water and precipitated asphaltene would occur. The results for the paraffinic treatment of the oil emulsion can then be compared to the model oil solution (Chapter 4).

Here, we give a brief review of the existing literature on the aqueous and paraffinic treatment for the removal of solids in oil emulsions.

5.2 Aqueous treatment of the oil solution for removal of solid particles

Aqueous treatment in our work is divided into two sections:

1) Adding water in small amounts to the model oil solution to agglomerate the silica particles.

2) Adding pentane to the model oil emulsion to have heteroflocculation of silica particles and emulsified water. By model oil emulsion, we mean modifying the model oil solution with water and prepare a stable model oil emulsion. The procedure for preparing the oil emulsion would be explained in details later.

The literature in each part is described below.

5.2.1 Addition of water as a cleaning phase

One mechanism for removing solids and impurities from an oil phase is the addition of an aqueous phase and the transfer of the solids from the oil phase to the aqueous phase. The effectiveness of this treatment will obviously depend on the energy barrier to transfer the solids across the oil-water interface. One of the main parameters that affect the transferring of the solid particles from the oil phase to the aqueous phase is the contact angle of the particles in the oil phase. In addition, other parameters such as mixing, pH of the aqueous phase, surfactant concentration, etc. effect the recovery of the particles.

Henry *et al.* (1984) studied the transfer of solid particles from an organic to water phase. A system containing xylene (oil phase), deionized distilled water (pH adjusted to water) and soda-lime glass microbeads in the size range of 5 - 20 μm (solid particles) was used as the model system. The purpose was to study the effect of emulsified water on transferring the solid particles from the oil phase to the aqueous phase. The model oil was 0.2 g solid particles in 100 ml of xylene. The particles were dispersed in the organic phase by using an ultrasonic bath. 50 ml of water phase was added to the oil phase while the solution was being mixed by using a turbine impeller with a 4 flat pitched blades. After the three phase mixing was completed, for breaking the emulsion, either a separatory funnel or an electrically induced coalescence was used. The mixture was separated into three phases; the organic, the interface and the aqueous phase. Each phase was filtered by using a 0.45 μm filter to determine the distribution of solid particles in each

phase. The filtration of each phase showed that most of the particles were transferred to the aqueous phase [1, 2].

The effects of five parameters on transferring the solid particles from the organic to the aqueous phase were studied: mixing time, mixing rate, surfactant concentration, contact angle, and pH [1, 2].

The results of Henry's work showed that increasing the mixing time increased the recovery until it reached a steady state. Recovery was defined as the number of the particles that transfer to the water phase divided by the total number of the particles. The steady state recovery was higher when the mixing speed was increased [1, 3].

When the suspended particles in the organic phase are hydrophilic, attachment of the particles to the emulsified water in the mixture is favorable. The water droplets should then coalesce and separate from the oil phase to remove the solid minerals. However, when the particles are hydrophobic, for instance the particles are coated with a layer of adsorbed asphaltene, the removal efficiency of the particles is low. In these cases, one can use a surfactant to change the hydrophobic surface characteristic of the particles to hydrophilic and make it possible for the particles to attach to water droplets [4]. Henry *et al.* used a nonionic ethoxylate as the surfactant to improve the attachment of hydrophobic particles to the emulsified water. Recovery is higher for hydrophilic particles in comparison to the hydrophobic ones. The addition of surfactant renders the hydrophobic particles, hydrophilic leading to a higher recovery of the particles [4]. Increasing

the pH of the aqueous phase and the surfactant concentration in the mixture also increased the recovery [1, 4].

When the particles are attached to the dispersed water, the next step is breaking the emulsion and separating the oil and water phase.

5.2.1.1 Emulsion breakdown mechanisms

5.2.1.1.1 Sedimentation/Creaming

When one phase is dispersed in another phase the density of the two phases are different. In W/O emulsions, the water droplets will settle down because of gravitational forces, and this process is called sedimentation. In the creaming process, in O/W emulsions, the oil droplets rise or float due to the difference in densities between the oil and water. Creaming and sedimentation bring the dispersed phase together (Figure 5-1) [5].

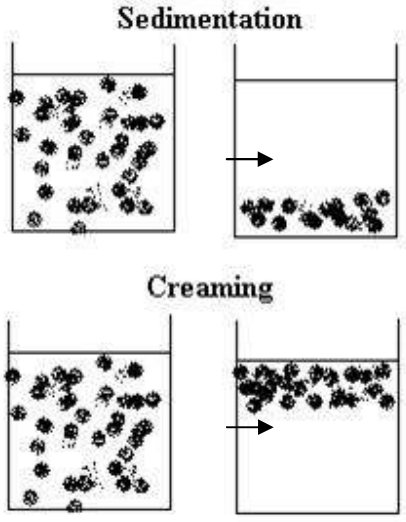

Figure 5-1 Sedimentation and Creaming

5.2.1.1.2 Coalescence

In coalescence, two single droplets merge and form a single new larger drop. As they approach, their surfaces deform and become planar between the two droplets. During coalescence the liquid film between the droplets would rupture and allow the droplets to approach closer (Figure 5-2).

When two particles coalesce, the total surface area is reduced due to the formation of a large particle. In order to unite the emulsified water in W/O emulsions, the stabilizing material on the interface, such as asphaltenes, solids and resins should be removed to make coalescence more favorable [6].

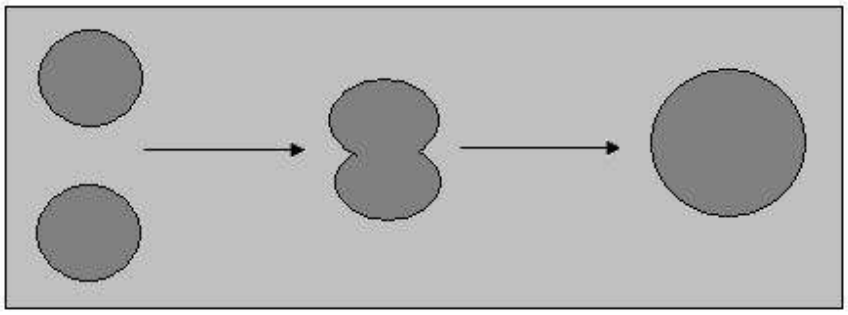

Figure 5-2 Coalescence

5.2.2 Paraffinic treatment of the model emulsion

In Shell-Albian froth treatment, by treating the bitumen phase with heptane, part of the asphaltene would precipitate. The precipitated asphaltene flocculate the solid particles and water droplets and form water/solids/asphaltenes aggregates that are larger than the original emulsified water droplets and dispersed solids and settle fast [7, 8].

In this process the amount of solids and water can reduce to less than 0.2 wt%. By using an aliphatic solvent such as hexane or pentane not only the emulsified water and micrometer size particles are removed but also some of the asphaltenic components of the bitumen that affects the upgrading strategies are separated [8, 9].

5.2.2.1 Heteroflocculation using asphaltene

Heteroflocculation describes the flocculation of colloidal dispersions consisting of more than one type of particle. Heteroflocculation is a complex phenomenon which accounts for various particle parameters such as particle size, surface potential, shape of the particle, surface charge density, etc. [10].

Uricanu (2001) claimed that there are two main cases in behavior of mixed colloids:

1. Selective flocculation or heteroflocculation between two sets of particles of comparable sizes and concentrations.
2. Bridging flocculation which is adsorption of smaller particles onto larger ones or flocculation of two sets of colloidal particles that differ greatly in size [11].

Long *et al.* (2002) studied the structure of aggregates formed of precipitated asphaltene (PA), dispersed solid (DS) and water droplets (WD) in bitumen froth. The effect of different solvents (C5/C6 and C7) and temperatures on aggregates settling rate was studied as well. It was found that aggregates of precipitated

asphaltene, dispersed solid and water droplets would form while treating with aliphatic solvents.

The size of the aggregates was measured using the settling rate. Increasing the mixing temperature increased the size of the aggregates. In addition, the aggregates formed by adding the C5/C6 solvent had larger diameters. By treating the diluted bitumen containing fine particles (9 wt%) and water (31 wt%) with n-hexane the water and ash contents in the clean oil zone were both less than 0.1 wt% for hexane-bitumen solution after 60 min [12, 13].

5.2.2.2 Characteristics of water in oil emulsions

5.2.2.2.1 Classification

An emulsion is a mixture of two immiscible liquids such as water and oil in which one liquid is dispersed in the form of droplets in the other liquid (continuous phase). Classification of the emulsions depends on which phase is the dispersed phased. The common emulsions in the oil industry are introduced in Table 5-1:

Table 5-1 Different types of emulsions in the oil industry

Type of emulsion	Dispersed phase	Continuous phase
Water in oil (W/O)	Water	Oil
Oil in water (O/W)	Oil	Water
Multiple emulsion	Droplets are dispersed in other dispersed droplets	

Emulsions are found in daily life and some of them are useful and essential, such as pharmaceutical, lubricant, paints, cosmetics, etc. In the petroleum

industry, however, some emulsions are undesirable and need physical and/or chemical treatment to separate the emulsified phase (water) from the oil.

5.2.2.2.2 Emulsion Stability

Emulsions are thermodynamically unstable due to excess energy for creation of a larger surface area in the system. As a result, there is a tendency to reduce the contact area between the phases to minimize the total energy. However, the processes involved to reduce contact area can be very slow and the emulsion can be kinetically stable for hours, days, or even years.

5.3 Experimental methods

5.3.1 Model oil preparation

The stock oil solution was prepared by mixing 5 wt% pitch material in toluene. The sample was shaken by means of a horizental shaker for 2 hours and then centrifuged at 4600 rpm and kept afterwards. Two types of oil solution were prepared to study the effect of water on the flocculation of silica particles:

5.3.1.1 Addition of water to the oil suspension

4 wt% silica particles were added to the stock oil solution and the suspension was shaken via a horizental shaker for 2 hours. Then the de-ionized water was added to the oil suspension and the emulsion was homogenized by using a homogenizer for 8 min at 26,000 rpm. The amount of added water in the oil

solution was 2, 4 and 10 wt%. Then the samples were transferred to a graduated cylinder and left for the desired time between 1 to 5 hours to measure the water and solid contents at various heights. All the glassware was soaked in dichlorodimethylsilane overnight and washed with toluene afterwards to prevent the water droplets from sticking to the walls of the glassware. The experiments were repeated for both hydrophilic and hydrophobic silica particles.

5.3.1.2 Addition of n-pentane to the stable oil emulsion

The target of this set of experiments was to have stable water in oil emulsion. For this purpose, 4 wt% water was added to the oil solution and the emulsion was homogenized at 26,000 rpm for 8 min by using a homogenizer. Then the emulsions were left overnight. Part of the water phase settled. The oil emulsion from the top was separated carefully by means of a pipette after 16 hours. Then the silica particles were added to the emulsion, shaken for 2 hours and homogenized at 26,000 rpm. N-pentane was added at various ratios and the samples were shaken for 25 min via a table shaker. The samples were then transferred to a graduatet cylinder and left for 1 hour (similar to the time for settling rate in chapter 4). Water and solid contents were measured for each sample at various heights after 1 hour.

5.3.2 Settling experiment

The details for the settling experiment have been described in section 4.2.1.

5.3.3 Water analysis

The oil emulsions were transferred to a graduated cylinder after preparation and left for the desired time. Then samples from specific heights were taken with a deflected non-coring septum penetration needle and water content was determined by Karl Fischer titration (Mettler model DL 18). For each height two samples were taken and the reported amount is the average between the two numbers. When the measured amount of water was more than 5 wt%, the samples from each height were diluted using a stock solution of 70:30 (by volume) of dry toluene: isopropanol to get more accurate results. The water content of these diluted solution were then measured and the accurate numbers were reported considering the dilution factor.

5.3.4 Ash analysis

The ash contents were determined for individual samples using ASTM 5142 to measure the silica content at each height. The samples from each height were taken with a 5 ml glass pipette and transferred to the crucibles that were oven dried. The samples were then burned to remove all the residues except silica. We used a programmed oven overnight to burn the samples in air. The oven temperature was raised to 800°C over 4 hours, maintained at the target temperature for 2 hours and then cooled for 4 hours.

5.4 Results

5.4.1 Stability of the water droplets in the oil solution

In chapter 4, it was observed that the suspension of 1μm silica particles in the oil solution was stable and that the silica particles did not settle down. Therefore, samples of oil solution with water droplets and without silica particles were prepared to check the stability of the water droplets in the oil solution. These results are shown in Figure 5-3.

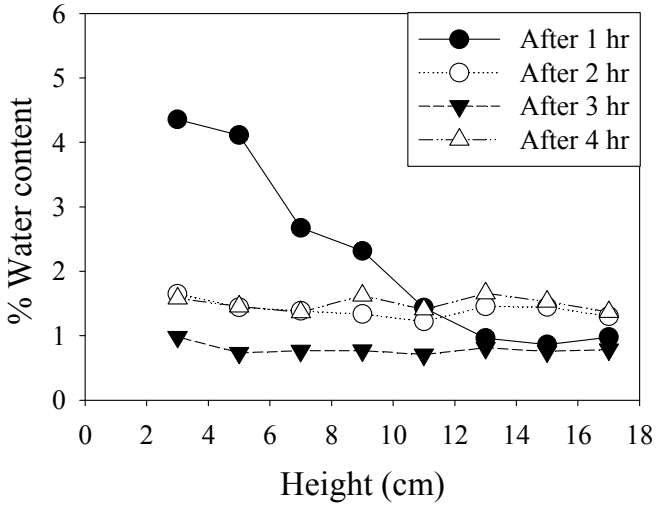

Figure 5-3 Profile of water content in oil solution with 4 wt% water and without silica particles

It is obvious from these results that the emulsion of water droplets was not stable and that they would start coalescence and settle in the oil solution. The water phase was recognized as a distinct phase at the bottom of the graduate cylinder. The experiment was repeated for different timing. Figure 5-3 shows that after 2 hours we would have less than 2 wt% water in the oil emulsion. Figure

5-4, is the microscopic image of the oil emulsion without silica particles after 1 hour. It can be seen in the image that the number of water droplets at the top (h = 17 cm) has decreased significantly.

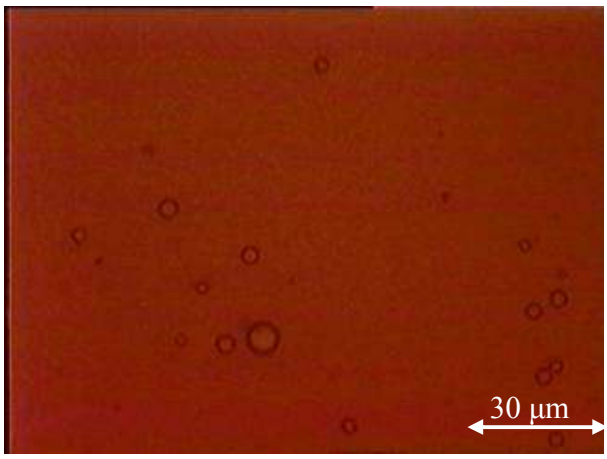

Figure 5-4 Water content in the oil solution after 1 hour at height = 17 cm

5.4.2 Aqueous treatment of the model oil solution

Various samples with 4 wt% water and 4 wt% silica particles were prepared and quickly transferred to a graduated cylinder. The samples were left for 1, 2, 3, and 4 hours and the water and ash content were measured at various heights. The experiments were repeated for both hydrophobic and hydrophilic silica particles. The results for the ash and water content at various heights of the solutions with hydrophobic and hydrophilic silica particles are presented in Figure 5-5 and Figure 5-6, respectively.

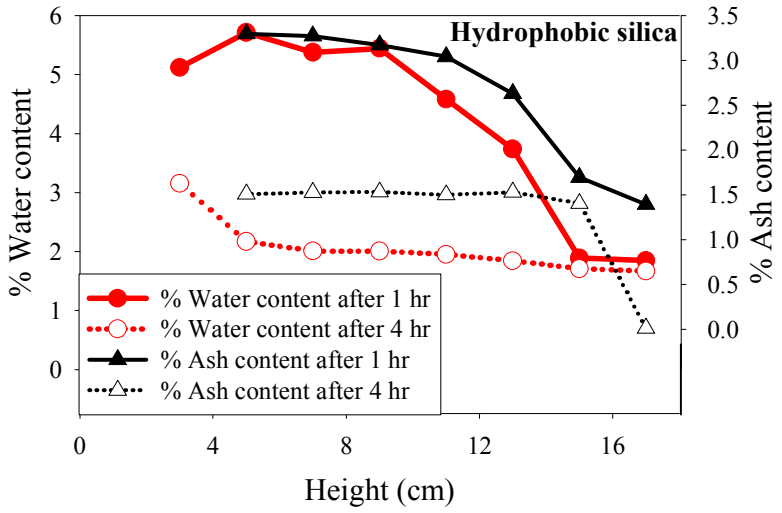

Figure 5-5 Water and ash content in the oil solution with 4 wt% water and 4 wt% hydrophobic silica particles at various heights. (Red symbols: water content; Black symbols: ash content at various timing)

The important issue in aqueous treatment of the oil solution is that the water content in the oil solutions should also decrease to meet the required industrial content. For instance, for pipeline transport, the maximum water content in the oil streams should be roughly 0.5 wt%. Otherwise, adding water can be considered as another problematic issue for industry.

The results in Figure 5-5 and Figure 5-6 for hydrophobic and hydrophilic silica particles, respectively, show that the ash and water content in the oil emulsions is still high after 1 hour. By leaving the oil emulsions for longer times, such as 4 hours, the water and ash content decreased to a lower amount (less than 3 wt% for hydrophobic silica and around 1 wt% for hydrophilic ones). However, the results in chapter 4 showed that paraffinic treatment of the oil emulsion led to low content of the silica particles in the supernatant only after 1 hour. Therefore,

it is obvious that efficiency of the paraffinic treatment of the oil solution for removal of solid particles is much higher than the aqueous treatment of the similar solutions.

It can be seen in Figure 5-5 and Figure 5-6 that the ash and water content for hydrophobic silica particles after 4 hours are higher than the hydrophilic ones. When the particles are hydrophilic, after 4 hours, water and ash content (around 1 wt%) have settled down and the supernatant is almost clean. In the hydrophobic case, however, even after 4 hours the ash and water content is still more than 1 wt% except in the very top layers.

This result could be due to the surface characteristics of the silica particles that do not interact with water droplets. Although the surface of the silica particles was modified by asphaltene adsorption, this adsorbed material did not completely control the interactions with the water droplets. Water droplets are hydrophilic; as a result they would normally tend to coalesce. The heteroflocculation of hydrophobic silica particles and water droplets is not favorable; therefore, hydrophobic silica would remain suspended in the oil solution. In the hydrophilic case, however, the water droplets tend to agglomerate these particles more; therefore, the settling of the particles and water droplets was higher in the oil solution of these particles in comparison to solutions with hydrophobic particles.

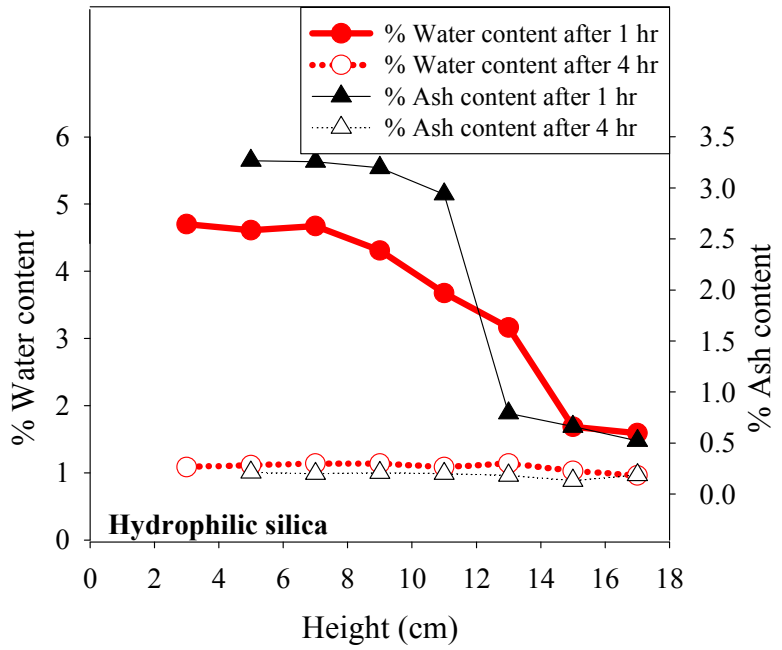

Figure 5-6 Water and ash content in the oil solution with 4 wt% water and 4 wt% hydrophilic silica particles at various heights. (Red symbols: water content; Black symbols: ash content)

5.4.3 Settling curve of silica particles - emulsified water - precipitated asphaltene at S/O = 0.6

The silica particles were initially shaken in the oil solution for 2 hours to enable adsorption of pitch components. The desired amount of water was then added to the oil solution and after homogenizing, it was sampled for examination under an optical microscope. Figure 5-7 shows the microscopic image for the oil emulsion. The large particles are water droplets and the dots are silica particles. The size of the water droplets is clearly less than 10 μm.

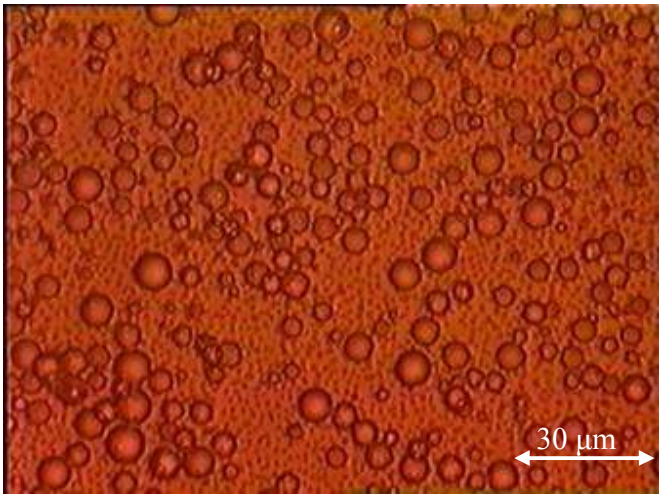

Figure 5-7 Microscopic image of water-in-oil emulsion with silica particles after homogenizing

The results for settling experiments of 5 wt% pitch and 4 wt% silica in toluene at S/O = 0.6 with different amounts of water and without water are shown in Figure 5-8. It was mentioned in chapter 4 that this ratio of pentane/oil solution was chosen due to visibility of the flocs (flocs are referred to aggrlomerate of water droplets, silica particles and asphaltene aggregates) at this ratio. The ratio of water contents were chosen to be 2, 4, and 10 wt%. These water contents were chosen to give water content less than, equal to and greater than the amount of silica in the oil solution. The results show that the addition of at least 2 wt% water would increase the settling rate of the flocs compared to the oil suspension without water. However, for 2 and 4 wt% oil emulsions, the settling rate did not show a significant difference. Therefore, we add 4 wt% water to the oil solutions for all the experiments.

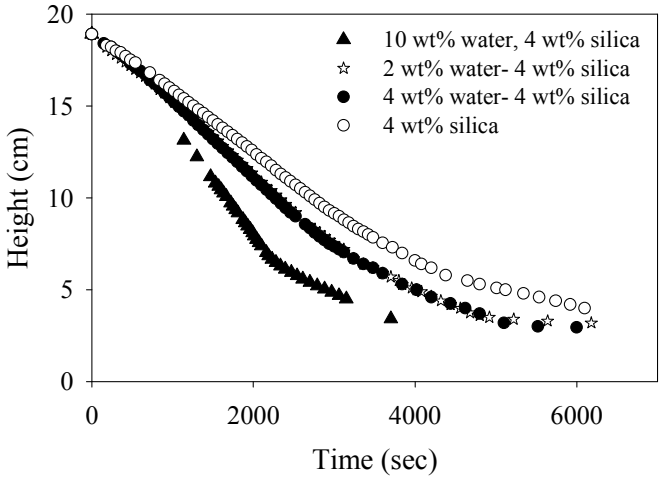

Figure 5-8 Change in the height of the interface versus time at S/O = 0.6 for various concentrations of water

5.4.4 Paraffinic treatment of the model oil solution in the presence of emulsified water

In the next set of experiments, by leaving the oil emulsion overnight, most of the water droplets settled down and no water droplets were observed by optical microscopy in samples taken from the supernatant. However, the water content of the oil emulsions that were left overnight (0.6 wt%) was higher than the water content of the original model oil solution (<0.05 wt%) which showed the presence of emulsified water in the oil emulsion. To determine if the suspension of silica particles in this new emulsion is stable, a control experiment (i.e. oil emulsion without pentane) was prepared to measure the stability of the suspended particles. The control experiments (S/O = 0) showed stable suspensions of silica particles in the model oil emulsion, which are shown in Figure 5-9 and Figure 5-10 for

hydrophilic and hydrophobic silica particles, respectively. The ash content at various heights was around 3.35 ± 0.8 wt% as compared to 4 wt% orginially. Part of the silica particles was lost during the preparation of the samples. The stability of these emulsified water-silica samples showed that low water contents in the solution did not destabilize the silica suspensions. The water content of the stable emulsion was between 0.4 - 0.6 wt%.

In the next series of experiments, n-pentane was used to determine the destabilization of silica suspensions in the oil emulsion. The results were then compared to the results previously obtained in the model oil without water in chapter 4. Two parameters are important while comparing the results for the aqueous and paraffinic treatment: the S/O for the destabilization of the silica suspension and the removal efficiency in each method. In these set of experiments, it can be seen in Figure 5-9 and Figure 5-10 that above S/O = 0.24 and S/O = 0.23 for hydrophilic and hydrophobic silica particles, respectively, addition of n-pentane would destabilize the silica suspensions in the oil emulsion. Therefore, fast sedimentation of the silica particles would occur and we had a clean supernatant after 1 hour for S/O > 0.24 in both cases.

The impact of water content at various heights of the oil emulsion are shown in Figure 5-11 and Figure 5-12 for hydrophilic and hydrophobic silica particles, respectively. It is obvious that the amount of water content is lower than 0.1 wt% for S/O > 0.24 in both cases. Considering the sedimentation of both water and ash at various heights in the oil emulsion shows that paraffinic treatment of the oil emulsion was successful for S/O > 0.24.

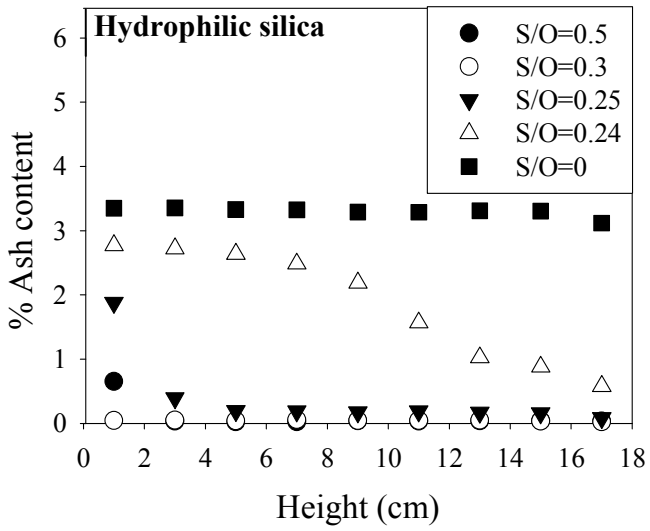

Figure 5-9 Ash content for various S/O in the oil emulsion after 65 min for solutions of 4 wt% hydrophilic silica particles

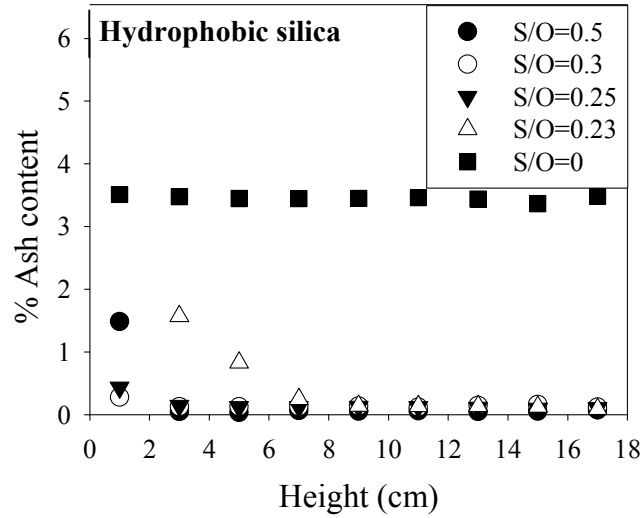

Figure 5-10 Ash content for various S/O in the oil emulsion with after 65 min for solutions of 4 wt% hydrophobic silica particles

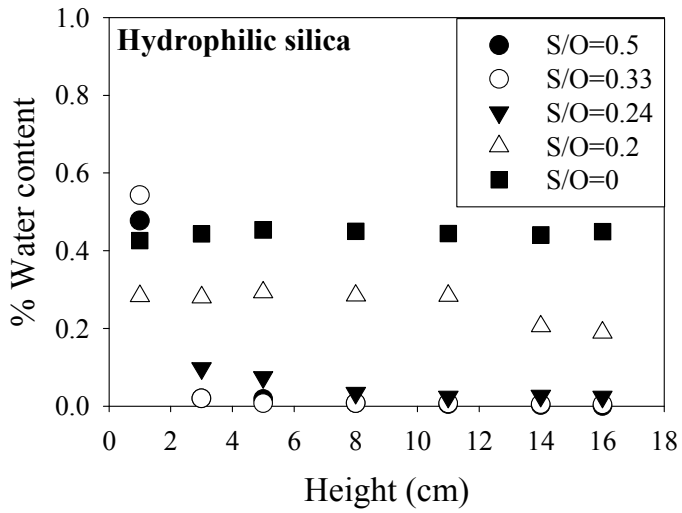

Figure 5-11 Water content in oil emulsion after 65 min in the oil solution with 4 wt% hydrophilic silica after 65 min

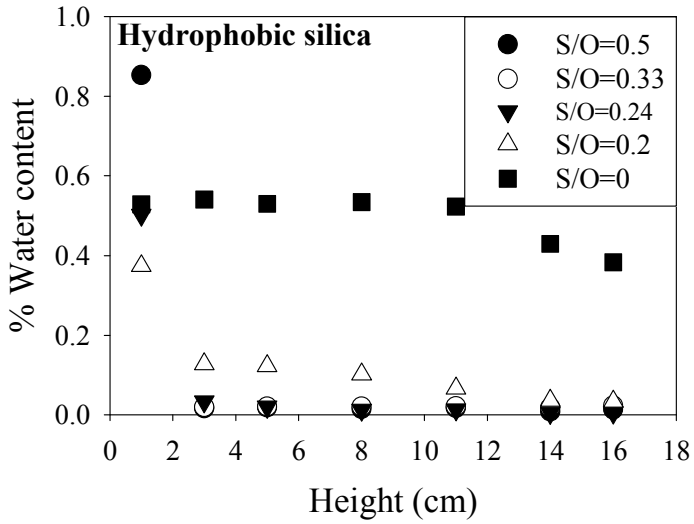

Figure 5-12 Water content in oil emulsion after 65 min in the oil solution with 4 wt% hydrophobic silica after 65 min

Removal efficiencies of silica particles in the oil solution without water (chapter 4) and in the presence of water (this chapter) are shown in Figure 5-13. It

can be seen in Figure 5-13 that in the presence of emulsified water, addition of n-pentane destabilize the particles suspended in the oil at lower S/O. Therefore, high removal efficiency of the silica particles happens at lower S/O in the presence of water, with a combination of heteroflocculation of the water, silica and asphaltenes. Therefore, we need less amount of a paraffinic solvent to clean the oil solution and less asphaltene would precipitate. The removal efficiency in both methods for S/O > 0.3 is more than 96%.

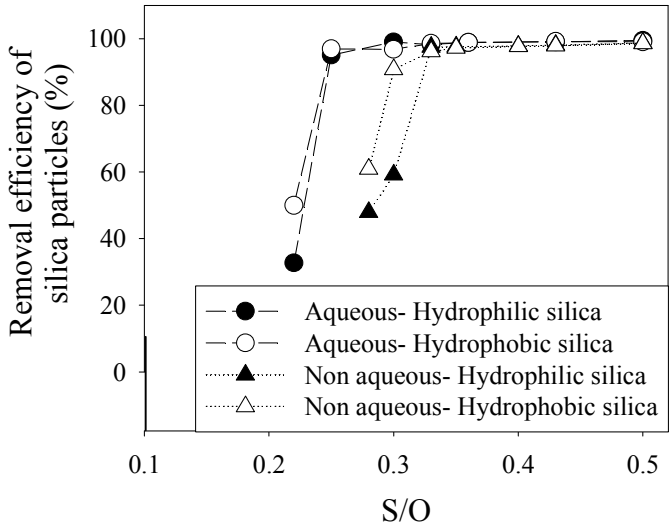

Figure 5-13 Removal efficiency (%) of the silica particles with different hydrophobicities in the aqueous and non-aqueous treatment of the oil solutions with paraffinic solvents

The ash content versus S/O at h = 5 cm for the oil solution and oil emulsion is compared in Figure 5-14. The water content in the oil emulsion for various S/O at h = 5 cm is also shown in Figure 5-14. In the oil sands industry the water and ash content in the pipelines should be less than 0.5 wt% [8]. The results in Figure

5-14 demonstrate that for S/O = 0.3 and higher ratios, in both oil models the ash and water content is less than 0.1 wt% which is acceptable from oil sands industry point of view.

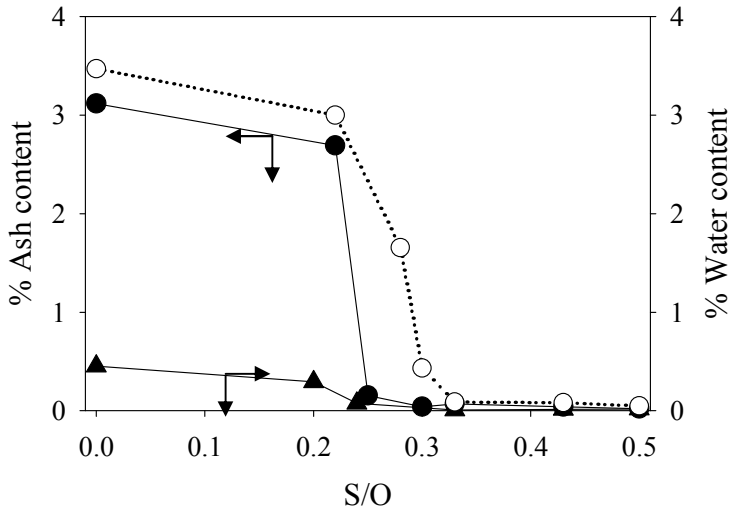

Figure 5-14 The ash content at h = 5 cm in the (○) paraffinic treatment of the oil solution and (●) paraffinic treatment of the model oil emulsion on the left axis. The water content (▲) at h = 5 cm in the oil emulsion by paraffinic treatment on the right axis

5.5 Discussion

This chapter investigated an aqueous treatment of the oil solution to determine if the addition of water would destabilize the silica suspensions. Two different approaches were chosen:

1) Aqueous treatment of the model oil solution: Preparing the oil solution plus the silica particles and emulsifying with small amounts of water afterwards. The water was used to agglomerate the silica particles.

2) Paraffinic treatment of the stable oil emulsion: Preparing a stable emulsion (leaving the oil solution with 4 wt% of water overnight) of water in the oil solution and adding the silica particles at the next step. The oil solutions were then treated with pentane to heteroflocculate the silica particles and emulsified water.

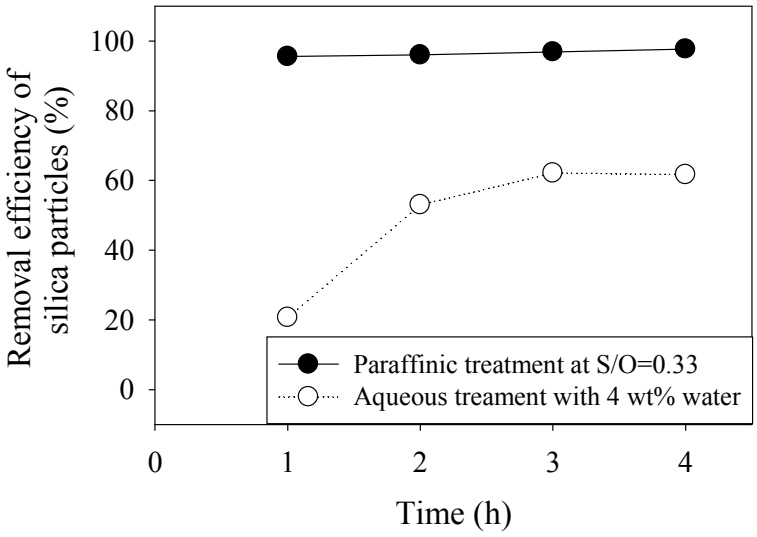

Figure 5-15 Removal efficiency (%) of hydrophilic silica particles with paraffinic and aqueous treatment of the model oil emulsion at h = 5 cm

Using the first approach, we observed that the addition of water removed the silica particles from the oil solution; however, the destabilization of the silica particles by this method is less efficient than by n-pentane. For instance, by adding 4 wt% water to the oil solution containing hydrophilic silica, the ash

content would be less than 1 wt% after 4 hours. For hydrophobic ones, the solution should be left for longer time to have less than 1 wt% ash content at different levels. In chapter 4, by paraffinic treatment of the oil solution at S/O = 0.33, for instance, the ash contents of samples at various heights were 0.09 ± 0.01 wt% only after 1 hour. The comparison between the efficiency of the two methods is shown in Figure 5-15. It is obvious that in the case of paraffinic treatment, much lower ash content was achieved in much shorter time (1 hour) with higher efficiency for removal of both hydrophilic and hydrophobic silica particles.

In chapter 4, we tested the hypothesis that addition of pentane destabilizes the stable suspension of silica particles in the model oil solution. Addition of n-pentane destabilized the solid suspensions in the water-free oil suspension at S/O = 0.33. In this chapter by using the second approach in the presence of emulsified water, destabilization of the silica particles occurred at lower S/O = 0.25. The amount of ash and water at S/O = 0.25 for hydrophilic silica particles were less than 0.3 wt% and 0.1 wt%, respectively. For hydrophobic silica particles, the destabilization started at S/O = 0.23 and the amount of ash and water was less than 0.1 wt%. In both emulsions with different hydrophobicities, the water and ash content, met the industry criteria which is less than 0.5 wt%.

Improvement of the flocculation and sedimentation of the silica particles in the presence of water can be due to amphiphilic characteristics of the asphaltene [14]. Asphaltenes are lyophobic with respect to low molecular weight paraffin hydrocarbon and lyophilic with respect to resins and aromatics. Asphaltenes ability to flocculate water droplets and fine solids has been reported previously in

the literature [15]. Zhao *et al.* (2008) has reported that the water in oil emulsion would facilitate the removal of asphaltenes from bitumen and improve the quality of the product [16]. In the case of our work, it is clear that in the presence of emulsified water, the removal of silica particles from the oil emulsions occur at a lower S/O. However, the mechanism of how the precipitated asphaltene facilitates the removal of solid particles from the oil solution in the presence of emulsified water is not fully understood. The interaction between the emulsified water with the precipitated asphaltene and silica particles can be an important factor to understand the heteroflocculation mechanism better.

Long *et al.* (2002) did similar experiments and diluted the bitumen containing fine particles (9 wt%) and water (31 wt%) with n-hexane and toluene. The ratio of solvent to bitumen was 1.5 in both cases (S/O = 1.5). The water and ash contents in the clean oil zone were both less than 0.1 wt% for hexane-bitumen solution after 60 min. For toluene-bitumen solution, however, the results were different. After 60 min settling in toluene, about 1.3 wt% water and 0.4 wt% ash remained in the oil phase, which was much higher than in the hexane solutions [12].

For any commercial process to remove the solid particles from the oil streams, the recovery efficiency is absolutely important. In addition, the amount of solvents and precipitated asphaltene can be other factors to affect the bitumen upgrading. Our results show that presence of emulsified water would facilitate the removal of solid particles in the paraffinic treatment of the oil solutions.

5.6 References

[1] Joseph D.Henry, Michael E.Prudich, and Chak Lau, 1980, "Liquid, Liquid, Solid Systems: Role of Water in Particle Removal from Hydrocarbon Suspensions," pp. 335.

[2] Ku, C. A., and Henry, J. D., 1987, "Mechanisms of Particle Transfer from a Continuous Oil to a Dispersed Water Phase," Journal of Colloid and Interface Science, 116(2) pp. 414-422.

[3] Henry, J. D., Prudich, M. E., and Vaidyanathan, K. R., 1979, "Novel Separation Processes for Solid-Liquid Separations in Coal Derived Liquids," Separation and Purification Methods, 8(2) pp. 81-118.

[4] Michael E.Prudich, and Joseph D.Henry, 1978, "The Mechanisms of Transfer of Hydrophobic Coated Mineral Matter Particles from a Hydrocarbon to an Aqueous Phase," 24(5) pp. 788.

[5] Buzzacchi, M., Schmiedel, P., and Von Rybinski, W., 2006, "Dynamic Surface Tension of Surfactant Systems and its Relation to Foam Formation and Liquid Film Drainage on Solid Surfaces," Colloids and Surfaces A: Physicochemical and Engineering Aspects, 273(1-3) pp. 47-54.

[6] Hiemenz, P., and Rajagopalan, R., 1997, "Principles of Colloids and Surface Chemistry,".

[7] Shelfantook, W., Tipman, R., Anderson, N. , C. Strand, 1996, "Effect of Alternate Diluents in Treatment of Bitumen Froths", CIM, Edmonton.

[8] Long, Y., Dabros, T., and Hamza, H., 2004, "Structure of water/solids/asphaltenes Aggregates and Effect of Mixing Temperature on Settling Rate in Solvent-Diluted Bitumen," Fuel, 83(7) pp. 823-832.

[9] Gray, M.R., 1994, "Upgrading petroleum residues and heavy oils " New York: M.Dekker.

[10] Islam, A. M., Chowdhry, B. Z., and Snowden, M. J., 1995, "Heteroaggregation in Colloidal Dispersions," Advances in Colloid and Interface Science, 62(2-3) pp. 109-136.

[11] Uricanu, V., Eastman, J. R., and Vincent, B., 2001, "Stability in Colloidal Mixtures Containing Particles with a Large Disparity in Size," Journal of Colloid and Interface Science, 233(1) pp. 1-11.

[12] Long, Y., Dabros, T., and Hamza, H., 2002, "Stability and Settling Characteristics of Solvent-Diluted Bitumen Emulsions," Fuel, 81(15) pp. 1945-1952.

[13] Long, Y., Dabros, T., and Hamza, H., 2004, "Structure of water/solids/asphaltenes Aggregates and Effect of Mixing Temperature on Settling Rate in Solvent-Diluted Bitumen," Fuel, 83(7) pp. 823-832.

[14] Li, X. , Elliott, J. A. W., McCaffrey, W. C., 2005, "Dynamic Surface Tensions of Athabasca Bitumen Vacuum Residue Including the Effect of Dissolved Air," Journal of Colloid and Interface Science, 287(2) pp. 640-646.

[15] Skuse, D. R., Tadros, T. F., and Vincent, B., 1986, "Controlled Heteroflocculation of Nonaqueous Silica Dispersions," Colloids and Surfaces, 17(4) pp. 343-360.

[16] Zhao, Y., and Wei, F., 2008, "Simultaneous Removal of Asphaltenes and Water from Water-in-Bitumen Emulsion. I. Fundamental Development," Fuel Processing Technology, 89(10) pp. 933-940.

6 Study of Asphaltene Adsorption on Surfaces by QCM and FTIR Spectroscopy

6.1 Introduction

The asphaltene solubility class of petroleum contains large and polar molecules that are formed from different aromatic groups and aliphatic chains. This fraction contains heteroatoms such as nitrogen, sulfur, oxygen, and metal components like vanadium and nickel. The asphaltene fraction also includes surface active components with a hydrophobic structure containing some hydrophilic functional groups [1, 2].

The stable dispersion of asphaltenes in crude oil can be destabilized by adding a paraffinic solvent, such as pentane or hexane, to give precipitation. Precipitated asphaltene can flocculate water droplets and solid particles, which is extremely useful in producing dry and solids-free bitumen from a water rich froth [3] and has potential for removal of fine solids from refinery streams (chapter 4). Asphaltenes adsorb on surfaces as individual molecules or colloidal aggregates of various sizes [4-10]. Accumulation of this material gives solid deposits which can

foul pipelines and process equipment. Asphaltenes can also adsorb on mineral surfaces and reservoir rocks, forming deposits that limit extraction of heavy oils from reservoirs and changing the wettability of the mineral surface [11, 12]. These behaviors motivate research activities on the deposition of asphaltenes onto various surfaces.

Fundamental studies of the deposition of asphaltenes on surfaces, under controlled conditions, help to identify the underlying processes. The amount of asphaltene deposited on solid surfaces has been measured by UV-Vis spectroscopy [13-16], quartz crystal microbalance (QCM) [6, 17-21], and X-ray photo-electron spectroscopy (XPS) [22].

Surfaces employed in previous adsorption studies included metallic and mineral surfaces. Langmuir adsorption asphaltene-toluene solutions was observed on clay minerals [23], on kaolin, $CaCO_3$, $BaSO_4$, FeS, Fe_3O_4, TiO_2 and SiO_2 [24], and on gold [6]. Multi layer adsorption was observed on oxidized surfaces, including silica, quartz, dolomite, calcite, kaolin, Fe_2O_3, and TiO_2 [11, 12, 25]. In multi layer adsorption, the amount of adsorption kept increasing on the surface of the solid particles, as a function of time, and it did not reach equilibrium. At low concentrations (10 - 10,000 ppm), the adsorption of asphaltenes on Berea sandstone, Bedford limestone and a Mexican dolomite rock showed monolayer adsorption. However, at higher concentrations (10,000 to 30,000 ppm) a stepwise-type of isotherm was observed, suggesting a change in the asphaltene adsorption behavior from toluene solution [15].

In chapter 4, we reported that a suspension of silica particles in asphaltene toluene solution was destabilized by the addition of pentane well below the onset of asphaltene precipitation (S/O = 0.43). In this chapter, we apply Fourier transform infra red (FTIR) spectroscopy and Quartz Crystal Microbalance (QCM) techniques to measure the amount and rate of asphaltene deposition on metal and mineral surfaces at various ratios of pentane (solvent) to oil solution. It was shown in chapter 4 that no asphaltene aggregates was observed by optical microscopy below S/O = 0.43. However, destabilization of silica particles occurred at S/O below the onset of asphaltene precipitation. Therefore, it is expected that asphaltene aggregates exist in size scales below the limit of optical microscopy. Our hypothesis is that even below the onset of asphaltene precipitation asphaltene material will adsorb on the surfaces of solid particles and give rise to flocculation.

The literatures on asphaltene deposition on solid surfaces focus mainly on two types of solutions:

1) A range of asphaltene concentration in toluene.

2) Addition of a paraffinic solvent (mainly heptane) to a specific concentration of asphaltene in toluene solution mainly in the range of 25:75, 50:50 and 75:25 of heptane:toluene.

In our work, however, we defined the onset of asphaltene precipitation precisely (chapter 4) and want to study the deposition properties at various ratio of pentane/oil (S/O) solution below and above the onset of asphatlene precipitation (i.e. S/O= 0 - 0.5). By increasing the amount of n-pentane from 0 -

0.5, more asphaltene would precipitate; therefore, we expect to observe more deposition on solid surfaces (on gold and silica particles with different hydrophobicity), especially after the onset of asphaltene precipitation. By studying the asphaltene deposition at various ratios of S/O, we want to see if asphaltene deposits would show any characteristics differences above and below the onset point.

The following sections provide brief descriptions on the literature about analysis of asphaltene adsorption by using QCM and FTIR spectroscopy. The comparison between different studies shows some discrepancies; however, one needs to note that the concentration range, the asphaltene type and the solid surfaces in each study are different.

6.2 Literature on measurement of asphaltene adsorption on solid surfaces by using FTIR

The literature on FTIR spectroscopy of asphaltenes is mainly on reactions and chemistry, including the asphaltene aging characteristics [26, 27] and elemental composition and functional groups of asphaltenes [28-33]. To our knowledge, there is no published work on the use of FTIR spectroscopy to measure the amount of asphaltene deposition on solid surfaces.

6.3 Literature on measurement of asphaltene adsorption on solid surfaces by using QCM

6.3.1 Asphaltene adsorption on metallic surfaces

Several published studies have focused on the adsorption of asphaltene on metal surfaces.

Rudrake (2009) used a combination of QCM and XPS to measure Cold Lake C7- asphaltene adsorption on gold. The amount of adsorption was estimated to be in the range of 2 - 9 mg/m^2 for 50 - 1500 ppm C7-asphaltene in toluene solution after 200 min. The adsorption process was diffusion controlled for the initial 40 seconds (i.e. the adsorbed mass showed a linear trend with square root of the time), following a first order kinetic process. The thickness of the adsorbed layer was reported to be 6 - 8 nm. The adsorption of C7-asphaltene on gold surfaces was described by a Langumir (type-I) isotherm after 200 min [6].

Abudu *et al.* (2008) studied the amount of adsorbed mass on gold from various concentrations of crude oil in toluene. The amount of adsorbed material for 0.5 - 30 wt% crude oil in toluene was 3.27 - 3.48 mg/m^2 which is almost constant for various concentrations. The amount of asphaltene adsorption at various concentrations of crude oil in heptane/toluene mixtures was studied as well. For instance, by increasing the ratio of heptane from 25% to 75% for 5 wt% crude oil in heptane/toluene, the amount of adsorption on the gold surface increased from 4.63 to 14.68 mg/m^2. The size of the asphaltene nano-aggregates was estimated from a diffusion model and the Stokes-Einstein equation to be

around 3 nm in a 3 wt% crude oil in toluene solution [34]. Unfortunately, their calculations of apparent diffusion coefficient were incorrect.

Ekholm *et al.* (2002) measured the adsorption of resin and asphaltenes on gold from solutions in toluene and toluene/heptane at various ratios. The amount of asphaltene adsorption for the concentration range of 50 - 1000 ppm in toluene and toluene/heptane (50:50) solution was 0.5 - 3 and 4.2 - 5.4 mg/m^2, respectively. For the same concentration range of asphaltene, heptane/toluene solutions showed more deposition on solid surfaces than the toluene solutions due to more precipitated asphaltene upon addition of heptane. They observed a Langmuir isotherm for adsorption of resins in heptane solution on gold surfaces and multilayer adsorption for asphaltene in toluene solution on the same surface, which did not reach equilibrium even after 300 min [20].

Xie *et al.* (2005) studied the adsorption of asphaltenes on metal surfaces in heptane/toluene solution by using R-QCM. It was reported that for 10 - 200 ppm asphaltene in heptane/toluene solution no equilibrium was observed even after 700 min. The amount of adsorption after 700 min was reported to be 4 - 22 mg/m^2 for C5-asphaltene in heptane/toluene solution (50:50) with concentrations of 10 - 200 ppm [21].

6.3.2 Asphaltene adsorption on mineral surfaces

The asphaltene adsorption has been studied on a variety of mineral surfaces, including clay [23, 35], mica [36], silica [25], montmorillonite [23], quartz [37], dolomite, and calcite [11].

Dudasova *et al.* (2008) studied the adsorption of 1 g/L of asphaltene in toluene or heptane/toluene on SiO_2, TiO_x, Al_2O_3, and FeO_x. The quartz crystal was spin coated with the above mentioned particles. The amount of adsorption was in the range of 1.5 - 9.8 mg/m^2 from heptane/toluene solution and 1.7 - 9.1 mg/m^2 for toluene solution. Silica surfaces had the highest adsorption from the heptane/toluene mixture. The diffusion coefficients for asphaltene in toluene solution were obtained by NMR and were in the order of 10^{-10} m^2/s. The size of the asphaltene aggregates was estimated by using Stokes-Einstein equation to be in the order of 1 nm [18].

Hannisdal (2006) studied the adsorption of 1 wt% of asphaltene and 1 wt% of resins in toluene solution on fumed silica nanoparticles (25 g particles/L) using QCM-D. Four different types of fumes silica were used in their study: Aerosil® 200, Aerosil® 7200, Aerosil® 202, and Aerosil® 972. The hydrophobic silica particles were the Aerosil® 202 and Aerosil® 972 treated with polydimethylsiloxane and dimethyldichlorosilane, respectively. The comparison between the amounts of adsorption on silica particles with different hydrophobicity showed that hydrophilic silica adsorbed more asphaltene and resins compare to the hydrophobic ones [19].

The lack of information in the literature that has been conducted in QCM area either on mineral or metallic surfaces is as follows:

1) The onset of asphaltene precipitation has not been measured precisely. Therefore, the amount of added heptane does not clarify the stage of asphaltene precipitation.

2) The swollen effect of the liquid has not been the focus of the mentioned studies.

3) The diffusion coefficient that has been calculated by QCM is much smaller than the diffusion coefficient calculated by other methods. The reason for this discrepancy has not been studied.

4) The reason that the amount of adsorption is different on mineral and metallic surfaces has not been clarified well.

The focus of the QCM study in this chapter is on part 1, 2 and 3. We studied the adsorption of asphaltene at various ratios of S/O above and below the onset point to observe the asphaltene deposition characteristics with respect to precipitation ratio.

6.4 Theory

We chose FTIR spectroscopy and QCM to measure the amount of asphaltene deposited on surfaces. In addition, we used QCM to study the solvent swelling of the asphaltenes and the transport of the asphaltenes to the solid surface.

6.4.1 Quartz Crystal Microbalane (QCM)

The detailed study of QCM has been described by many authors [38-46]. Here we give a brief discussion about its behavior in liquid media.

Sauerbrey was the first to use QCM technology to measure mass changes in gas phase. The quartz crystal oscillates at a certain frequency when an AC voltage

is applied. If any mass is adsorbed on the surface of the crystal, the frequency will drop. From the change in frequency it is easy to calculate the mass from the Sauerbrey equation:

$$\Delta f = -C_f . \Delta m \tag{6-1}$$

C_f is the sensitivity factor for the quartz crystal and depends on the properties of the crystal ($56.6\, Hz \cdot \mu g^{-1} cm^2$ for a 5 MHz AT-cut quartz crystal at room temperature), Δm is the adsorbed mass on the surface of the quartz crystal and Δf is the change in frequency upon adsorption of mass on the crystal surface.

For many years, QCMs were used as gas-phase mass detectors; however, Konash and Bastiaans in 1980 showed that QCM can be used in liquid media as well [61]. In liquid media, the characterization of the adsorbed layer is different than in gas phase; therefore, both resonance frequency and dissipation of the quartz oscillator must be considered. The loading of the liquid on the crystal causes the frequency to shift from its frequency in air. The change in frequency is not due to mass adsorption in this case, but is due to the liquid phase damping as follows:

$$\Delta f_{loading} = -\frac{f_0^{3/2}}{\pi^{1/2}} \frac{(\rho_L \eta_L)^{0.5} - (\rho_S \eta_S)^{0.5}}{\rho_q \nu_q} \tag{6-2}$$

where f_0 is the fundamental resonant frequency ($f_0 = 5 \times 10^6$ Hz), ρ_q is the specific density of the quartz (2650 kg/m^3) and ν_q is the shear wave velocity of the quartz (3340 m/s) [17, 34]. Throughout this chapter, the subscript *S* refers to a solution of toluene-pentane, and L refers to oil-toluene-pentane.

In some QCM instruments, the dissipation (ΔD) or resistance (ΔR) is measured. The shift in the dissipation factor and the resistance in a liquid medium are given as follows:

$$\Delta D = 2\frac{f_0^{0.5}}{\rho_q \nu_q}\left(\frac{\rho_L \eta_L}{\pi}\right)^{0.5} \tag{6-3}$$

$$\Delta R = \frac{\pi \mu_q h_q}{8 e_{26}^2 A_M \rho_q \nu_q}\left(\frac{1}{f_0}\right)^{0.5}\left(\frac{\rho_L \eta_L}{\pi}\right)^{0.5} \tag{6-4}$$

$A_m = 0.3149 \times 10^{-4}$ m^2 , $h_q = 3.31701662 \times 10^{-4}$ m, $e_{26} = 0.0966$ C/m^2, $\nu_q = \sqrt{\frac{\mu_q}{\rho_q}}$,

and $\mu_q = 2.947 \times 10^{10}$ Pa is the shear modulus of the quartz.

When mass is adsorbed on the quartz, a frictional energy is created that increases the dissipation (ΔD). If the film is viscous, energy is dissipated due to the oscillatory motion induced in the film. Hence, a rigid adsorbed layer gives no change in dissipation and equation (6-1) applies, while a loose layer gives a dissipation or resistance increase. The QCM instrument either measures the resistance (ΔR) with frequency or dissipation (ΔD). In equation (6-3) and (6-4), the term $(\rho_L \eta_L)^{0.5}$ would change according to the density and viscosity of the medium; however, the rest of the parameters in the equations are constants and only depend on the characteristics of the quartz crystal. Therefore, either measuring the dissipation or resistance can be used to characterize the rigidity of the material deposited on the crystal surface.

6.5 Kinetic study of asphaltene deposition

Adsorption of any type of solutes from a solution, and adhesion of colloids from a suspension onto a planar surface can be considered as a diffusion process. Initially, the concentration of the adsorbing species is the same at the vicinity of the surface and in the bulk. The species in the solutions move randomly in all directions, however, the net flux is towards the surface due to adsorption or adhesion. Ward and Tordai assumed that the area next to the surface with a thickness of few molecules in the bulk solution is considered as the sub-surface [47]. At the beginning of the diffusion process, the surface is bare and there are many available sites for the adsorption or adhesion. Therefore, when the solute molecules arrive at the sub-surface, they pass the area between the subsurface and surface faster than diffusing through the bulk of the solution. As more molecules are adsorbed on the surface the availability of the empty sites for adsorption decreases. Therefore, some of the solute molecules remain in the sub-surface area. When the concentration of subsurface is not zero anymore, back diffusion from the subsurface to the bulk starts. The concentration of solute molecules in the sub-surface keep increasing until it reaches a concentration similar to the bulk [47].

The concentration of the solutes in the solution at distance x from the surface at time t can be consists of two terms: one term attributed to the diffusion of the solutes to the surfaces ($\frac{\partial n_1}{\partial x}$) and the second term is back diffusion of the solutes from the surface to the bulk of the solution ($\frac{\partial n_2}{\partial x}$). Therefore, the concentration of the solutes in the solution can be considered as the following equation [47]:

$$\frac{\partial n}{\partial x} = \frac{\partial n_1}{\partial x} + \frac{\partial n_2}{\partial x} \tag{6-5}$$

The first term in the right hand side of equation (6-5) attributed to the diffusion from the bulk to the surface and is as follows [47]:

$$\frac{\partial n_1}{\partial x} = \frac{n_0}{(\pi D t)^{1/2}} \exp\left(-\frac{x^2}{4Dt}\right) \tag{6-6}$$

Where n_0 is the bulk concentration and D is the diffusion coefficient.

The second term in equation (6-5) can be defined as (the back diffusion of the solutes) [47]:

$$\left(\frac{\partial n_2}{\partial x}\right)_{x=0} = -\frac{1}{2(\pi D)^{1/2}} \int_0^t \frac{\varphi(\tau)}{(t-\tau)^{1/2}} d\tau \tag{6-7}$$

where τ is a variable for time and $\phi(\tau)$ is the subsurface concentration. It should be noted that the concentration in the bulk remains constant (n_0) at all the time. The concentration at the subsurface (express by $\varphi(t)$), however, varies with time.

The rate of diffusion at $x = 0$ is [47]:

$$\left(\frac{\partial M}{\partial t}\right)_{x=0} = -D\left(\frac{\partial n}{\partial x}\right)_{x=0} \tag{6-8}$$

Therefore, the amount diffuses towards the surface at time t, M_1, and the amount of solutes difusses backward from the subsurface to the bulk, M_2, is then given by [47]:

$$M_1 = \int_0^t \left(\frac{\partial M_1}{\partial t}\right)_{x=0} dt = 2n_0 \left(\frac{Dt}{\pi}\right)^{1/2} \tag{6-9}$$

$$M_2 = \int_0^t \left(\frac{\partial M_2}{\partial t} \right)_{x=0} dt = -\left(\frac{D}{\pi} \right)^{1/2} \int_0^t \frac{\varphi(\tau)}{(t-\tau)^{1/2}} d\tau \tag{6-10}$$

Using equation (6-9) and (6-10) and rearranging the equations, the total amount of solutes can be calculated as follows [47]:

$$M(t) = 2\sqrt{\frac{D}{\pi}} \left[n_0 \sqrt{t} - \int_0^{t^{1/2}} \phi(\tau) d[(t-\tau)^{1/2}] \right] \tag{6-11}$$

where M(t) is the dynamic adsorption, If $\phi(\tau) = 0$, equation (6-11) is reduced to:

$$M(t) = 2n_0 \left(\frac{Dt}{\pi} \right)^{1/2} \tag{6-12}$$

The condition $\phi(\tau) = 0$ is true if there is no back diffusion of the solutes from the subsurface to the bulk, i.e. when the adsorption is irreversible. Thermal motion of the particles may lead to the detachment of the particles from the surface. The irreversible adsorption in the case of asphaltenes corresponds to adsorption in a deep primary energy minimum with possible chemical bonds being formed between the asphaltene and the substrate. In the case of our work, asphaltene are assumed to have strong attachment to the surfaces. Therefore, the probability of removal of deposited asphaltene from the gold surface is very low.

This condition ($\phi(\tau) = 0$) should be satisfied not only at the beginning of the adsorption but also during the adsorption process at all the times. If this condition is true then the apparent diffusion coefficient may be calculated from the slope of M versus $\sqrt{t}$.

$$Slope = 2n_0\left(\frac{D}{\pi}\right)^{1/2} \tag{6-13}$$

For a spherical particle, the diffusion coefficient is given by Stokes-Einstein equation as follows:

$$D = \frac{k_B T}{6\pi\eta r} \tag{6-14}$$

where k_B is the Boltzmann constant ($1.3806503 \times 10^{-23}$·m^2·kg·s^{-2}·K^{-1}), T is the temperature (296 K), η the viscosity of the surrounding fluid, and r is the radius of the hard sphere. From this equation and the diffusion coefficient, one can estimate the radii of the particles, asphaltene molecules or aggregates in the case of our study, as equivalent spheres [48].

6.6 Experimental methods

6.6.1 Materials

The model oil was prepared as a 5 wt% concentration of pitch material in toluene (model oil) , as described in previous chapters.

Asphaltenes were separated by first mixing pitch material with chloroform with a 1:0.4 weight ratio of pitch to chloroform. The mixture was shaken with a table shaker for 2 hours until all the pitch material was dissolved in chloroform. Then pentane was added to the mixture with a 40:1 volume ratio of pentane to pitch mixture. The mixture was stirred for 4 hours and left overnight to allow the precipitated asphaltenes to settle. Then the supernatant was removed, and the remaining precipitate was further diluted with pentane at a 4:1 volume ratio of

pentane to asphaltenes. After 4 hours shaking, the final mixture was filtered using 0.22 μm Millipore filter paper to filter out the asphaltenes, which were washed thoroughly with pentane until the filtrate became colorless. The precipitated asphaltenes were dried in an oven at 80°C [49]. The solvents were separated from the filtrate by using a rotary evaporation, then the remaining maltenes were dried in an oven at 80°C. The asphaltene and maltenes were kept in desicator for further experiments.

Solutions of asphaltenes and maltenes were prepared to determine the contributions of these fractions to adsorption on surfaces. The original asphaltene content of the pitch material was 60%. To examine the contributions of each fraction in a 5 wt% solution of pitch a sample with 3 wt% asphaltene in toluene and a sample with 2 wt% maltenes in toluene were prepared.

6.6.2 Viscosity measurements

The viscosity was measured by using a Viscolab 3000 rheometer (Cambridge Applied Systems, Massachusetts, USA). All the sample viscosities were measured in a thermostatic bath using a glass capillary viscometer as well. The viscosities were measured at 22°C.

For the samples in which pentane was added to the oil solution, the mixture was left for 1 hour to allow any flocculated material to sediment, then the density and viscosity was measured for the supernatant.

6.6.3 FTIR spectroscopy experiments

After the model oils were prepared, the silica particles were left in the oil solution for 2 hours; the silica particles were then separated from the oil phase by centrifuging each sample. The silica particles were washed with toluene until the supernatant was colorless and then oven-dried at 105ºC overnight.

Samples were prepared for FTIR spectroscopy by mixing the coated silica particles with potassium bromide (KBr) to prevent scattering effects from the particles (1 gr KBr and 1 - 5 mg coated silica). This powder mixture was then hand-ground and put in the sample container. The reference sample was a mixture of KBr with clean silica particles at the same weight ratio. Infrared spectra of the pure and coated silica products were recorded in the range between 600 and 4000 cm^{-1}. Infrared spectra were obtained using an FTIR spectrometer in diffuse reflectance mode (Bio-Rad FTS 6000, Midland, Ontario, Canada). The spectra were obtained at a spectral resolution of 2 cm^{-1} using 128 scans per spectrum. We used the spectra range between 2800 and 3000 cm^{-1} with characteristic adsorption bands from C-H stretching in methyl and methylene groups (2962 cm^{-1} ν_{as} CH_3, 2872 cm^{-1} ν_s CH_3, 2924 cm^{-1} ν_{as} CH_2, 2853 cm^{-1} ν_s CH_2) as a measure of the mass of hydrocarbon adsorbed on the silica surface. These strong bands were present in all fractions of the pitch; therefore, any selectivity in the adsorption on the silica was unlikely to change the absorbance in these bands significantly.

6.6.3.1 Calibration curve

The FTIR spectra consist of absorbance versus the wave number for a given concentration of sample. For quantitative measurements of the amount of adsorbed material on the surface of silica particles, a calibration experiment was designed as follows: KBr was mixed with pitch material (10 gr KBr and 50 mg pitch). The mixture was ground to have a uniform mixture of pitch and KBr. Then for the sample container, KBr, pitch+KBr mixture and clean silica were hand-ground. The experiment was repeated for different weights of pitch+KBr mixture with the same amount of clean silica particles for each sample and the absorbance curve was measured. If we assume that the mixture of KBr and pitch material was uniform, then for each sample the amount of pitch and the absorbance peak was known. Therefore, the calibration curve was plotted based on different weight of pitch versus the height of measured absorbance at 2924 cm^{-1}. From this graph, by knowing the height of absorbance for various ratios, the amount of adsorbed material was estimated.

6.6.4 QCM experiments

QCM is a sensitive technique to measure the adsorbed and adhered mass on different surfaces. Two types of measurements are feasible; QCM-D with measurement of dissipation and R-QCM with measurement of resistance. We used R-QCM in this study to measure the amount of asphaltene deposition on solid surfaces.

In this set of experiment, we used a 5 MHz AT-cut quartz crystals and QCM25 crystal oscillator (QCM200 from Stanford Research Systems (SRS), Santa Barbara, US). The constants of the crystals were C = 33 fF, L = 30 mH, and R = 10 Ω (for a dry crystal). The capacitance, C_0, was zeroed each time the crystal was changed.

6.6.4.1 Immersion experiments

In all the experiments, both resonant frequency (f) and resistance (R) data were collected. After the crystal was mounted, the response was measured in air for at least 10 min to obtain a stable baseline (stage 1). The probe was then immersed in a pentane-toluene solution until a stable reading was obtained (stage 2), then transferred to an oil- toluene-pentane solution with the same pentane-toluene ratio as in stage 2 (stage 3). The frequency was measured in the toluene-pentane-oil solution for 2 hours, then the probe was rinsed with pure toluene and immersed in toluene until a stable reading was obtained (stage 4). In all the cases, the sample container was covered carefully to avoid evaporation of the solvents. The probe was then removed from the toluene, washed with excess toluene, and allowed to stand in the air until the frequency became constant (stage 5). The mass adsorbed on the crystal was calculated after washing with toluene and drying in air at the end of the experiment.

6.6.4.2 Flow Through Cell (FTC)

In order to measure the amount of adsorption on silica particles at various S/O, the flow through cell (FTC) method was used to avoid losing the silica particles during immersion in the solution. To compare the results from adsorption on silica with results on gold, the same experiments were repeated for the gold surface as well. The flow cell (SRS QCM, Santa Barbara, US) is used in place of the crystal retainer ring of the crystal holder. Once installed, the volume of the cell is around 0.15 mL. The flow cell includes two inlet and outlet ports with 0.040″ ID through hole and fitted with barbed hose adapters for 0.062″ ID tubing. A 5 mL syringe was used for injecting the sample in the cell. The sample was injected at a rate of around 5 mL/min. First a stable baseline in the air was established, then the oil solution was mixed with pentane at various ratios and injected in the cell for a period of nearly 2 hours while the data were collected.

Spin coating (Laurell Technologies Corporation, USA) was used to coat the gold quartz crystal with silica particles. A solution with 0.1 wt% silica particles in isopropyl alcohol (IPA) was prepared and the sample was shaken with a vortex for 20 min. Then droplets of the sample were placed on the surface of the gold crystal. The quartz was spun at 500, 1000, 2000, 3000, 4000, 5000 rpm for 30 sec each and then for 2 min at 6000 rpm. The coating was checked with a microscope to make sure that there was a monolayer adsorption of silica particles on the surface of the gold crystal. For concentration of silica particles in IPA higher than 0.1 wt% we observed multilayer accumulation of particles in some spots, while decreasing the amount to less than 0.1 wt% gave empty areas on the surface of the

crystal. Although the surface was not covered completely with silica particles, we avoided increasing the concentration of silica particles in IPA to avoid multilayer accumulation of silica particles on the surface of the gold-plate crystal.

6.7 Results and discussion

6.7.1 FTIR Spectroscopy results

In order to examine the interactions between precipitated asphaltene and silica, we used FTIR spectroscopy to measure the amount of adsorbed material on silica (mainly asphaltene) as a function of S/O. At low S/O values, the absorbance due to the asphaltene on the silica particles was low. By increasing the ratio of added n-pentane to the oil phase, the intensity of the IR spectrum of the asphaltene on the silica particles was increased (Figure 6-1). The height of the adsorbance peaks in the range of 2850 - 2950 cm^{-1} increased with increasing S/O, which indicated that more material was adsorbed on the surface of the silica particles.

Using a calibration curve from mixtures of pitch and silica, the amount of adsorbed asphaltenes was estimated as a function of S/O (Figure 6-2). The calibration curve was based on a mixture of pitch material with silica, whereas the adsorbed material on the surface of the silica particles was mainly asphaltene, due to addition of n-pentane as a solvent. Both pitch and asphaltene have strong absorbance bands at 2924 cm^{-1}, but the extinction coefficient of the adsorbed

material could depend on its composition, therefore, we consider the results of these measurements to be semi-quantitative.

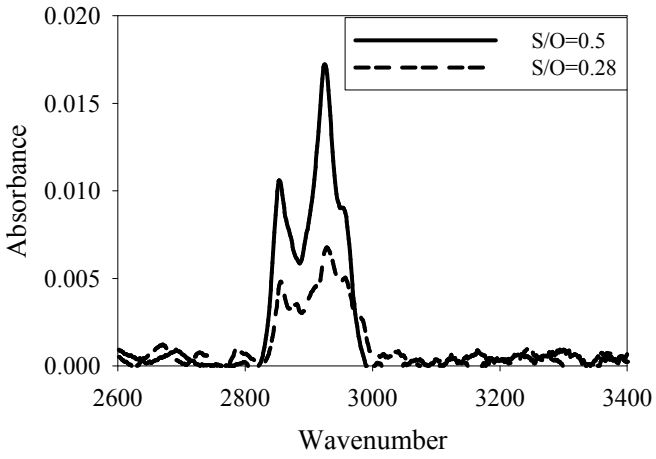

Figure 6-1 FTIR spectra for treated silica particles in model oil solution at various S/O. Particles were washed, dried and mixed with KBr for collection of spectra by diffuse reflectance. These results from FTIR spectroscopy confirmed that some asphaltene material adsorbed on the silica particles, even well before the onset of precipitation.

At S/O = 0 the amount of hydrocarbon adsorption on silica particles was the lowest (at circa 0.01 mg/g silica). The amount of adsorbed material increased with S/O to the onset of asphaltene precipitation at S/O = 0.43, then increased more with subsequent addition of pentane. For example, an increase in S/O from 0.25 to 0.4 increased adsorption by 20%, however, when S/O was increased from 0.43 to 0.7, the amount of adsorbed material increased by 84%.

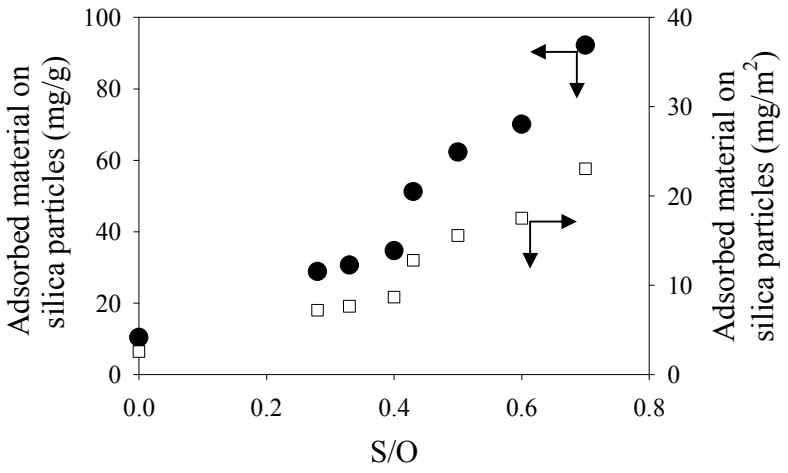

Figure 6-2. Asphaltene adsorption on the silica surface at various S/O

The amount of adsorbed material (mainly asphaltene) on silica particles was measured by FTIR spectroscopy, based on the absorbance at 2924 cm^{-1}. The right hand axis shows the amount of adsorbed material calculated in mg/m^2 from a surface area of the silica particles of 4 m^2/g.

The surface area of the silica particles is 4 m^2/g. Bases on this surface area, the amount of adsorbed material was calculated in mg/m^2 and plotted in Figure 6-2 on the right hand axis. The coverage of 9 mg/m^2 at S/O = 0.4, just before the onset of flocculation, corresponded to a mean thickness of 7.5 nm of asphaltene material, based on a density of 1200 kg/m^3. Given that the minimum size of the asphaltene aggregates is 5 - 10 nm, based on several methods as discussed earlier, these results suggest that a monolayer coverage of asphaltene aggregates was achieved on the silica prior to the onset of flocculation. Clearly, the higher concentrations of asphaltenes on the silica at S/O > 0.4 would correspond to multiple layers of deposition.

6.7.2 QCM results

6.7.2.1 Stages in QCM immersion experiment

As explained earlier, the QCM immersion experiment in this work had 5 stages which are shown in Figure 6-3, giving first deposition then rinsing of the surface material in toluene, followed by air drying.

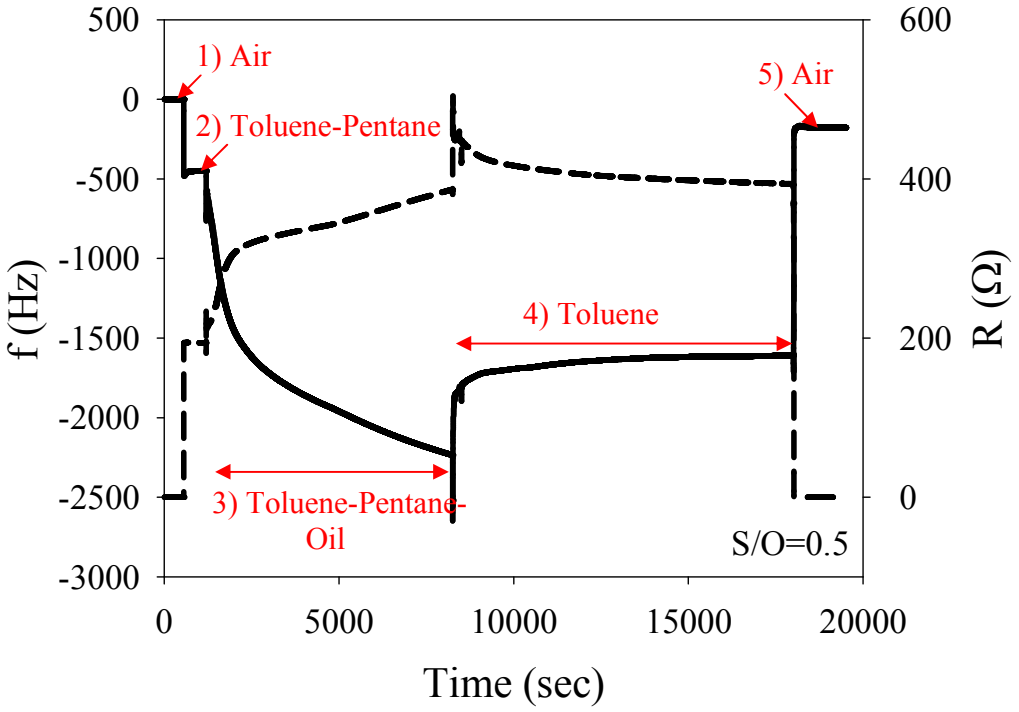

Figure 6-3 Sequence stages for the QCM immersion experiment (S/O = 0.5).

(Solid line - frequency; dashed line - resistance)

Stage 1: Mounting the quartz crystal in air; Stage 2: Exposing the quartz crystal to pentane and toluene; Stage 3: Transferring the probe to the oil-toluene-pentane solution; Stage 4: Washing the probe with toluene; Stage 5: Drying the probe in air

The data in table 6.1 summarize the significant shifts in frequency due to changing the surrounding medium of the quartz crystal and due to adsorption and removal of the asphaltenes. In the transition from stage 1 to stage 2, exposing the quartz crystal to any solvent (pentane and toluene in this study), gave a change in both frequency and resistance due to the changes of the density and viscosity of the medium. As there is no adsorption, the frequency reaches a new equilibrium in few seconds and becomes stable. The change in resistance follows the same pattern as the frequency.

Table 6-1 Experimental changes in frequency due to immersion in different solutions for various S/O

S/O	Δf (Hz) (1→2)	Δf (Hz) (2→3)	Δf (Hz) (4→1)	Δf (Hz) (5)
0.5	-443	-1768	-1609	-195
0.43	-450	-771	-1065	-72
0.36	-460	-213	-686	-29.5
0.0	-585	-114	-638	-1.8

When the probe was immersed in the oil solution (oil-toluene-pentane) in stage 3, the frequency steadily decreased and the resistance steadily increased. The change of the frequency in this stage is due to two contributions:

a) Change of viscosity and density of the medium (the medium has changed from toluene-pentane to oil-toluene-pentane).

b) The deposition of asphaltene on the surface of the quartz crystal.

However, the changes are mainly due to the adsorption of asphaltene, not the change in density and viscosity of the media except for S/O = 0. The solvent in

the oil mixture in stage 3 is similar to the solvent in stage 2, i.e. toluene-pentane with the same ratio. The change in frequency due to liquid loading for transferring from stage 2 to 3 was calculated by using equation (6-2) and is shown in Table 6-1. Comparing the experimental change in frequency for stage 2 to 3 (Table 6-1) with calculates Δf (2→3) due to liquid loading (Table 6-2) shows that most of the frequency change in the transition from stage 2 to the end of stage 3 for S/O > 0 is due to the deposition of asphaltene on the surface of the quartz. At S/O = 0, the total frequency shift was -114.4 Hz, compared to an expected shift of -68.5 Hz due to the change in the solvent medium. Therefore, the effect of solvent loading at S/O = 0 was larger than the contribution of asphaltene deposition on the surface. In contrast, at higher values of S/O, the shifts due to the solvent alone were smaller; therefore, the contribution of the asphaltene deposits was dominant.

Table 6-2 Density and viscosity of toluene-pentane (stage 2) and oil-toluene-pentane (stage 3) for various S/O. Δf (2→3), is calculated by using equation (6-2)

S/O	**Density of stage 2 (kg/m^3)**	**Viscosity of stage 2 ($\times 10^3$) (Pa·s)**	**Density of stage 3 (kg/m^3)**	**Viscosity of stage 3 ($\times 10^3$) (Pa·s)**	**Calculated Δf for stage (2→3), (Hz)**
0.5	770	0.39	776	0.47	-38.6
0.43	779	0.41	785	0.48	-34.9
0.36	789	0.43	796	0.50	-36.4
0	867	0.62	876	0.78	-68.5

In stage 4, the quartz was washed with toluene and remained in toluene for 2 hours. If any materials adsorbed on the surface reversibly, then they would be dissolved in toluene during this period. After stage 4, the probe was washed with

excess toluene and brought back to air (stage 5). The probe remained in the air until a stable reading in frequency was obtained. The frequency in this step is due to irreversibly adsorbed material and no other factor affects this signal.

During the immersion in the asphaltene solution during stage 3, for S/O = 0.43 (Figure 6-4) and S/O = 0.5 (Table 6-3), there is a sharp continuous change in frequency with time, with no achievement of a stable value. The sharp changes in the frequency for these two ratios are due to the onset of asphaltene precipitation. This progressive change was due to the ongoing deposition of asphaltenes during most of this time interval of 2 hours. This accumulation of adsorbed mass was only partly reversed by subsequent immersion in toluene; therefore, the frequencies in stage 4 (in toluene) and 5 (in air) are higher for these solvent:oil ratios as well.

The frequency values for stage 4 reveals some interesting facts. In stage 4, part of the frequency is due to the adsorption of material from the pitch and partly due to toluene trapped in the deposited layer. This contribution is particularly clear when we analyze the results from the end of stage 4, where a stable layer of adsorbed material remains in toluene (the frequency became stable), and in stage 5 in air. The experimental and predicted frequency shifts for Δf (4→1) are given in Table 6-3.

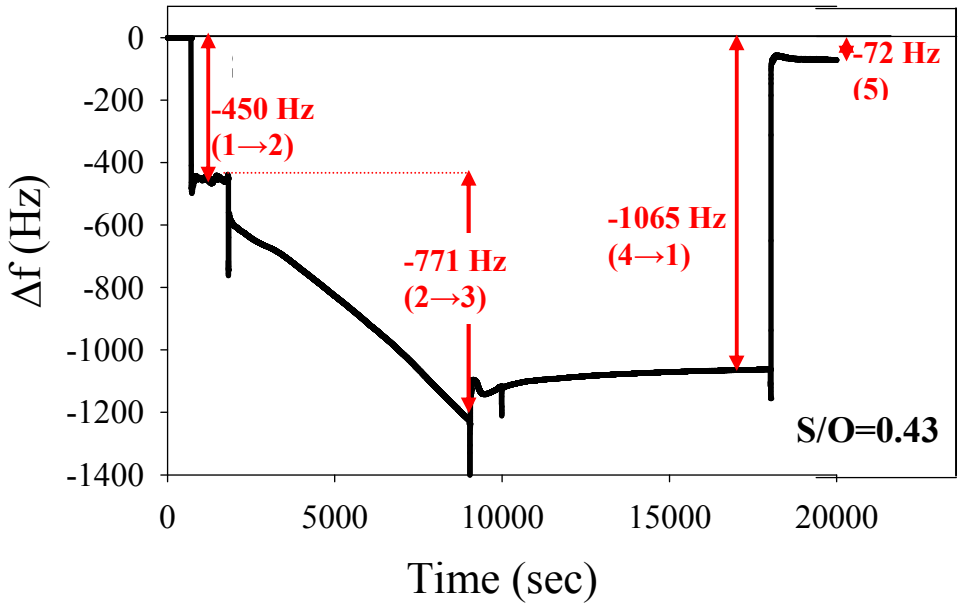

Figure 6-4 Change in frequency with stages of immersion for S/O = 0.43.

Table 6-3 Experimental and predicted changes in frequency in stage 4 for various S/O. Expected $\Delta f\ (4\rightarrow1) = \Delta f_{\text{Liquid loading due to toluene by using equation (6-2)}} + \Delta f_{\text{Stage 5}}$

S/O	Experimental Δf (Hz) (4→1)	Expected Δf (Hz) (4→1)
0.5	-1609	-705
0.43	-1065	-582
0.36	-686	-539
0.0	-638	-509.8

When the quartz crystal is loaded with toluene, the calculated frequency due to toluene (by using equation (6-2)) is around 509.8 Hz. In addition, we have the experimental amount of deposited mass on the quartz crystal at each S/O in the air (stage 5). Therefore, for a simple solid film on the crystal, we would expect that

the Δf (4→1) to be the frequency in the air (stage 5) due to the asphaltene film plus the frequency due to toluene, i.e. Δf (4→1) = Δf (stage 5) + 509.8. For instance, for S/O = 0.5, the frequency due to deposited mass on the quartz in stage 5 is -195.4 Hz. Therefore, we expect that the Δf (4→1) for S/O = 0.5 to be -705.2 Hz (i.e. -509.8 + (-195.4)). However, the experimental Δf (4→1) for S/O = 0.5 is much larger, at -1609 Hz. For S/O = 0, the frequency due to deposited mass on the quartz in stage 5 is -1.8 Hz. Therefore, we expect that the Δf (4→1) to be -510.6 Hz (i.e. -509.8 + (-1.8)) for S/O = 0. However, the experimental Δf (4→1) is -638 Hz. The data of Table 6-3 compare the experimental and expected Δf (4→1) values for various S/O.

The simplest explanation is that the asphaltene layer traps toluene solvent, so that the effective mass in stage 4 is much larger than the mass of dried asphaltene film in stage 5. The amount of trapped toluene in the structure of asphaltenes depends on the S/O value. At higher S/O, especially above the onset of asphaltene precipitation, asphaltene starts precipitating and forming aggregates with high porosity. At higher S/O, the volume of the solvents increases in these porous structures. Therefore, the adsorbed mass would become swollen with the toluene so the solvent swollen weight increases more rapidly than the dry weight of the asphaltenes. Therefore, there would be a bigger difference between the expected and experimental frequency in stage 4 for higher S/Os.

6.7.2.2 Changes in dissipation (ΔD) and resistance (ΔR)

The change in dissipation factor, D, indicates how much energy is dissipated in the layer adjacent to the surface of the quartz resonator. In the case of our work, R-QCM was used with the ability to record the resistance. Using equations (6-3) and (6-4), the dissipation and resistance parameters were calculated and the results for some of the solvent ratios are shown in Table 6-4.

Table 6-4 Calculated dissipation and calculated and measured resistance due to oil-toluene-pentane solution loading

S/O	ΔD (calculated)$\times 10^4$	ΔR (measured)	ΔR (calculated)
0.5	1.73	234	225
0.43	1.75	232	229
0.36	1.80	226	235
0	2.35	287	308

When liquid is coupled to the surface of the gold crystals, this liquid loading behavior is manifested by a linear variation of ΔD versus Δf. Aung *et al.* [50] found that ΔR and ΔD are correlated well with each other and both parameters gave similar characterization to the viscoelastic properties of the adsorbed material on the surface of the quartz crystal. If we assume that this analysis applies to the case for asphaltene as well, we can use the resistance data to get information about the viscoelastic properties of the attached layers to the gold crystals. Using equations (6-2) and (6-4) we can calculate the ratio of change in frequency to change in resistance:

$$\frac{|\Delta f|}{\Delta R} = \frac{8e_{26}^2 f_0^2 A_M}{\pi \mu_q h_q} = 1.92 \tag{6-15}$$

The ratio of the changes in ΔR and Δf leads to a constant which is independent of the liquid characteristics and can be used as a verification for proper operation of the instrument. If this ratio is much higher than 1.92, the surface roughness is assumed to increase [41]. Table 6-5 shows $\frac{|\Delta f|}{\Delta R}$ for some values of S/O for both the liquid loading and adsorption stages of each experiment.

Table 6-5 Ratio of change in frequency to change in resistance for different stages of the QCM experiments

S/O	$\frac{\lvert\Delta f\rvert}{\Delta R}$ **liquid loading (1→2)**	$\frac{\lvert\Delta f\rvert}{\Delta R}$ **during adsorption process (stage 3)**	$\frac{\Delta R}{\lvert\Delta f\rvert}$ **during adsorption process (stage 3)**
0.5	2.30	8.29	0.12
0.43	2.12	5.67	0.18
0.36	2.17	5.53	0.18
0	2.38	3.93	0.25

The data of the calculated ratio for liquid loading is close to the expected value of 1.92, with a mean value of 2.26 ± 0.04 that was not dependent on the S/O ratio. This constant relative response showed that the instrument was working properly.

When asphaltenes are adsorbed on the crystal, however, $\frac{|\Delta f|}{\Delta R}$ in stage 3 are significantly greater than 1.92, and increase systematically with S/O ratio.

According to Cho *et al*. the $\frac{|\Delta f|}{\Delta R}$ higher than five shows a rough surface which is the case in stage 3 [41].

Previous work with QCM has shown that when ΔR = 0, the adsorbed mass on the surface of the quartz is elastic [51]. However, when viscoelastic materials are adsorbed on the surface, the changes in ΔR are no longer negligible. For all the S/Os, the change in resistance during the adsorption part (stage 3) was not zero, which shows that the adsorbed materials on the surface of the gold for all S/Os are not rigid. As the ratio of S/O increased, larger changes in the resistance would be observed in stage 3. However, $\frac{\Delta R}{|\Delta f|}$ becomes larger for lower S/O. For all the S/O, $\frac{\Delta R}{|\Delta f|} \neq 0$ (last column in Table 6-5) shows a viscoelastic deposition of materials on the quartz surface.

6.7.2.3 Amount of adsorbed asphaltene at various S/O by immersion method

For each S/O, the adsorbed mass was calculated in the air after washing the crystal with toluene (stage 5). When the mass is calculated in the air, we can assume that there is no viscosity and density effect, and that the mass of deposit can be calculated without considering the liquid loading, using the Sauerbrey equation (6-1). In this case, the change in frequency is due to irreversibly adsorbed mass. The data in Figure 6-5 show that even below the onset of asphaltene precipitation, which is at S/O = 0.43, there is evidence of adsorbed

materials on the surface of the gold. The amount of the adsorbed mass, however, increased significantly after this point.

The adsorbed mass on the quartz crystal after 2 hours immersion in the oil solution at various S/Os (stage 3) are shown in Table 6-6. The $\frac{M_{Stage(3)}}{M_{Stage(5)}}$ shows the ratio of the effective mass (adsorbed mass plus the trapped solvent) to the dry mass. It can be seen that the solvent swollen effect is more for higher S/O due to more porous structure of the deposited asphaltene on the gold surfaces.

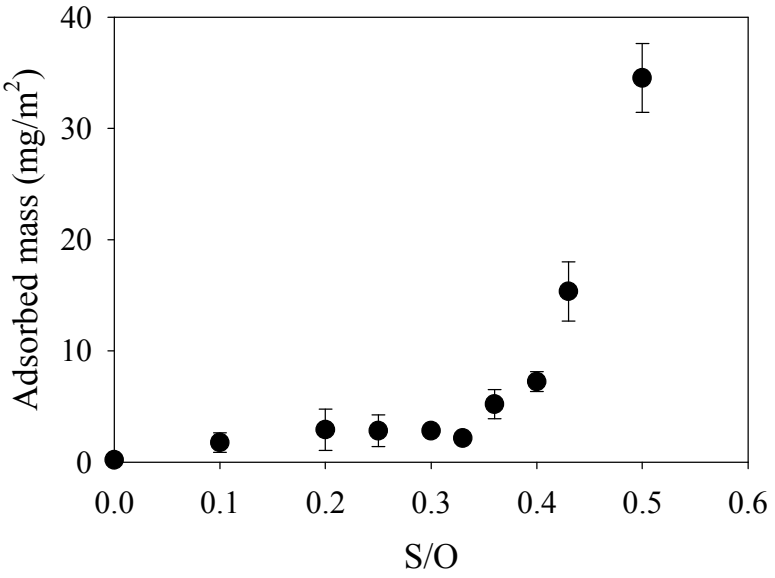

Figure 6-5 Amount of adsorbed mass on gold at various S/Os. Quantity measured after washing with toluene and dried in air

The results from literature on asphaltene adsorption by using QCM are summarized in Table 6-7. Comparing the results in Table 6-7 with the results from our work show that the amount of asphaltene adsorption in the case of our work is similar to other works considering the concentration of asphaltene and the

origins of the sample. The amount of the asphaltene deposition in the case of Xie *et al*. work is mainly higher than the rest of the works. In the literature the paraffinic solvent has been added to the oil solution at some defined ratios (such as 25:75, 50:50, and 75:25) without considering the precise point for the asphaltene precipitation. In our work, however, we studied the amount of deposition at specific ratio of pentane/oil solution by considering the onset of asphaltene precipitation.

Table 6-6 Estimated mass in stage 3 and 5. $\frac{M_{Stage(3)}}{M_{Stage(5)}}$ shows the solvent swollen effect at various S/O

S/O	$M_{Stage(3)}$, (mg/m^2)	$M_{Stage(5)}$, (mg/m^2)	$\frac{M_{Stage(3)}}{M_{Stage(5)}}$
0.5	305.5	34.5	8.8
0.43	130.1	15.4	8.5
0.36	31.2	5.2	6

Table 6-7 Literature results on comparison of asphaltene adsorption on gold surfaces

Work	**Solvent**	**Concentration**	**Amount of adsorption (mg/m^2)**
Abudu *et al.* (2008) [34]	Heptane-toluene (25:75)	5 wt%	4.63
	Heptane-toluene (50:50)		13.24
	Heptane-toluene (75:25)		14.68
Ekholm *et al.* (2002) [20]	Toluene	50 - 10000 ppm	0.2 - 8.5
	Heptane-toluene (50:50)	25 - 1000 ppm	0.8 - 5.4
Xie *et al.* (2005) [21]	Heptane-toluene (50:50)	10 - 200 ppm	4 - 22
This work	Pentane-toluene (S/O = 0-0.5)	5 wt%	0.2 - 34.5

6.7.2.4 Adsorption of asphaltene and maltene in toluene solution

In all of our deposition experiments, the solution of pitch in toluene was used as the model oil. Most of the adsorbed material on the solid surfaces was assumed to be asphaltene. To make sure that this assumption is true, the amount of adsorption on gold was measured in solutions of separated C5 asphaltenes and maltene. The results for these experiments are shown in Table 6-8. When no pentane is added (S/O = 0), the amount of adsorption in asphaltene solution (13.09 mg/m^2) was higher than both the maltene solution (4.86 mg/m^2) and the pitch solution (7.95 mg/m^2). Although the wt% of asphaltene in both pitch and asphaltene solution was the same, the amount of adsorption was consistently lower in the pitch solution. This result shows that the deposition behavior of asphaltene in the presence of resins is different than in pure asphaltene solution. In addition, it is obvious that the maltene components compete with asphaltene to adsorb on the surface of gold in pitch solution. Adsorption of maltene components, mainly as molecular species from solution, would fill some of the available sites on the surface of the gold, reducing the mass of adsorbed asphaltene aggregates in the pitch solution and the total adsorbed mass. When pentane is added, the oil solution is destabilized and asphaltene starts precipitating. A portion of the adsorbed mass at higher values of S/O is still due to maltenes, which is constant; however, the fraction due to the asphaltenes was dominant.

Table 6-8 Comparison between mass adsorbed from asphaltene, maltene and pitch in toluene

Solid material	Solid concentration in toluene (wt%)	Wt% of each component in pitch	Density (kg/m^3)	Viscosity (Pa·s)	Adsorbed mass (mg/m^2)
Pitch	5	-	876.19	0.00078	7.95
Asphaltene	3	59.5	870.63	0.00074	13.09
Maltenes	2	15.8	867.04	0.00073	4.86

6.7.2.5 Adsorption on silica particles with different hydrophobicity

For the FTIR spectroscopic analysis, the hydrophilic silica particles were immersed in the oil solution for 2 hours, and then washed with toluene; then the amount of asphaltene adsorption was determined. The same time was chosen here to measure the amount of asphaltene adsorption on silica particles with different hydrophobicity by using QCM. The gold quartz crystal was covered with a monolayer of silica particles with spin coating. The crystal was mounted in the flow cell and the oil solutions at various S/O were injected carefully with a very low flow rate (5 ml/min) in the flow cell to eliminate removal of the silica particles from the surface of the gold.

The data shown in Figure 6-6 give the comparison between adsorbed mass of asphaltene on silica particles with different hydrophobicity and on the gold surface. The surface of the silica particles was calculated based on hexagonal monolayer of one micrometer silica particles on the gold quartz crystal. From the results it is obvious that hydrophilic silica particles adsorbed more material above

the onset of asphaltene precipitation in comparison to hydrophobic particles. Below the onset of precipitation, however, the amount of adsorption was similar in both cases. These results are in agreement with Hannisdal (2006) and Dudaova (2008), [18, 52]. The amount of adsorption on gold is higher than adsorption on silica particles.

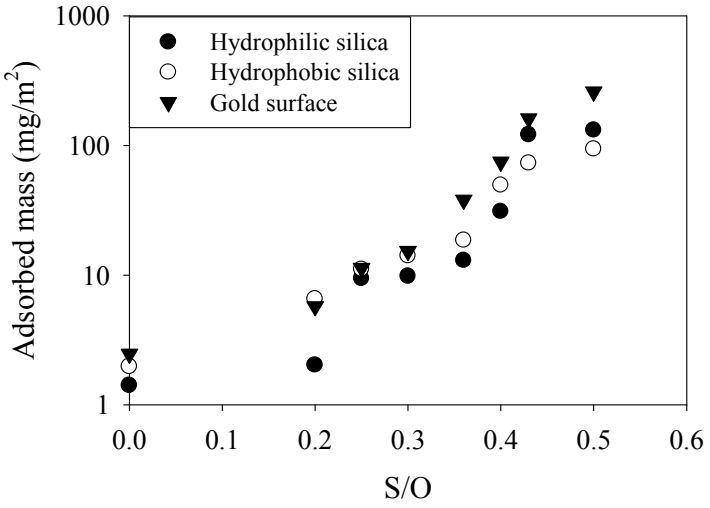

Figure 6-6 Comparison of mass deposited from pitch solutions on different surfaces using Flow Through Cell (FTC) method with QCM

Figure 6-7 shows the amount of asphaltene adsorption on hydrophilic silica particles that were measured with FTIR and QCM at various S/O. The amount of adsorbed material in the QCM experiments is higher than the FTIR measurements simply due to the washing of the particles with excess toluene in FTIR experiments. In the FTIR experiments, after suspending the silica particles in the model oil for 2 hours, the particles were separated by centrifuge and were washed with toluene until the supernatant were colorless (washing for three days). In the QCM method, we did not wash the quartz crystal coated with silica particles with

toluene to avoid losing the silica particles from the surface. However, the trend of increasing the amount of adsorbed material on the surface of the particles before and after the onset of asphaltene precipitation is similar in both methods.

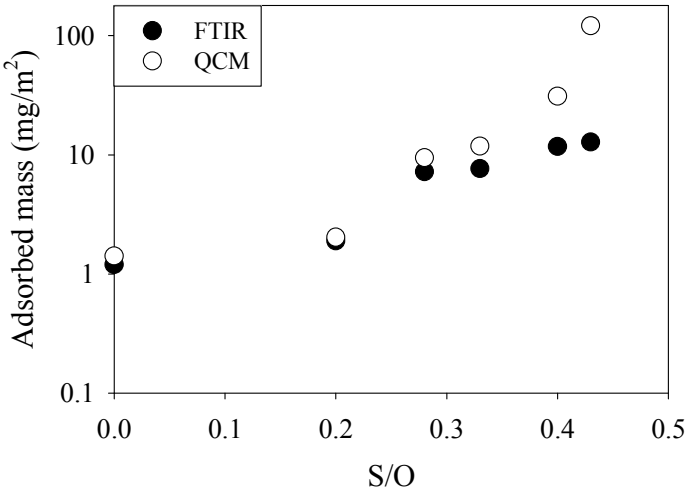

Figure 6-7 Amount of asphaltene adsorption on hydrophilic silica particles with FTIR and QCM methods at various S/O

6.7.2.6 Kinetic study of asphaltene adsorption

Solutions with 0.05, 0.1, 0.25, 0.5, 1, and 1.5 g/L pitch in toluene were prepared to measure the rate of deposition. The gold-coated probe was immersed in these solutions for both short times and for 16 hours. The purpose of doing the experiments for 16 hours was to detremine if an equilibrium mass of deposit would be achieved. Running the experiment overnight showed that there was ongoing built up of asphaltene molecules on the surface of the gold over the entire time interval, and no equilibrium condition was observed over the duration of the experiment.

The adsorption experiments were run for each concentration for 1 hour. The adsorbed mass was plotted versus $t'^{1/2}$ ($t' = t - t_{\text{immersion of the quartz in the solution}}$). Figure 6-8 shows the adsorbed mass versus $t'^{1/2}$ for 0.05 and 1 g/L pitch in toluene. These slopes change linearly with $t'^{1/2}$ which indicate infinite adsorption kinetics and corresponds to a diffusion-controlled process.

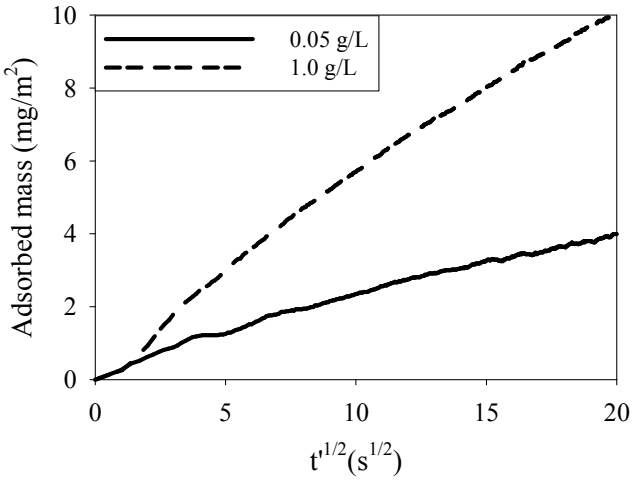

Figure 6-8 Comparison between the amount of adsorbed mass of asphaltene on gold versus $t'^{1/2}$ for 0.05 and 1.0 g/L pitch in toluene. Time $t' = 0$ corresponded to the instant that the probe was immersed in the solution

Figure 6-9 shows the comparison between the amounts of adsorbed mass versus $t'^{1/2}$ for various concentrations of the oil solution for the first 20 seconds of each experiment. These data show that the slopes of the adsorbed mass with $t'^{1/2}$ increased with increasing concentration, consistent with Abudu *et al.* (2009). These slopes were used to calculate the apparent diffusion coefficient using equation (6-13), and in turn the apparent diffusion coefficients gave the corresponding size of the asphaltene aggregates from the Stokes-Einstein equation

(See Table 6-9). The calculated size shows an increasing trend with increasing the concentration of pitch (and asphaltene) in toluene solution. Whereas, the diffusion coefficient kept decreaseing for higher concentration of asphaltene in toluene.

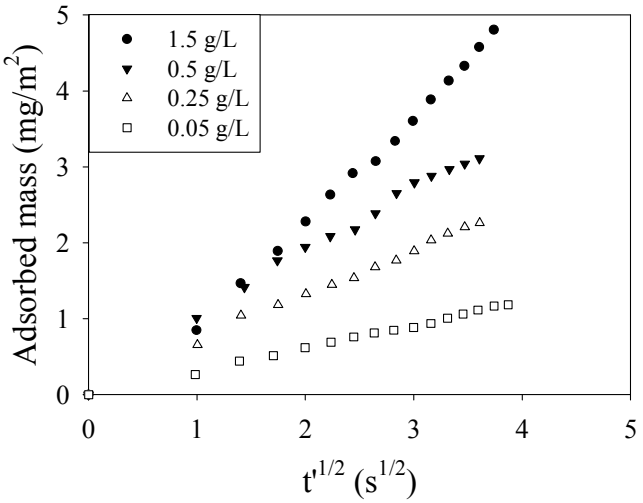

Figure 6-9 Mass of asphaltene deposited on gold during the first 20 s with different concentrations of pitch material in toluene

Table 6-9 Effect of the concentration of pitch material in toluene on the apparent diffusivity and apparent hydrodynamic diameter of adsorbed particles. Diffusion coefficients (D) are estimated from equation (6-13), and the diameter (d) is from equation (6-14)

Concentration (g/L)	**Slope $\times 10^{-7}$ ($kg \cdot m^{-2} \cdot s^{-1}$)**	**D $\times 10^{-12}$ (m^2/s)**	**Viscosity (mPa·s)**	**d (nm)**
0.05	3.05	21.8	0.545	18.22
0.1	3.83	6.74	0.546	46.0
0.25	6.39	9.86	0.545	102.2
0.5	9.24	2.68	0.547	191.9
1	11.6	1.16	0.549	472.0

Abudu *et al*. [34] and Xie *et al*. [21] used QCM and the same experimental method to calculate the diffusion coefficient for various concentrations of asphaltene in toluene. The results of their work are shown in Table 6-10.

Table 6-10 Literature results on the calculated size of asphaltene aggregates by using Stokes-Einstein equation

Abudu *et al.* (2009) [34]			**Xie *et al.* (2005) [21]**	
C_{asphal} (g/L)	**d (nm)**	**Our correction to Abudu work for calculating d (nm)**	**C_{asphal} (g/L)**	**d (nm)**
0.139	1.07 ± 0.29	Data not available	0.05	34
0.278	0.79 ± 0.17	1220	0.1	78
0.835	3.64 ± 0.97	Data not available	0.15	120
			0.2	110

Our results are similar to what Xie *et al.* [21] observed within a factor of two to three over the common range of concentration from 0.05 to 0.2 g/L; however, the size of the calculated asphaltene aggregates was at least an order of magnitude larger than the results of Abudu *et al*. [34]. The major difference between Abudu *et al*. and our work is the calculation of the time for determination of the slope by using equation (6-13). We used the difference between the recorded time and the time when the samples were immersed to calculate $t'^{1/2}$, giving values of the ordinate axis from 0 to 10 $s^{1/2}$ as illustrated in Figure 6-9. In contrast, Abudu *et al*. did not subtract the time before immersion, so their x-axis values included times before the samples were immersed, giving apparent slopes that were one order of magnitude smaller. Consequently, the calculated aggregate size in their work was an underestimate. This lack of correction for time was inconsistent with the

derivation of the governing equation 6-13. The size of the aggregates based on their work was recalculated and is shown in Table 6-9. By using the correct value for $t'^{1/2}$, we obtain similar trends for the size of the asphaltenes from their data to the experiments results on pitch.

The size of the asphaltene molecules from different sources has been estimated by different methods. Groenzin *et al.* evaluated the size of the molecular asphaltenes to be roughly 1.2 - 2.4 nm using depolarization techniques and by using theoretical models [53]. Schneider *et al.* used fluorescence correlation spectroscopy and estimated an average molecular size of 1.2 nm for a variety of asphaltene samples [54]. Chen *et al.* estimated the size of four different types of asphaltene to be in the range of 1.07 - 1.66 nm based on diffusion measurement by using a diaphragm cell [55]. Indo *et al.* observed molecular asphaltene with sizes around 2.6 nm by centrifugation [56]. Durand *et al.* estimated the size of asphaltenes to be 1.56 nm by using ^{1}H diffusion-ordered nuclear magnetic resonance spectroscopy [57]. Therefore, based on literature the molecular size of the asphaltenes can be estimated to be around ~ 1.2 – 2.6 nm.

Dechaine (2009) reported the size of the asphaltene aggregates to be 5 - 9 nm in 1 g/L asphaltene in toluene. Small-angle neutron scattering (SANS) and X-ray scattering (SAXS) gave estimates of the asphaltene aggregate size to be in the range of 3-11 nm [58, 59], and 3.3 - 25.2 nm [60]. Therefore, the size of asphaltene aggregates can be assumed to be around 5 - 25 nm, and almost certain a distribution of values in this range presents the size of asphaltene rather than a single value.

The calculated size of the asphaltene components in our work is much larger than the literature data based on scattering and diffusion, and increases significantly with concentration. Consequently, we conclude that the apparent diameters in Table 6-9 are invalid estimates, and we need to analyze the factors that could account for unreasonably small apparent diffusion coefficients. Some of the possible reasons for deviation of the apparent size of the asphaltene are presented below.

6.7.2.7 Potential error in estimated diffusion coefficients for aggregates

6.7.2.7.1 Liquid trapping

Asphaltene aggregates are assumed to have a fractal structure. In the case of measuring the amount of adsorbed asphaltene on the gold surface crystal by using QCM, the solvent is trapped in the porous structure of asphaltenes and are vibrated with the adsorbed mass.

Table 6-11 shows the result for the amount of change in the resistance during the adsorption part. Even though the changes in the resistance are very low, they are not zero. Therefore, the attached layer is not totally rigid and solvent swelling of the asphaltene aggregates would give an artificially large estimate of the mass of attached material. This result would also affect the apparent hydrodynamic radii that we determine from a kinetic curve.

Table 6-11 The change in Resistance and frequency during the adsorption part

Concentration (g/L)	ΔR during the adsorption part (Ω)
1.5	11
1	11
0.5	14
0.25	9
0.05	4

6.7.2.7.2 Activation barrier

Several investigators have measured the diffusion coefficient of asphaltenes in toluene. Durand *et al.* (2009) used ^{1}H diffusion-ordered spectroscopy (DOSY) nuclear magnetic resonance (NMR) to investigate the behavior of asphaltenes diluted in toluene for the concentration range of 0.01 to 15 wt %. The results show that the diffusivity is highly dependent upon solute concentration. At infinite dilution, the diffusion coefficient was estimated to be $2.4 \pm 0.1 \times 10^{-10}$ m^2/s [57]. Kawashima *et al.* (2008) used pulsed-field gradient spin-echo ^{1}H NMR to measure the diffusion coefficient for three types of asphaltenes from the vacuum residue of Khafji, Iranian Light and Maya crude oils over the range of 0.1 to 30 g/L asphaltene in toluene. The calculated diffusion coefficient for the three types of the asphaltenes was almost similar. For instance, for the Maya asphaltene, the diffusion coefficient was estimated to be 5.1, 2.2, 1.3, and 1.0×10^{-10} m^2/s for 0.1, 1, 10, and 30 g/L asphaltene in toluene, respectively [61]. Wargadalam *et al.* obtained a value of 6.26×10^{-10} m^2/s for a coal derived asphaltene using Taylor dispersion [62]. Ostlund *et al.* obtained a value of 5.7×10^{-10} m^2/s for a North Sea asphaltene using PFG-SE NMR [63]. Ballard *et al.* used fluorescence correlation

spectroscopy to obtain a value of 3.4×10^{-10} m^2/s for a UG8 asphaltene [64]. Lisitza *et al.* used stimulated-echo pulsed field gradient NMR to obtain a value of 2.9×10^{-10} m^2/s for UG8 asphaltenes at infinite dilution, and a value of $\sim1\times10^{-10}$ m^2/s at a concentration of 2.1 g/L [65]. Ostlund *et al.* found the infinite dilution diffusion coefficient for Venezuelan asphaltenes in toluene to be 2.2×10^{-10} m^2/s using pulsed field gradient spin echo NMR (PFG-SE NMR) [66]. Dechaine *et al.* (2009) estimated the diffusion coefficient of 0.1 g/L asphaltene in toluene solution to be around 0.52×10^{-10} m^2/s and 1.7×10^{-10} m^2/s for two different type of membrane. Therefore, the values for the infinite dilution diffusion coefficients of asphaltenes in toluene range from $2.2 - 6.3\times10^{-10}$ m^2/s.

Comparing the results of our work with the diffusion coefficient obtain in literature shows that the calculated diffusion coefficient in our work is much smaller. Particles approaching a solid surface can be trapped in a primary energy minimum. While capturing in the energy minimum the probability of escaping from the surface would be finite. Ward *et al.* (1946) mentioned that calculation of the diffusion coefficient by equation (6-5) assumes that instantaneous equilibrium is achieved between the surface and sub-surface. Therefore, no barrier should exist between the surface and sub-surface. If so, the calculated D is a complex parameter of both diffusion and the crossing of the barrier. In the presence of a barrier, the calculated D is smaller than the real diffusion coefficient.

The main problem is that no experimental work has yet been designed to investigate the nature of the barrier. However, if the bulk diffusion coefficient is known, from the calculated diffusion coefficient, the existence of the activation

barrier would be clear. In the presence of an energy barrier, the calculated D is much smaller than the bulk diffusion coefficient. If we assume that the calculated D for asphaltene in toluene solutions in the literature are the bulk diffusion coefficient, then our results can be evidence of the existence of an activation barrier between the surface of the gold and the subsurface which leads to lower apparent diffusion coefficients.

6.7.2.7.3 Parameters affecting the deposition of the particles on a solid surface

Some of the other parameters that affect the amount of the deposition of the particles on the surface are the hydrodynamic conditions around the solid particles. It is assumed that particles are deposited on smooth and clean solid surfaces, however, the roughness of the surfaces affect the particles deposition by creating tangential forces on the particles. These forces affect the number of particles that are attached to the surface. On the other hand coagulation of the particles may occur due to instability of the particles dispersion. All these parameters affect the coating characteristics and mass transfer rates of the aggregates to the surface.

6.8 Summary

The quartz crystal microbalance (QCM) and Fourier Transform Infra-Red (FTIR) methods were used to measure the asphaltene adsorption on gold surfaces

and silica particles having different hydrophobicities. The results from QCM and FTIR were in agreement with the results in chapter 4, demonstrating that even below this S/O value, adsorption of asphaltenes and possibly other components on solid surfaces was detectable. The amount of material adsorbed increased significantly after the onset of asphaltene precipitation. For instance, the amount of adsorption increased from 0.4 to 36 mg/m^2 when the solvent ratio increases from 0 to 0.5. Adsorption was more pronounced on the gold surface than on the silica particles, especially after the onset of asphaltene precipitation. For S/O = 0.43, for instance, the adsorption was 160, 125 and 75 mg/m^2 for gold surface, hydrophilic and hydrophobic silica particles, respectively. Hydrophilic silica particles adsorbed more material compared to hydrophoblic particles above the onset point; however, the adsorption amounts were similar below the onset point for both types of particles.

The solvent swelling of the aggregates were also studied at various S/Os showing more solvent trapped in the structure of the aggregates at higher S/O. Larger swelling effect is due to higher porous structure of the aggregates at higher S/O. The adsorbed materials at all ratios showed viscoelastic characteristics on the surface of the gold.

The experimental diffusion coefficient obtained by kinetic study using QCM led to incorrect size prediction of the asphaltene aggregates. The simple explanation for this discrepancy is due to the combined effects of the solvent and adsorbed asphaltene on the mass. Any reorganization of the deposits on the crystal to reduce solvent fraction appears as a loss of mass, which offsets the

adsorption from solution. This measurement of "net mass gain" is unreliable as a measure of adsorption rate. With increasing the rate of adsorption, the solvent restructuring becomes more significant; therefore, the apparent mass increase with time is reduced. The reduction in the mass measurements, lower the apparent diffusion coefficients as the rate of adsorption increases. Therefore, the obtained diffusion coefficients for asphaltene solution measured by QCM are lower than the results from other methods. As a result, the calculated diffusion coefficient calculated by Ward and Tordi equation and using QCM is not reliable. Modern theory considering proper interaction between the adsorbing asphaltene and the substarte may lead to better interpretation of these data.

6.9 References

[1] Rahmani, N. H. G., Dabros, T., and Masliyah, J. H., 2005, "Settling Properties of Asphaltene Aggregates," Energy and Fuels, 19(3) pp. 1099-1108.

[2] Yarranton, H. W., and Masliyah, J. H., 1996, "Molar Mass Distribution and Solubility Modeling of Asphaltenes," AICHE Journal, 42(12) pp. 3533-3543.

[3] Long, Y., Dabros, T., and Hamza, H., 2002, "Stability and Settling Characteristics of Solvent-Diluted Bitumen Emulsions," Fuel, 81(15) pp. 1945-1952.

[4] Jamialahmadi, M., Soltani, B., Muller-Steinhagen, H., 2009, "Measurement and Prediction of the Rate of Deposition of Flocculated Asphaltene Particles from Oil," International Journal of Heat and Mass Transfer, 52(19-20) pp. 4624-34.

[5] Hamadou, R., Khodja, M., Kartout, M., 2008, "Permeability Reduction by Asphaltenes and Resins Deposition in Porous Media," Fuel, 87(10-11) pp. 2178-2185.

[6] Rudrake, A., Karan, K., and Horton, J. H., 2009, "A Combined QCM and XPS Investigation of Asphaltene Adsorption on Metal Surfaces," Journal of Colloid and Interface Science, 332(1) pp. 22-31.

[7] Amin, J. S., Ayatollahi, S., and Alamdari, A., 2009, "Fractal Characteristics of an Asphaltene Deposited Heterogeneous Surface," Applied Surface Science, 256(1) pp. 67-75.

[8] Nabzar, L., and Aguilera, M. E., 2008, "The colloidal approach. A promising route for asphaltene deposition modelling," Anonymous Editions Technip, 27 rue Ginoux, Paris Cedex 15, 75737, France, 63, pp. 21-35.

[9] Ramirez-Jaramillo, E., Lira-Galeana, C., and Manero, O., 2006, "Modeling Asphaltene Deposition in Production Pipelines," Energy and Fuels, 20(3) pp. 1184-1196.

[10] Wang, S., and Civan, F., 2005, "Modeling Formation Damage by Asphaltene Deposition during Primary Oil Recovery," Transactions of the ASME.Journal of Energy Resources Technology, 127(4) pp. 310-17.

[11] Marczewski, A. W., and Szymula, M., 2002, "Adsorption of asphaltenes from toluene on mineral surface," Anonymous Elsevier, 208, pp. 259-266.

[12] Saraji, S., Goual, L., and Piri, M., 2010, "Adsorption of Asphaltenes in Porous Media Under Flow Conditions," Energy and Fuels, 24(11) pp. 6009-6017.

[13] Nassar, N. N., 2010, "Asphaltene Adsorption Onto Alumina Nanoparticles: Kinetics and Thermodynamic Studies," Energy and Fuels, 24(8) pp. 4116-4122.

[14] Marchal, C., Abdessalem, E., Tayakout-Fayolle, M., 2010, "Asphaltene Diffusion and Adsorption in Modified NiMo Alumina Catalysts Followed by Ultraviolet (UV) Spectroscopy," Energy and Fuels, 24(8) pp. 4290-4300.

[15] De, l. C., Castellanos-Ramirez, I., Ortiz-Tapia, A., 2009, "Study of Monolayer to Multilayer Adsorption of Asphaltenes on Reservoir Rock Minerals," Colloids and Surfaces A: Physicochemical and Engineering Aspects, 340(1-3) pp. 149-54.

[16] Alboudwarej, H., Pole, D., Svrcek, W. Y., 2005, "Adsorption of Asphaltenes on Metals," Industrial and Engineering Chemistry Research, 44(15) pp. 5585-5592.

[17] Goual, L., Horvath-Szabo, G., Masliyah, J. H., 2005, "Adsorption of Bituminous Components at oil/water Interfaces Investigated by Quartz Crystal Microbalance: Implications to the Stability of Water-in-Oil Emulsions," Langmuir, 21(18) pp. 8278-8289.

[18] Dudaova, D., Silset, A., and Sjoblom, J., 2008, "Quartz Crystal Microbalance Monitoring of Asphaltene Adsorption/ Deposition," Journal of Dispersion Science and Technology, 29(1) pp. 139-146.

[19] Hannisdal, A., Ese, M., Hemmingsen, P. V., 2006, "Particle-Stabilized Emulsions: Effect of Heavy Crude Oil Components Pre-Adsorbed Onto Stabilizing Solids," Colloids and Surfaces A: Physicochemical and Engineering Aspects, 276(1-3) pp. 45-58.

[20] Ekholm, P., Blomberg, E., Claesson, P., 2002, "A Quartz Crystal Microbalance Study of the Adsorption of Asphaltenes and Resins Onto a Hydrophilic Surface," Journal of Colloid and Interface Science, 247(2) pp. 342-350.

[21] Xie, K., and Karan, K., 2005, "Kinetics and Thermodynamics of Asphaltene Adsorption on Metal Surfaces: A Preliminary Study," Energy and Fuels, 19(4) pp. 1252-1260.

[22] Abdallah, W. A., and Taylor, S. D., 2008, "Study of Asphaltenes Adsorption on Metallic Surface using XPS and TOF-SIMS," Journal of Physical Chemistry C, 112(48) pp. 63-72.

[23] Pernyeszi, T., and Dekany, I., 2001, "Sorption and Elution of Asphaltenes from Porous Silica Surfaces," Colloids and Surfaces A: Physicochemical and Engineering Aspects, 194(1-3) pp. 25-39.

[24] Dudasova, D., Simon, S., Hemmingsen, P. V., 2008, "Study of Asphaltenes Adsorption Onto Different Minerals and Clays. Part 1. Experimental Adsorption with UV Depletion Detection," Colloids and Surfaces A-Physicochemical and Engineering Aspects, 317(1-3) pp. 1-9.

[25] Acevedo, S., Ranaudo, M. A., Garcia, C., 2000, "Importance of Asphaltene Aggregation in Solution in Determining the Adsorption of this Sample on Mineral Surfaces," Colloids and Surfaces A: Physicochemical and Engineering Aspects, 166(1-3) pp. 145-152.

[26] Costa, S. D., Farcas, F., Santos, L., 2010, "Chemical and thermal characterization of road bitumen ageing," 5th International Materials Symposium

Materials 2009 - 14th meeting of SPM - Sociedade Portuguesa de Materiais, April 5, 2009 - April 8, Anonymous Trans Tech Publications Ltd, Lisbon, Portugal, 636-637, pp. 273-279.

[27] Le Guern, M., Chailleux, E., Farcas, F., 2010, "Physico-Chemical Analysis of Five Hard Bitumens: Identification of Chemical Species and Molecular Organization before and After Artificial Aging," Fuel, 89(11) pp. 3330-3339.

[28] Chiaberge, S., Guglielmetti, G., Montanari, L., 2009, "Investigation of Asphaltene Chemical Structural Modification Induced by Thermal Treatments," Energy and Fuels, 23(9) pp. 4486-4495.

[29] Khvostichenko, D. S., and Andersen, S. I., 2009, "Electrodeposition of Asphaltenes. 1. Preliminary Studies on Electrodeposition from Oil-Heptane Mixtures," Energy and Fuels, 23(2) pp. 811-819.

[30] Gu, G., Zhang, L., Xu, Z., 2007, "Novel Bitumen Froth Cleaning Device and Rag Layer Characterization," Energy and Fuels, 21(6) pp. 3462-3468.

[31] Li, Y. Z., Xu, Z., and Masliyah, J. H., 2005, "Characterisation of Adsorbed Athabasca Asphaltene Films at Solvent-Water Interfaces using a Langmuir Interfacial Trough," Industrial and Engineering Chemistry Research, 44(5) pp. 1160-1174.

[32] Peralta-Martinez, M., Vazquez-Ramirez, R., Blass-Amador, G., 2008, "Determination of Functional Groups in Mexican Vacuum Residua," Petroleum Science and Technology, 26(1) pp. 91-100.

[33] Zhang, L. Y., Lopetinsky, R., Xu, Z., 2005, "Asphaltene Monolayers at a toluene/water Interface," Energy and Fuels, 19(4) pp. 1330-1336.

[34] Abudu, A., and Goual, L., 2009, "Adsorption of crude oil on surfaces using quartz crystal microbalance with dissipation (QCM-D) under flow conditions," Anonymous American Chemical Society, 2540 Olentangy River Road, P.O. Box 3337, Columbus, OH 43210-3337, United States, 23, pp. 1237-1248.

[35] Gaboriau, H., and Saada, A., 2001, "Influence of Heavy Organic Pollutants of Anthropic Origin on PAH Retention by Kaolinite," Chemosphere, 44(7) pp. 1633-1639.

[36] Drummond, C., and Israelachvili, J., 2004, "Fundamental Studies of Crude Oil-Surface Water Interactions and its Relationship to Reservoir Wettability," Journal of Petroleum Science and Engineering, 45(1-2) pp. 61-81.

[37] Gonzalez, G., and Middea, A., 1991, "Peptization of Asphaltene by various Oil Soluble Amphiphiles," Colloids and Surfaces, 52(3-4) pp. 207-217.

[38] Martin, S. J., Granstaff, V. E., and Frye, G. C., 1991, "Characterization of a Quartz Crystal Microbalance with Simultaneous Mass and Liquid Loading," Analytical Chemistry, 63(20) pp. 2272-2281.

[39] Reed, C. E., Kanazawa, K. K., and Kaufman, J. H., 1990, "Physical Description of a Viscoelastically Loaded at-Cut Quartz Resonator," Journal of Applied Physics, 68(5) pp. 1993-2001.

[40] Kanazawa, K. K., and Gordon, J. G., 1985, "The Oscillation Frequency of a Quartz Resonator in Contact with a Liquid," Analytica Chimica Acta, 175(SEP) pp. 99-105.

[41] Cho, N., D'Amour, J. N., Stalgren, J., 2007, "Quartz Resonator Signatures Under Newtonian Liquid Loading for Initial Instrument Check," Journal of Colloid and Interface Science, 315(1) pp. 248-254.

[42] Antonio Arnau Vives, 2008, "Piezoelectric transducer and applications," Springer-Verlag Berlin Heidelberg, Spain.

[43] Martin, B. A., and Hager, H. E., 1989, "Velocity Profile on Quartz Crystals Oscillating in Liquids," Journal of Applied Physics, 65(7) pp. 2630-2635.

[44] Martin, B. A., and Hager, H. E., 1989, "Flow Profile Above a Quartz Crystal Vibrating in Liquid," Journal of Applied Physics, 65(7) pp. 2627-2629.

[45] Muramatsu, H., Tamiya, E., and Karube, I., 1988, "Computation of Equivalent-Circuit Parameters of Quartz Crystals in Contact with Liquids and Study of Liquid Properties," Analytical Chemistry, 60(19) pp. 2142-2146.

[46] Viitala, T., Hautala, J. T., Vuorinen, J., 2007, "Structure of Anionic Phospholipid Coatings on Silica by Dissipative Quartz Crystal Microbalance," Langmuir, 23(2) pp. 609-618.

[47] Ward, A. F. H., and Tordai, L., 1946, "Time-Dependent of Boundary Tensions of Solutions. I. the Role of Diffusion in Time-Effects," 14(7) pp. 453.

[48] Elimelech, M., Gregory, J., Jia, X., 1995, "Particle deposition and aggregation : measurement, modelling and simulation,".

[49] Rahmani, N. H. G., Masliyah, J. H., and Dabros, T., 2003, "Characterization of Asphaltenes Aggregation and Fragmentation in a Shear Field," AICHE Journal, 49(7) pp. 1645-1655.

[50] Aung, K. M. M., Ho, X., and Su, X., 2008, "DNA Assembly on Streptavidin Modified Surface: A Study using Quartz Crystal Microbalance with Dissipation Or Resistance Measurements," Sensors and Actuators B-Chemical, 131(2) pp. 371-378.

[51] Zhou, L., Chen, H., Jiang, X., 2009, "Modification of Montmorillonite Surfaces using a Novel Class of Cationic Gemini Surfactants," Journal of Colloid and Interface Science, 332(1) pp. 16-21.

[52] Nordgard, E. L., Srland, G., and Sjoblom, J., 2010, "Behavior of Asphaltene Model Compounds at W/O Interfaces," Langmuir, 26(4) pp. 2352-2360.

[53] Groenzin, H., and Mullins, O. C., 1999, "Petroleum Asphaltene Molecular Size and Structure." Abstracts of Papers of the American Chemical Society, 218pp. 61.

[54] Schneider, M. H., Andrews, A. B., Mitra-Kirtley, S., 2007, "Asphaltene Molecular Size by Fluorescence Correlation Spectroscopy," Energy and Fuels, 21(5) pp. 2875-2882.

[55] Chen, Z., Xu, C., Gao, J., 2010, "Hindered Diffusion of Residue Narrow Cuts through Polycarbonate Membranes," AICHE Journal, 56(8) pp. 2030-2038.

[56] Indo, K., Ratulowski, J., Dindoruk, B., 2009, "Asphaltene Nanoaggregates Measured in a Live Crude Oil by Centrifugation," Energy and Fuels, 23(9) pp. 4460-4469.

[57] Durand, E., Clemancey, M., Lancelin, J., 2009, "Aggregation States of Asphaltenes: Evidence of Two Chemical Behaviors by 1H Diffusion-Ordered

Spectroscopy Nuclear Magnetic Resonance," Journal of Physical Chemistry C, 113(36) pp. 16266-16276.

[58] Gawrys, K. L., Blankenship, G. A., and Kilpatrick, P. K., 2006, "On the Distribution of Chemical Properties and Aggregation of Solubility Fractions in Asphaltenes," Energy and Fuels, 20(2) pp. 705-714.

[59] Sirota, E. B., 2005, "Physical Structure of Asphaltenes," Energy and Fuels, 19(4) pp. 1290-1296.

[60] Fenistein, D., and Barre, L., 2001, "Experimental Measurement of the Mass Distribution of Petroleum Asphaltene Aggregates using Ultracentrifugation and Small-Angle X-Ray Scattering," Fuel, 80(2) pp. 283-287.

[61] Kawashima, H., Takanohashi, T., Iino, M., 2008, "Determining Asphaltene Aggregation in Solution from Diffusion Coefficients as Determined by Pulsed-Field Gradient Spin-Echo 1H NMR," Energy and Fuels, 22(6) pp. 3989-3993.

[62] Wargadalam, V. J., Norinaga, K., and Iino, M., 2002, "Size and Shape of a Coal Asphaltene Studied by Viscosity and Diffusion Coefficient Measurements," Fuel, 81(11-12) pp. 1403-1407.

[63] Ostlund, J., Nyden, M., Auflem, I. H., 2003, "Interactions between Asphaltenes and Naphthenic Acids," Energy and Fuels, 17(1) pp. 113-119.

[64] Andrews, A. B., Guerra, R. E., Mullins, O. C., 2006, "Diffusivity of Asphaltene Molecules by Fluorescence Correlation Spectroscopy," Journal of Physical Chemistry A, 110(26) pp. 8093-8097.

[65] Lisitza, N. V., Freed, D. E., Sen, P. N., 2009, "Study of asphaltene nanoaggregation by nuclear magnetic resonance (NMR)," Anonymous American

Chemical Society, 2540 Olentangy River Road, P.O. Box 3337, Columbus, OH 43210-3337, United States, 23, pp. 1189-1193.

[66] Ostlund, J., Andersson, S., and Nyden, M., 2001, "Studies of Asphaltenes by the use of Pulsed-Field Gradient Spin Echo NMR," Fuel, 80(11) pp. 1529-1533.

[61] Konash, P. L., & Bastiaans, G. J. (1980). Piezoelectric-Crystals as Detectors in Liquid-Chromatography. Analytical Chemistry, 52(12), 1929-1931.

7 Measuring the forces on asphaltene coated surfaces in organic solutions by using AFM

7.1 Introduction

Atomic Force Microscopy (AFM) is a powerful and important tool for analyzing the topography and characteristics of surfaces. In addition, AFM can be used to measure the forces between solid surfaces (substrate and the cantilever tip) either in air or liquid over length scales of 0.1 - 100 nm due to electrostatic interactions, van der Waals forces, chemical interactions, and steric effects. Force measurements between surfaces have been reported extensively in literature in various fields such as polymers, bacterial studies, petroleum research, etc. [1-8]. However, measuring the force interactions between asphaltene coated surfaces in organic solvents is a novel and important area of research.

Knowing the nature of interaction between the asphaltene molecules, asphaltenes with surrounding solvent and asphaltene in vicinity of solid surfaces gives valuable information about the precipitation behavior of asphaltene. Van der Waals and steric forces are the main forces that are observed between asphaltene

surfaces in organic solvents [7]. Many researchers have measured the forces in aqueous systems using AFM. However, force measurement in non-aqueous systems has been studied less due to difficulties with liquid cell of AFM. There are only a few publications applying force measurements in non-aqueous media [6, 7, 9]. Yet, there is no single agreement on the interaction mechanism of asphaltene aggregation. Therefore, there is a need for direct measurement of interaction between asphaltene surfaces in non-aqueous environments to investigate the behavior of deposited asphaltene on solid surfaces.

In chapter 4, destabilization of silica particles occurred at S/O lower than the destabilization of asphaltene due to addition of pentane. Flocculation and sedimentation of the suspended silica particles were observed even below the onset of asphaltene precipitation. The QCM results in chapter 6 showed that asphaltene adsorption on any types of solids occur in oil solution. The data showed that the amount of asphaltene deposition on the gold surface increases significantly after the onset of asphaltene precipitation. Here, by using AFM we want to measure the interactions between adsorbed asphaltene at various S/O deposited on the gold surface with the cantilever tip. By measuring the interaction forces, we would observe the type of interactions that exist between asphaltene coated surfaces and bare surfaces.

QCM results show that the deposition of asphaltene on gold and on silica particles (both hydrophilic and hydrophobic) follows the same trend with S/O. Therefore, we expected that if we measure the interaction forces between the gold surfaces coated with precipitated asphaltene, the same interaction could be

modeled between coated silica particles. In this chapter, we want to analyze if the interaction forces between solid surfaces (regarding the adhesion forces, the deflection distance for the cantilever, etc) in the presence of asphaltene would follow a similar trend with S/O as in previous chapters, i.e. the interaction would increase for higher S/O.

In addition, previous studies with AFM imaging showed that asphaltene precipitation on solid surfaces gives a heterogeneous deposition. By using force measurements we want to see how the heterogeneous deposition of asphaltenes on surfaces would change at various S/O.

7.2 Forces between colloidal particles

Colloidal interactions are short range forces and do not extend to distances that are larger than the size of the particles. The dominant interactions between the colloidal particles are the universal attractive van der Waals forces, the repulsive electric double layer forces (in aqueous media) and steric forces (mainly in non-aqueous media) [10-12]. Here, we give a brief review about the nature of these forces in colloidal systems.

7.2.1 Van der Waals interactions

The attractive force between atoms and molecules is known as van der Waals forces (VDW). Atoms and molecules can be electrically uncharged. Polar molecules have a permanent dipole moment. A non polar molecule, on the other

hand, can have an induced dipole moment under an electric field. Therefore, all the molecules can be charged instantaneously. Fluctuation of the electronic cloud in one material can cause a corresponding fluctuation in a neighboring material, leading to an attractive force between the particles. The attraction between the particles depends on the particles size, the distance between them and the nature of the particles [13].

The expressions for the attractive forces were derived with the assumption that the speed of light is infinite. The correction due to the finite speed of light is called the retardation correction [13].

The unretarded VDW interaction energy between a sphere of radius *a* and an infinite flat plate can be calculated from Hamakar's approach as follows:

$$F_{VDW} = -\frac{A_H}{6}\left[-\frac{a}{h^2} - \frac{a}{(h+2a)^2} + \frac{2a}{h(h+2a)}\right] \tag{7-1}$$

where h is the closest approach between the two bodies and A_H is the Hamaker constant. In the Hamaker's approach (1937), the dispersion potential between two colloidal particles is the summation of the dispersion interaction between pairs of atoms located within the two particles. For complicated geometries, application of Hamaker's approach is troublesome and approximate techniques are used to evaluate the interaction energies.

One of the classical techniques used for approximate evaluation of VDW interaction energy is the Derjaguin approximation [12]. In Derjaguin approximation the two opposing section of the surfaces are treated as parallel plates. The dispersion potential is then the summation of the interaction between these parallel plates.

The unretarded van der Waals interaction force using Derjaguin's approximation between a spherical particle of radius *a* and an infinite flat plate is as follows:

$$F_{VDW} = -\frac{A_H a}{6h^2} \tag{7-2}$$

The Hamaker constant accounts for the material properties. For two bodies of composition 2 and 3 and medium 1 the Hamaker constant is as follows:

$$A_{213} = \left(A_{33}^{1/2} - A_{11}^{1/2}\right)\left(A_{22}^{1/2} - A_{11}^{1/2}\right) \tag{7-3}$$

When the bodies are similar, i.e. $A_{22} \equiv A_{33}$, equation (7-3) gives:

$$A_{212} = \left(A_{11}^{1/2} - A_{22}^{1/2}\right)^2 \tag{7-4}$$

For all the values of A_{11} and A_{22}, equation (7-4) is positive. This result indicates that for similar bodies, energy of interaction calculated from equation (7-2) is always negative which means that the interaction between similar bodies is always attraction [12].

7.2.2 Van dar Waals interactions with retardation

Suzuki *et al.* proposed the retarded VDW attraction between a sphere and an infinite planar surface to be as follows:

$$\frac{F_{VDW}}{a} = -\frac{A_H}{6}\frac{\bar{\lambda}\left(\bar{\lambda} + 22.232h\right)}{h^2\left(\bar{\lambda} + 11.116h\right)^2} \tag{7-5}$$

where *a* is the particles radii, A_H is the Hamaker constant for interaction between surfaces, $\bar{\lambda}$ is the London retardation wavelength (usually being of the order of 10^{-7} m) and *h* is the distance between the sphere and the infinite surface [14, 15].

7.2.3 Comparing the forces in aqueous and non aqueous media

The electric double layer is of great importance when studying colloidal particles immersed in an aqueous or polar medium. In non-aqueous and non-polar media on the other hand, the double layer phenomenon seems to be relatively insignificant. The minor effect of the double layer in such settings is related to the small values of dielectric permittivities and refractive indices of non-polar fluids. As ions have very low solubilities in non-polar liquids, the diffuse part of the double layer does not form. In non-aqueous systems, therefore, the concept of the double layer thickness or the Debye length is undefined and one can claim that for such systems the Debye length is equal to infinity [16].

Debye-Hückel approximation gives the electrical potential as follows:

$$\psi = \psi_0 \exp(-\kappa x) \tag{7-6}$$

where, κ is the Debye-Hückel parameter. Electric potential is equal to ψ_0 at the surface and is zero in the bulk. This distance '$\frac{1}{\kappa}$' is known as the "double layer thickness".

In order to have strong repulsive forces between the particles in a dispersed system, a large potential gradient (i.e. $-\frac{d\psi}{dx}$) is required in addition to high surface potentials. As these conditions are not satisfied in non-aqueous medium, strong electrostatic repulsion cannot be present between the particles dispersed in such systems [13]. However, stabilized non polar systems have been observed. This can be an evidence of electrostatic region between the particles. However, the magnitude and range of these forces is unknown [16]. The dominant type of

interaction in non-aqueous systems containing polymers is known to be of steric nature. For the approaching surfaces covered with polymers, the main interaction forces are steric repulsive forces. The attached polymers can have large sizes; therefore, the range of these forces can be much larger than VDW forces [13].

7.3 Atomic Force Microscopy (AFM)

7.3.1 Basic principles of AFM

AFM was first used by Binnig *et al.* in 1986 to image the topography of surfaces in nanometer scales. AFM uses a sharp tip mounted at the far end of a flexible cantilever as a probe. The probe scans the surface and by measuring the deflection of the cantilever and using the interaction between the tip and the surface of the sample an image can be built. AFM has the ability to image in air and liquid media.

The cantilevers that are used in AFM are normally made of silicon nitride. The cantilevers are mainly V-shaped or rectangular and are used as the probe for identifying the interactions between surfaces. The tips of the cantilevers are square-based pyramid or a cylindrical cone. The coating of the tip is normally either gold or aluminum.

A simple schematic of AFM is shown in Figure 7-1. Optical lever detection is the most common method used in AFMs to sense the force on the cantilever. Piezos are used as actuators for AFM scanners to bring the sample towards and away from the surface. Movement in this direction is referred to as z-direction. In

the MFP-3D^{TM} (Asylum research, Santa Barbara, US) a photodiode shines onto the back of the cantilever which is mounted at roughly eleven degrees with respect to the sample. A lens focuses the light on the cantilever. The light beam reflected from the cantilever is received by a sensitive photodetector. Any deflection of the cantilever, changes the position of the laser and the photodiode monitors these changes. The position of the reflected beam on the photodiode is determined by the angle of the deflected cantilever.

The configuration of the photodiode is normally a quadrant divided into four similar parts shown in Figure 7-1. Depending on the amount of light that each segment receives, a voltage is generated proportionally.

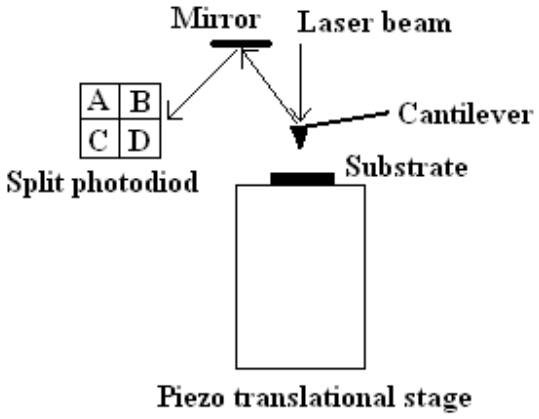

Figure 7-1 Schematic of AFM

The deflection is the difference between the detected signals from the upper and lower two halves of the detector (i.e. Deflection = $V_{A+B} - V_{C+D}$). The lateral, however, is the difference between the detected signals from the left and right halves of the detector. When the cantilever is not deflected the light source hits the centre of the photodiode. However, when the cantilever is deflected it creates

either positive or negative signals. The deflection is positive when more light hits the upper level and it happens when the spot moves upward. This is the case when the cantilever goes through a repulsive force and it deflects upward. When the cantilever experiences an attractive force (as it pushes down on the surface) it deflects downward and the spot moves down on the detector. More light hits the bottom than the top, so the deflection becomes negative.

When the probe is in contact with the surface, from the information of the deflection, height information of the topographic features of the surface are detected and an image can be created. More details on the AFM force measurements will be described in the following section.

7.3.2 Modes of operation in AFM

Contact Mode: In this mode the tip remains in continuous contact with the surface while transferred over the sample. This mode is associated with high shear forces, which can remove the sample from the substrate or damage the surface. This mode is not suitable for soft samples.

Ac Mode (Tapping Mode): In AC mode the damage to the sample surface due to the tip of the cantilever would be minimized. In this mode, the AFM tip taps the sample surface at the end of an oscillation cycle instead of dragging the tip along the surface. The destructive effects on the surface are reduced by using this mode.

7.3.3 AFM force measurement

The AFM has evolved from an imaging tool into a powerful instrument that can probe intermolecular forces at specified locations on a sample surface. Force is measured in the AFM tool as the deflection of the cantilever versus the distance between the sample and the surface along the z-axis. Hook's law is used to calculate the force:

$$F = -k \cdot D \tag{7-7}$$

where k is the spring constant of the cantilever and D is the cantilever deflection.

A force curve is a plot of the measured deflection versus the displacement of the z-piezo device. Normalization has to be applied to the deflection-distance data to obtain a force-distance curve. Description of the normalization procedure can be found elsewhere [17]. Attractive forces lead to a negative cantilever deflection, whereas repulsive forces lead to a positive cantilever deflection.

7.3.4 Approach and retraction curves

There are two types of operating models in a typical force measuremen: approach and retraction. The approach curve gives information on the cantilever deflection when the tip is going towards the surface; however, the retraction curve contains deflection data when the cantilever is separating from substrate and going away. The steps for the approach and retraction curves are shown in Figure 7-2. The red line is the approach curve and the black line shows the retraction curve. When the tip is far away from the surface, there is no interaction between the tip and the substrate; therefore, forces are absent and the cantilever is not

deflected (a). When the tip approaches the surface, a repulsive long-range force or attractive force can be distinguished (b). The dominant force between two similar approaching bodies in a low-dielectric medium is van der Waals. This force results in a negative deflection just before the contact of the tip with the surface in the approach curve. This negative deflection is often very sharp. If the force between the approaching bodies is repulsive, then the deflection is positive and starts increasing as the tip go closer to the surface. As the tip moves closer to the substrate, the surface force exerted by the tip increases and a mechanical instability known as snap-in occurs. Snap-in is due to similar values of the positive force gradient and the spring constant. For hard substrates, the sample displacement and cantilever deflection are proportional; therefore, the slope of the force curve becomes -1 (contact line). The distance between the tip and the sample remains constant along this contact line (c).

After the contact is made, the tip is retracted from the substrate. This retraction leads to a positive deflection which decreases continuously until the point where the tip is separated from the sample surface i.e. snap-off point (d). The retraction curve sometimes follows the approach curve; however, often hysteresis is observed. The hysteresis is normally due to adhesion between the tip and the surface and it appears as a minimum in the force plot (negative deflection). After the tip pulled off the substrate, the tip is disconnected from the surface and the deflection becomes zero as the cantilever returns to its natural state (e).

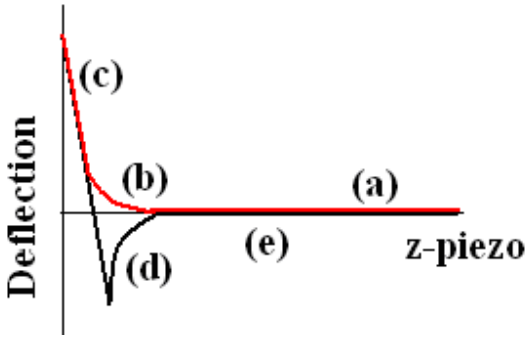

Figure 7-2 The steps of the approach and retraction curve; the red line is the approach curve and the black line shows the retraction curve

(a) The tip is far away from the surface; no interaction between the tip and the substrate; (b) The tip approaches the surface; a repulsive long-range force (positive deflection) or attractive force (negative deflection) can be distinguished; (c) The tip moves closer to the substrate; a mechanical instability known as snap-in occurs; (d) Snap-off point; negative deflection due to adhesion; (e) The tip pulls off the substrate, zero deflection.

Different features for the approach and retraction curves can be observed due to the forces between the tip and the surface. On the approach curve, the repulsive forces are mainly due to long-range electrostatic (for like charges) in aqueous media and polymer-brush and steric forces in non-aqueous media. These forces appear as a positive deflection on the approach curve (Figure 7-2- red line). The attraction force is due to van der Waals interaction which appears as a negative deflection on the approach curve (Figure 7-3 (a)-red line). In the retraction curve, the attraction between the tip and the surface before the snap off point can be due to capillary forces and polymer extension.

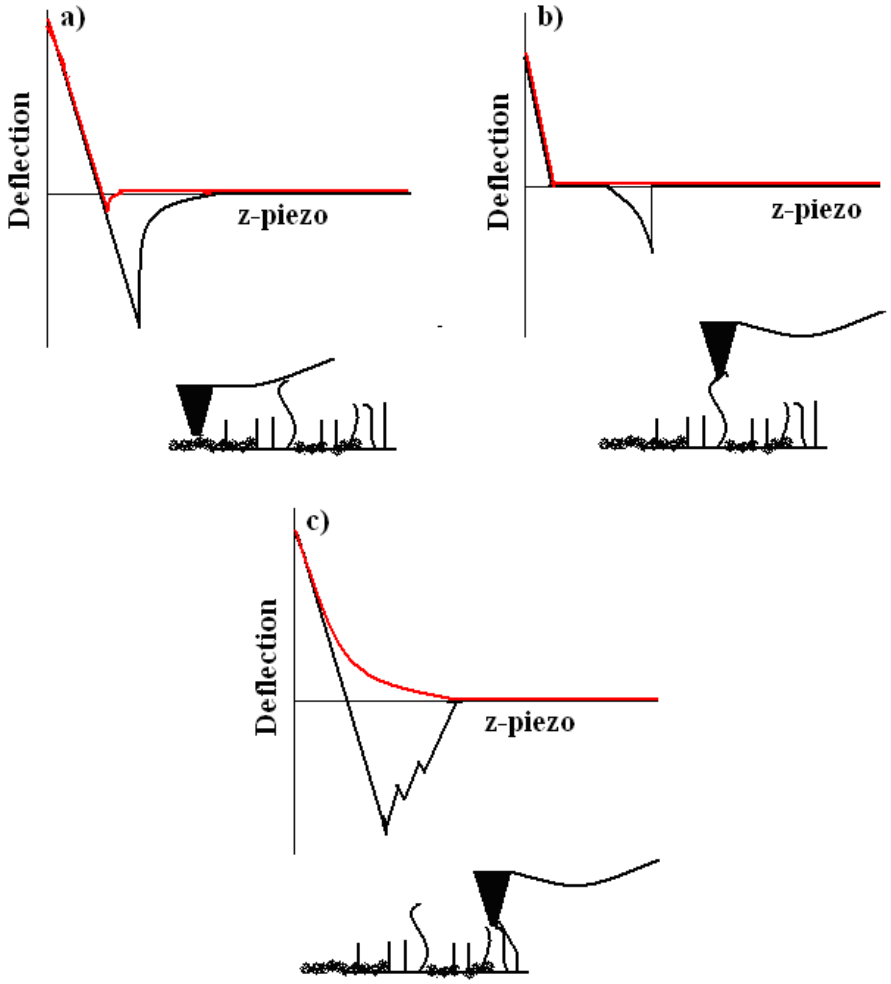

Figure 7-3 Different features of the approach and retraction curve; red line shows the approach curve and the black line is the retraction curve

Approach curves: a) van der Waals attraction forces; c) long range repulsion forces. Retraction curves: a) Simple adhesion; b) Attachment of loose structures to the tip; c) Attachment of multiple hairy structures to the tip

In air, nanometer-sized water droplets exist on most of the samples and form a bridge between the tip and the surface. Pulling the tip out of the bridge deflects

the cantilever negatively and leads to an attractive force between the tip and the surface. In solvents, however, the deflection extension of the cantilever due to adhesion can change depending on the characteristics of the solvent. When polymers exist on the surface or in the case of our work, asphaltene aggregates are deposited on the substrate, different types of adhesive forces can occur between the tip and the substrate. If there is simple adhesion of the aggregates to the tip, we refer to it as **simple** structure which is the black line shown in Figure 7-3 (a). When a loose aggregate is attached to the tip, the aggregate stretches until it breaks or detaches. In this case, we refer to this type of adhesion in the retraction curve as **loose** structure. The retraction curve follows the approach curve near the surface.

However, away from the surface, a negative deflection is observed in the retraction curve and the cantilever returns to the zero-deflection line (Figure 7-3 (b) - black line). If multiple asphaltene aggregates attach to the tip and substrate, there is a sequential unbinding of the attached aggregates from the tip. Therefore, a stepwise return to the zero deflection line is observed in the force plot (Figure 7-3 (c) - black line). We refer to this type of structure as **multiple** structure [17].

7.4 Literature on AFM force measurements for asphaltene coated surfaces

In this section, a brief review is presented on the few prior papers about the interaction of asphaltene surfaces in organic solvents.

Wang *et al.* studied the interactions between deposited asphaltene on oxidized silica wafers (using a mixture of nitric acid and hydrogen peroxide for oxidizing the wafers) and silica spheres by using AFM in organic solvents in two different studies.

Oxidized silica wafers and silica spheres, either by a Langmuir−Blodgett deposition technique (LB asphaltene film) or a dip-coating method, was coated with asphaltenes from a 2 mg/ml asphaltene-toluene solution. The thickness of the asphaltene film by LB method was 4 nm, which did not decrease while soaking in toluene. On the other hand, the thickness of the film in the dip coating method was 10 nm, which reduced to 3.5 nm while soaking in toluene for several minutes. The 3.5 nm film thickness remained constant by further soaking in toluene which shows irreversible deposition of asphaltene on the silica wafer. The tapping mode was chosen for imaging.

The studies focused on how different ratios of heptol and coating method effect the force interactions. In pure toluene, steric long-range repulsion was detected in the approach curves between asphaltene coated surfaces. However, for lower volume fraction of toluene in heptol, the steric repulsion was decreased and a weak attraction at a ratio of toluene/heptane < 0.2 was observed in the approach curves [7, 9].

The results showed that the preparation method can effect the magnitude and range of the repulsive forces. In the LB method, compact and organized deposited asphaltenes on the surface resulted in higher and a longer range of the repulsive forces as compared to the interaction on asphaltene surfaces prepared by the dip

coating method. No adhesion was observed between the coated surfaces in the retraction curves. The deposition of asphaltenes on surfaces, however, was less organized when the dip-coating method was used. In the dip coating method, there is no compression on the surface of the wafers for asphaltene deposition. Wang *et al.* assumed that when preparing the coated surfaces by the dip coating method, asphaltene tangles to the surface by some portion of the polar parts in its structure, while leaving the rest of the polar parts extending into the solvent. Therefore, bridging of the polar parts could occur between two silica surfaces coated with asphaltene. On the other hand, in LB method all the polar parts of the asphaltene molecules are attached to the substrate leaving no free polar structures in the solvent.

The retraction curves in the dip coating method showed hysteresis. The magnitude of repulsion forces would decrease for the surfaces that are prepared by dip coating method as some attraction occurs between the polar parts of the approaching surfaces. For instance, at a distance of 10 nm, the magnitude of the interacting forces was estimated to be 1.26 ± 0.15 and 0.93 ± 0.14 mN/m for the LB coating and the dip coating method, respectively [9].

In another study by Long *et al.* (2007), asphaltenes from a 2 mg/ml asphaltene in toluene solution were deposited on mica substrate and the forces were measured by using a silicon nitride cantilever. The mica surface was left in 2 - 3 ml of asphaltene solution and the toluene was allowed to evaporate. The substrate was then washed with deionized water to remove the unattached asphaltene to the mica sheets. The medium was chosen to be water, heptane and toluene. The main

focus of the work was to establish the length of the extended aggregates (L_{max}) and the maximum pulling force of the aggregates (F_{max}). The modified worm like chain model (M-WLC) was used to model the length and rupture strength of the aggregates.

Electrostatic repulsion was observed between the asphaltene aggregates in water. The large asphaltene aggregates present on the substrate were negatively charged due to ionization in aqueous media. In contrast, asphaltene molecules are neutral in organic solvents, such as heptane. The L_{max} in deionized water was in the range of 100 - 300 nm, as compared to 300 - 900 nm in heptane. Therefore, the aggregates sizes were longer and higher rupture forces were obtained in n-heptane (0.3 - 0.6 nN) than in deionized water (0.15 - 0.3 nN). The asphaltene aggregates were stretched in heptane indicating that the asphaltene aggregate under pulling forces would act as a worm-like polymer chain. The force measurement in toluene did not show any stretching of the aggregates due to solubility of the asphaltenes in toluene [6].

Amin *et al.* studied the heterogeneous property of asphaltenes on glass substrate by AFM. Asphaltene (the concentration of asphaltene in the solution was not mentioned) in toluene/heptane solution (3:1) was deposited on glass substrate at various pressures in a high pressure cell (maximum working pressure was 200bar) at 100°C. At P = 35 bar, asphaltenes started precipitating. The glass substrate was left for 2 hours in the pressure cell and afterward the solvents were drained and the coated glass substrate was used for the AFM imaging (the AFM mode was not mentioned in this work). Heterogeneous surfaces were observed by

AFM imaging in all the pressures. By increasing the pressure inside the pressure cell to 90 and 135 bar, the precipitated asphaltene was detached from the gold surface. For p = 35 bar, the precipitated asphaltene created tall peaks on the surface. The height of the peaks, on the other hand, became shorter for higher pressure. At higher pressure, solubility of the asphaltene in the solution increases; therefore, the heights of the peaks became shorter.

The existing literature in the force measurements in the organic solvents media was discussed above. The differences between our research and these studies are presented in the following paragraphs.

Wang *et al.* studied the force measurement between gold substrate and cantilever tip both coated with asphaltene. However, in our work, only the substrate was coated with asphaltene and the force measurement was measured between asphaltene coated substrate and clean cantilever. The other difference between the two works was the asphaltene concentration in the solution. The concentration of asphaltene in toluene solution was 2 mg/ml in Wang *et al.*'s research. However, we used a model oil solution with 45.57 g/L of pitch in toluene.

The other difference between Wang *et al.*'s work and ours is in the preparation of the coated substrate for the force measurement. In their work, the gold substrates were coated with the same material in all sets of experiments. On the other hand, in our work, the gold substrate was coated with precipitated asphaltene at various S/Os which leads to different types of materials on the gold surface.

7.5 Materials and Methods

7.5.1 AFM instrument: MFP-3D™

The instrument used to measure the forces was MFP-3D™ (Asylum Research Centre, Santa Barbara, CA). The view of the instrument is showing in Figure 7-4.

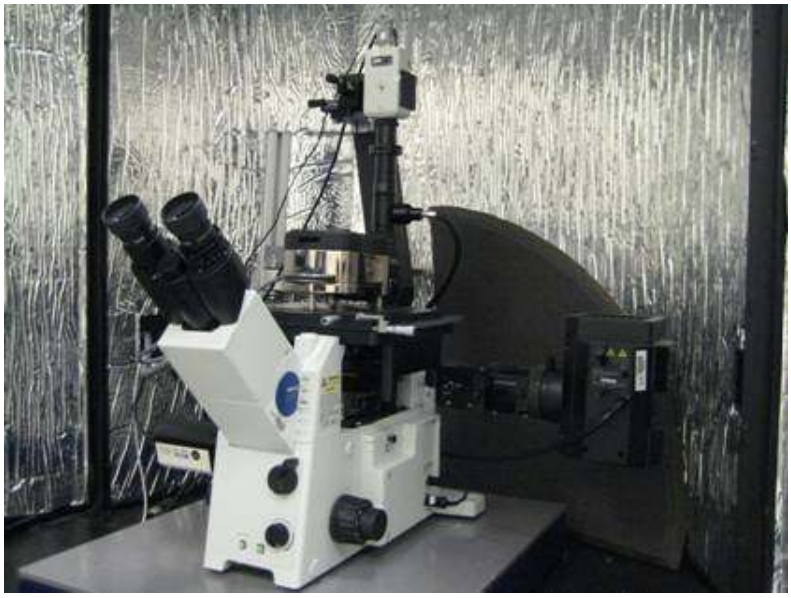

Figure 7-4 View of MFP-3D™

7.5.2 AFM Tip: TR400PB

In all the experiments the TR400PB cantilever (Asylum Research Centre, Santa Barbara, CA) was used. TR400PB has two levers which makes it useful for both AC and contact mode and for imaging and force measurements. For force measurement on hard surfaces the smaller lever should be used. The vendor specification of the lever and the tip is shown in Table 7-1 and Table 7-2, respectively. The SEM (Scanning Electron Microscopy) image of the lever and the tip is shown in Figure 7-5.

Table 7-1 TR400PB lever specification

Spring k (N/m)	0.09 (0.03 - 0.26)
Frequency (kHz)	32 (20 - 49)
Length (µm)	100 (90 - 110)
Shape	Triangular
Material	Silicon nitride
Reflex Coating (nm)	Cr/Au (5/50)

Table 7-2 TR400PB tip specification

Tip radius (nm)	42 ± 12
Tip shape	4-sided
Tip material	Silicon nitride
Tip coating (nm)	Cr/Au (5/40)

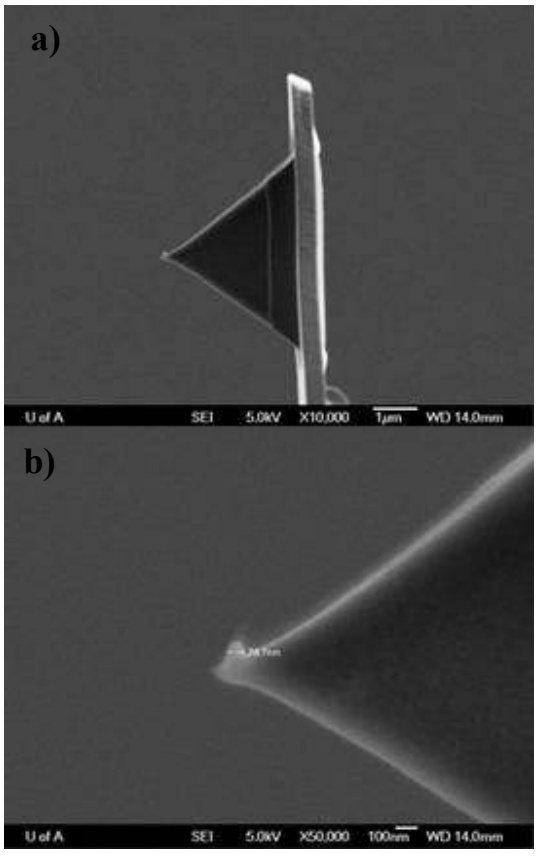

Figure 7-5 a) Lever of TR400PB, b) Cantilever tip

7.5.3 Closed cell

While performing the AFM measurements in liquid, for non–volatile solvents, the solvent can easily be placed on top of the substrate. However, working with volatile solvents such as toluene and pentane makes it necessary to use the closed cell to avoid evaporation of the solvent during the experiment. The closed cell configuration is shown in Figure 7-6.

Due to strong solvency of toluene, the materials for various parts of the closed cell should be resistant to this solvent. Therefore, the material for the closed cell was chosen to be Viton to eliminate the corrosion with these solvents.

Figure 7-6 Closed cell

7.5.4 Deposition of precipitated asphaltenes on gold surface

The gold surface (Gold500C, Asylum research centre) was cut into 1 cm×1 cm pieces and was glued to a 35 mm×1 mm glass disc (Figure 7-7). A two component thermal glue (EP21LV) purchased from Master Bond Epoxy (Hackensack, NJ, USA) was used to glue the gold pieces to the glass disc. The two components of the EP21LV glue were mixed with the same ratio and the gold pieces (substrate) were glued to the glass disc and left for 48 hours. This two component thermal glue is resistant to toluene and pentane solvents.

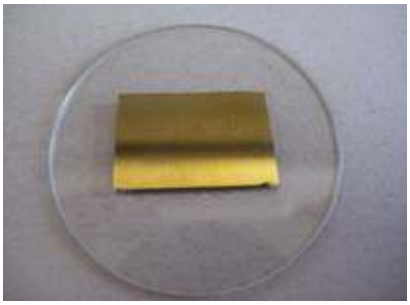

Figure 7-7 Gold piece on a 35mm×1mm glass disc

In the QCM experiments (chapter 6), the quartz crystal was left in the oil solution for 2 hours; therefore, in the AFM experiments, this timing (2 hours) was also chosen for coating the gold substrate with asphaltene. The gold substrate was left in the oil solution (oil-toluene-pentane) at various S/O (0 - 0.5) for 2 hours. After removing the substrate from the solution and rinsing with toluene, the substrate was quickly installed in the closed cell. The medium for each experiment was toluene-pentane with the same ratio of oil-toluene-pentane. After the closed cell was installed, it was sealed and 2 ml of the solvent was injected to the closed cell by means of Luer-Lok tip BD 5 mm syringe (Figure 7-6).

7.5.5 Cleaning procedure for the gold substrates

After each experiment the gold substrate was left in chloroform for 24 hours and in toluene for another 24 hours. It was expected that this procedure removes the deposited asphaltene from the gold surfaces.

7.5.6 Force measurements by AFM

A silicon nitride TR400PB cantilever was used as received. The actual spring constant of each cantilever was calibrated using the thermal tune method. Force measurements were carried out in an organic solvent (pentane-toluene) in the fluid closed cell. After injecting the solvent in the closed cell, the system (the substrate, tip and liquid) was left for 10 minutes to reach equilibrium prior to force measurements. Then the substrate was brought into contact with the AFM tip. The photodiode records the deflection of the cantilever as a function of the AFM piezo displacement. The data generated by the AFM instrument for the approach and retraction curves are the deflections versus z-piezo distances shown in Figure 7-8. This data needs normalization to convert to force-separation distance curves. The normalization procedure can be found elsewhere [17].

All force measurements were conducted at room temperature. For each S/O, the experiment was repeated twice and the force curves were obtained at five different points on the gold surface. For S/O = 0.43 which is the onset of precipitation, the force measurements were conducted at 30 points on the substrate. A new cantilever was used for each experiment.

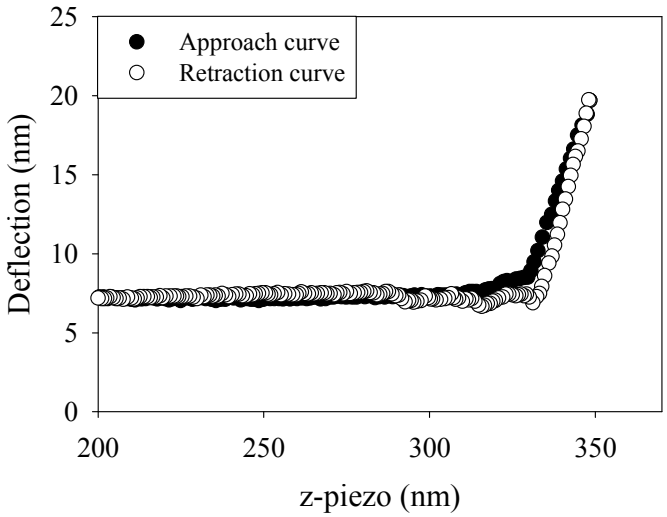

Figure 7-8 A typical raw data approach-retraction curve generated by AFM instrument for S/O = 0.43

7.6 Results and discussion

7.6.1 Interaction forces between bare gold surfaces in organic solvents

The interaction between the clean gold surface and the gold tip was measured in toluene, pentane and a mixture of these solvents to confirm the performance of the instrument. Figure 7-9. shows the approach and retraction curves between bare gold surfaces in toluene. The results measured in pentane and pentane/toluene = 0.43 are similar to toluene. A weak attractive force is observed as the two gold surfaces approach each other in toluene, shown in Figure 7-9. The force profile indicates that the electrical double-layer forces in organic solvents are negligible and the dominant interaction is attractive VDW force.

Equation (7-5) was used to calculate the VDW interaction between two approaching gold surfaces. The Hamaker constants for various materials are shown in Table 7-3. When the medium was the combination of toluene and pentane, the effective Hamaker constant was calculated by using equation (7-8):

$$A_{PenTol} = \sum \phi_i A_{ii} \tag{7-8}$$

Where ϕ_i is the volume fraction of each solvent.

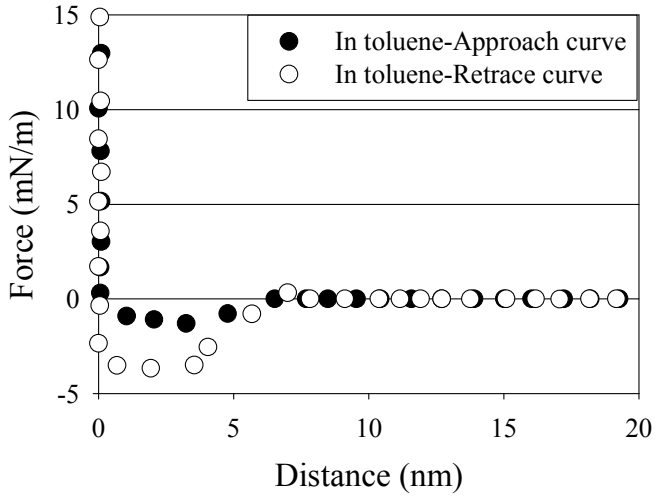

Figure 7-9 AFM force measurement between bare gold surfaces in toluene. The van der Waals attraction is the dominant force

Table 7-3 The Hamaker constant for various material in air [12]

Material	**Hamaker constant $\times 10^{-20}$ (A_{11}), J**
Pentane	3.8
Toluene	5.4
Gold	40.0
Asphaltene	6.0

The Hamaker constants for the interaction between gold-gold in various solvents were calculated by using equation (7-8) and are as follows:

$A_{Gold\text{-}Toluene\text{-}Gold} = 1.6 \times 10^{-19}$ J

$A_{Gold\text{-}Pentane\text{-}Gold} = 1.92 \times 10^{-19}$ J

$A_{Gold\text{-}S/O=0.43\text{-}Gold} = 1.71 \times 10^{-19}$ J

For pentane/toluene = 0.43, the interacting forces between the gold surfaces were calculated and compared with experimental results in Figure 7-10. The theoretical data is in good agreement with the experimental results for separations larger than 3 nm. VDW forces are short range forces. Therefore, it is obvious from experimental and theoretical results that the interaction between the surfaces becomes obvious at distances less than 10 nm. For separations of 10 to 3 nm, attractive forces (i.e. forces less than zero in Figure 7-10) were observed in the calculated results. However, for the experimental results the attractive forces are observed when the distance is less than 7 nm. These forces were almost consistent with the calculated results. At distances less than 3 nm in the theoretical results, the attractive force between the surfaces should grow when they are close. In the experimental results, on the other hand, attachment between the tip and the surface would occur and the deflection starts increasing. The distance between the surfaces becomes zero afterward. There was no evidence of repulsion forces (positive deflection) between the surfaces and the dominant force was attractive. The attractive forces that were predicted and measured by theory and experiment were consistent and showed van der Waals attraction between the two surfaces.

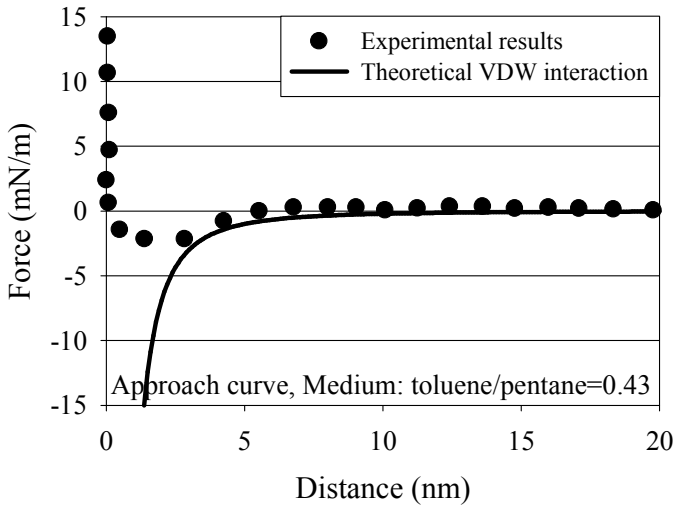

Figure 7-10 Comparison between the experimental (solid circles) and theoretical (solid line from equation (7-5)) interaction forces between bare gold in pentane/toluene = 0.43. The attractive interaction between the surfaces becomes obvious at distance less than 10 nm

7.6.2 Interaction forces between cleaned gold surfaces in organic solvents

After each exposure to asphaltenes, the cleaning procedure for the treated gold surface in the oil solution was to leave the gold pieces in chloroform for 24 hours and then leaving them in toluene for another 24 hours. It was expected that this cleaning method would remove the asphaltene from the surface. However, measuring the interaction forces on these cleaned gold substrates showed a small amount of repulsion in the approach curves. The results for the approach curves for the cleaned gold in various solvents are shown in Figure 7-11. The measured interactions show evidence of irreversibly adsorbed asphaltene on the gold surfaces that leads to repulsion between the surfaces over a distance of approximately 1.5 nm. Consequently, only longer range interactions can be

distinguished on the cleaned gold surfaces. When asphaltene is deposited on the surfaces, some portion of the deposited material can be removed by rinsing with solvents, such as toluene. However, the remaining deposited asphaltene on the surface has strong bonding with the gold and it could not be removed by solvents.

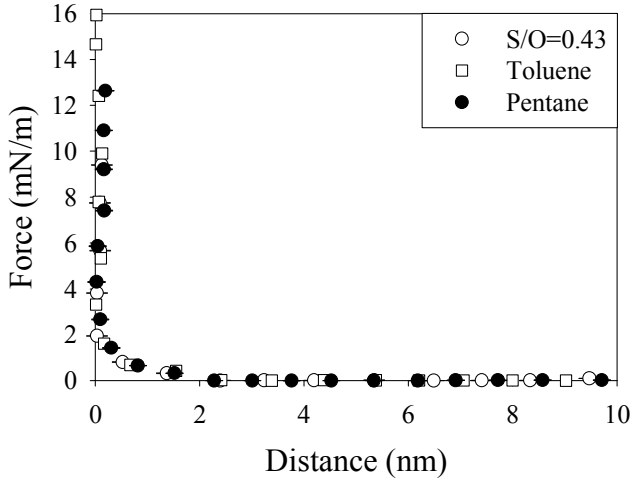

Figure 7-11 Approach curves for the interaction between cleaned gold (left overnight in chloroform and toluene separately) in toluene, pentane and pentane/toluene = 0.43. Repulsion forces are due to irreversible asphaltene deposition on the gold surface.

7.6.3 Interaction forces for asphaltene coated surfaces in organic solvents

Solutions of asphaltene in toluene are assumed to be destabilized upon addition of pentane. For the model oil solution that we used, the onset of asphaltene precipitation was at S/O = 0.43. However, our experiments in chapter 4 showed that destabilization of silica particles by pentane is observed below the visible onset of asphaltene precipitation by optical microscopy. Therefore,

changes in the interactions between asphaltene with the solvent medium should be observed even below S/O = 0.43.

The model oil solution was blended with pentane at ratios in the range of 0 - 0.5. The gold surface was soaked in each oil – toluene – pentane solution for 2 hours (the same time as for QCM immersion during stage 3), rinsed with toluene and transferred to the closed cell; the solvent was then injected to the closed cell. The medium in the closed cell was toluene – pentane at the same ratio as the oil – toluene – pentane solution. The plots for some of the important values of S/O such as 0 (no pentane) and 0.5 (above the onset point) in toluene – pentane media are shown in Appendix C. Here, we show the results for S/O = 0.43 which is the onset of asphaltene precipitation and S/O = 0.2 which is below the onset point.

For S/O = 0.43 in toluene – pentane medium, the force measurements were conducted at 30 positions on the surface of the gold and the time of each measurement was recorded. The result for the distance that the cantilever returns to zero deflection on the approach curves versus the time of each measurement is shown in Figure 7-12. The distances in Figure 7-12. do not follow a trend versus time. Therefore, one can assume that the adsorbed material was deposited irreversibly and they did not dissolve in the solution of toluene – pentane. If the adsorbed material dissolves back into the media (toluene – pentane), the height of the adsorbed material should decrease with time which is not observed in Figure 7-12.

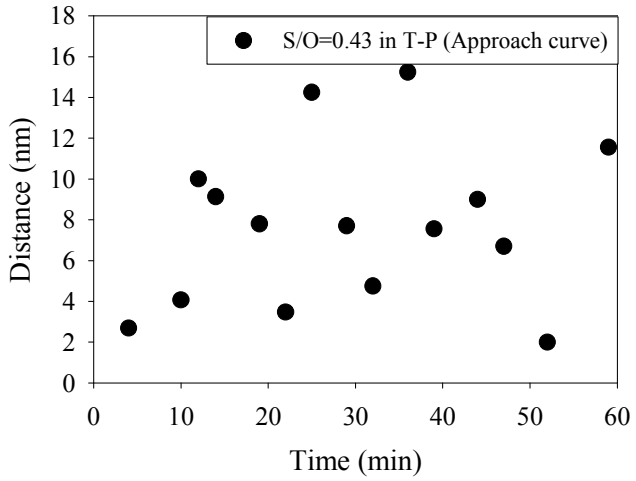

Figure 7-12 Distances on the approach curves (where the cantilever starts deflecting) versus time at S/O = 0.43 in toluene - pentane media

Different types of force curves were observed depending on the location of the tip on the surface. Examples of force curves that were observed at S/O = 0.43 (30 point of measurement on the substrate) and S/O = 0.2 (10 points of measurements on the substrate) are shown in Figure 7-13 and Figure 7-14, respectively.

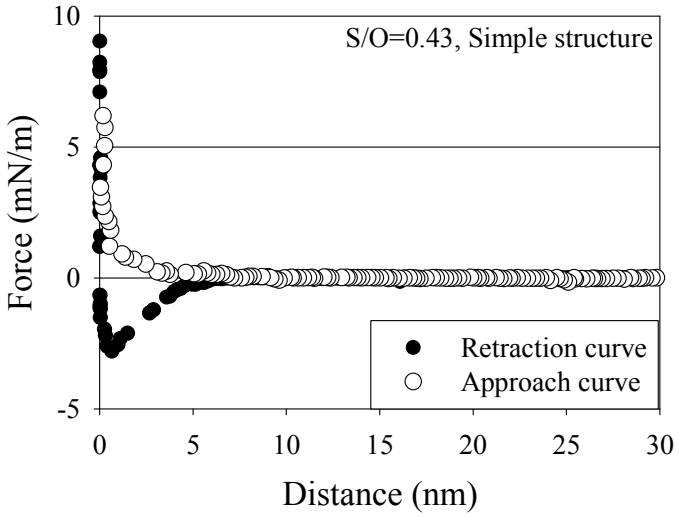

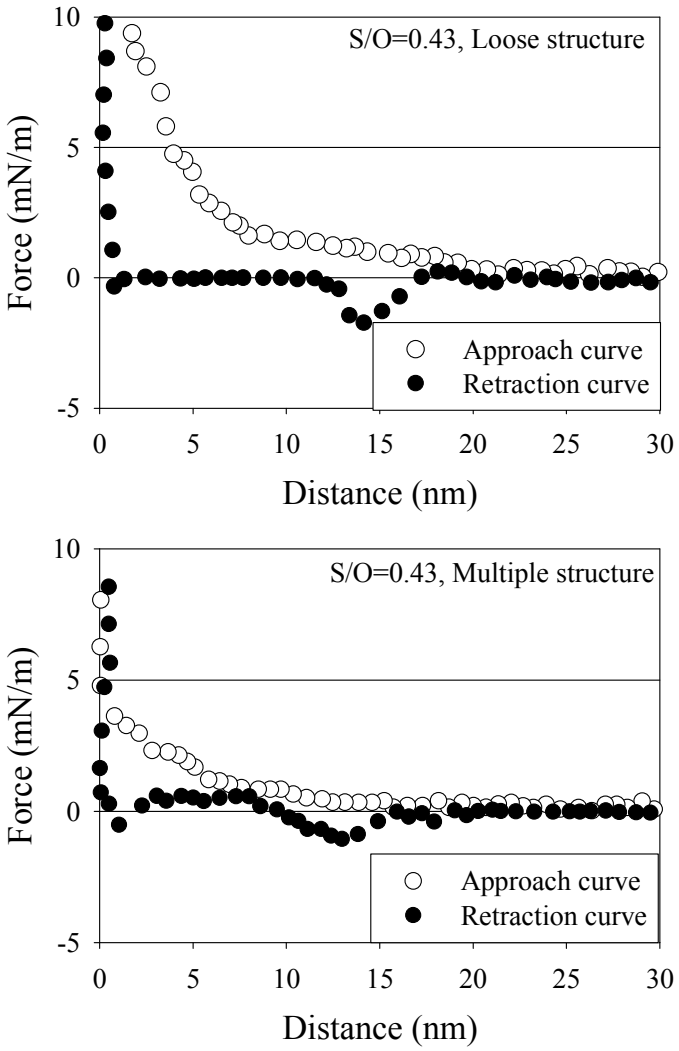

Figure 7-13 Representative force measurements between the AFM tip and the asphaltene coated surface prepared in oil – toluene – pentane solution at S/O = 0.43. The medium was pentane/toluene = 0.43

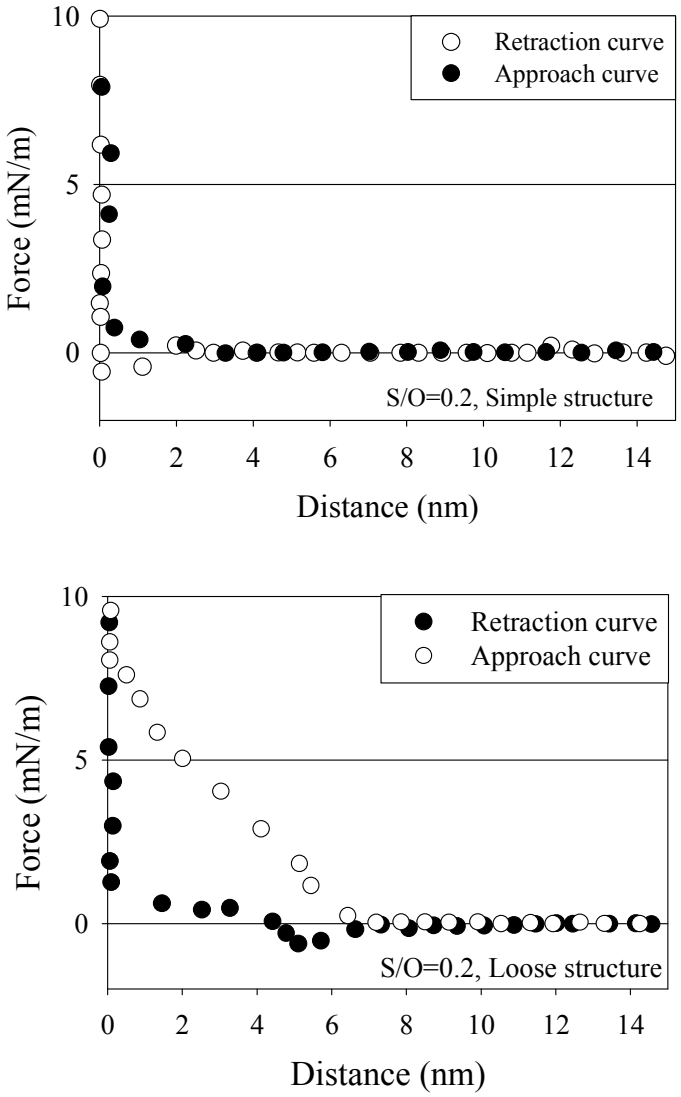

Figure 7-14 Representative force measurements between the AFM tip and the asphaltene coated surface prepared in oil – toluene – pentane solution at S/O = 0.2. The medium was pentane/toluene = 0.2

The parameters of interest were:

1) The distance where the cantilever starts deflecting in the approach curve, indicating the height of the adsorbed material.

2) The distance where the cantilever returns to zero deflection on the retraction curve, indicating the maximum separation for adhesive force.

3) The adhesion force during retraction, showing the elasticity of the attached aggregates.

For S/O = 0.43, the measured curves, including both approach and retraction curves, varied on different locations on the gold substrate, giving mainly three types of curves (Figure 7-13). In the approach curves, only positive deflections (repulsive forces) were observed and the distance of the repulsive forces from the surface varied with different positions on the gold substrate. The separation distances for the adhesive forces during retraction were also variable from point to point on the surface and different patterns of adhesion forces (simple, loose and multiple structure) were observed. The correlation coefficient was calculated for the distances of the cantilever deflection on the approach and retraction curves and the value was 0.61. This result shows that the differences in the maximum separation distance for the adhesive forces from point to point were not simply due to the thickness of the asphaltene coating at each location. From this result, we conclude that the deposited asphaltenes were heterogeneous both in thickness and in adhesion, and that the two features were not highly correlated. In addition, the variety of the patterns of adhesion forces on the gold substrate shows that different aggregates have different elasticity.

For S/O = 0.2, the measured curves including both approach and retraction curves varied on different locations on the gold substrate, however, mainly two types of curves were observed (Figure 7-14).

Although the distances for the change in the deflection of the cantilever on the approach and retraction curves varied at different positions on the substrate, an average threshold distance was calculated at various S/O and is presented in Figure 7-15. The threshold distance on the approach and retraction curves has two different concepts:

- Threshold distance on the approach curve: The distance where the cantilever starts deflecting and is considered as the onset of steric repulsion.

- Threshold distance on the retraction curve: The distance where the cantilever goes back to zero deflection.

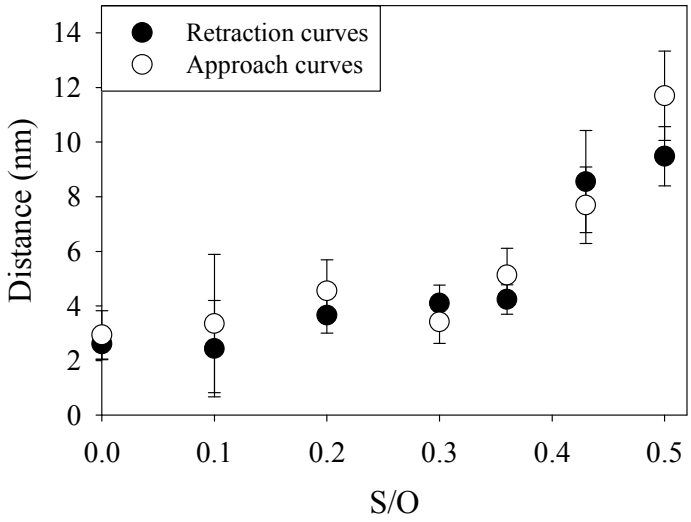

Figure 7-15 Height of the deposited materials on the gold substrate for various S/Os. The error bars show the standard deviation on 10 points on the gold surface from two different substrates for each S/O

The threshold distances in the approach and retraction curves are different for each S/O showing that the deposited aggregates do not have the same elongation

due to the AFM tip (in the retraction curve) and extension in the solution (approach curve). The threshold distances below S/O = 0.43 are in the range of 2 - 4.5 nm. These distances increase significantly after S/O = 0.43, showing that the heights of the deposited materials increase after the onset point. It should be noted that the height of the materials on the substrate would change at different positions and the data shown in Figure 7-15 is a rule of thumb for estimating the heights of the deposited materials.

The distances observed for S/O = 0 in the approach curve was around 2.9 nm, which is smaller than the size of asphaltene aggregates predicted by various methods in the literature to be in the range of 5 - 20 nm. The distances on the approach curves were 1.5, 0.1, 1.9, 3.2, 1.5, 7.4, 1.8, 6.1 nm at different positions on the substrate for S/O = 0. It is obvious the heights of the materials vary at different locations on the substrate and aggregates with different heights are observed.

Figure 7-16 shows the adhesion forces between the tip and asphaltene coated substrates at various S/Os. The results show that the tendency of asphaltene attachment to the gold substrate exist in the oil solution. This interaction becomes stronger by addition of pentane, and becomes obvious especially after the onset of asphaltene precipitation. However, the interacting forces are clearly observed even for lower S/O.

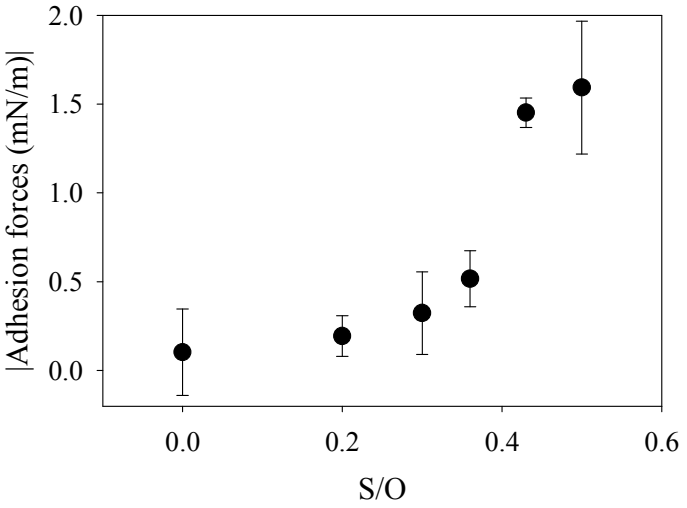

Figure 7-16 Adhesion forces observed in the retraction curves for various S/O in toluene-pentane medium. The error bars show the standard deviation on 10 points on the gold surface from two different substrates for each S/O

Among all the ratios, the interaction forces for S/O = 0.43 and 0.2 are going to be discussed in details below.

For S/O = 0.43 at the onset of precipitation, the force measurements were repeated for two gold substrates coated at S/O = 0.43 at approximately 30 points (n = 30) on each substrate. Based on the data, the normalized frequency for the shape of the retraction curves, the threshold distance on the approach and retraction curves and the adhesion forces in the retraction curves were plotted. The discrepancy in the shape of the retraction curves (Figure 7-17) at different positions on the same substrate shows that the structure and behavior of the asphaltenes on the surface differs from point to point, giving either simple, loose, or multiple adhesions.

Three main structures of the deposited asphaltene on the gold at S/O = 0.43 were observed, however, different rupture strength for the aggregates with similar structure is possible. This conclusion can be seen in Figure 7-18 that aggregate with both strong (2.4 to 2.8 mN/m) and weak (0.4 to 0.8 mN/m) attachment to the tip have been observed at different locations on the substrate.

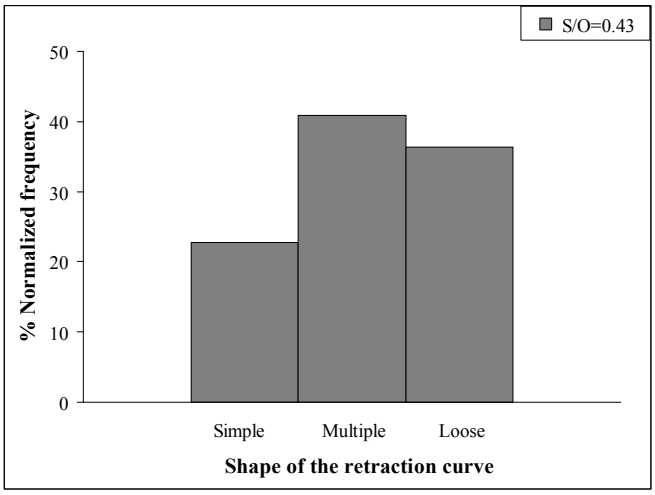

Figure 7-17 Distribution for the type of the adhesion forces in the retraction curves, with deposition at S/O = 0.43, measured in pentane/toluene = 0.43 (n = 30)

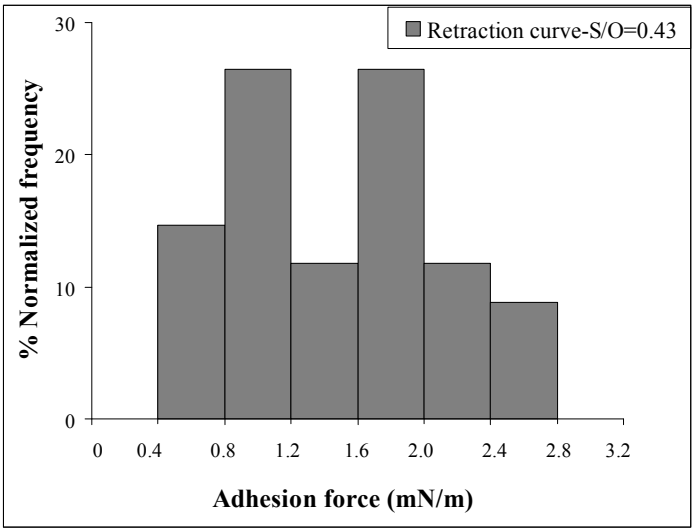

Figure 7-18 The normalized frequency for the adhesion forces in the retraction curve measured in pentane/toluene = 0.43

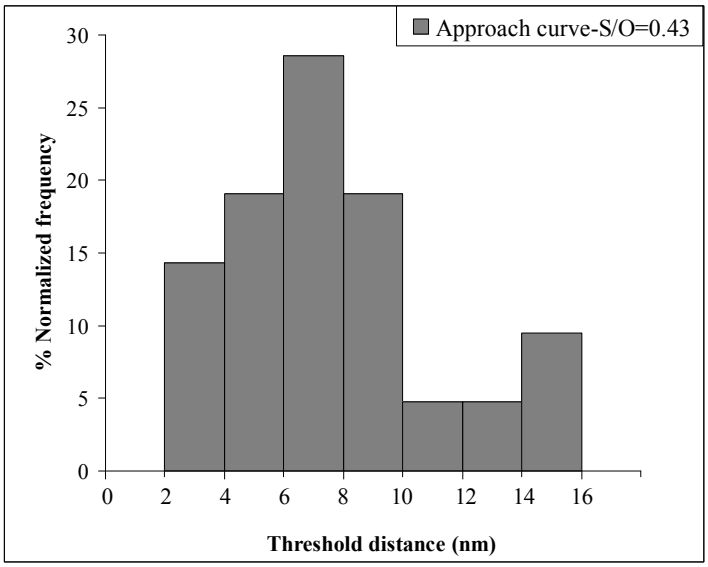

Figure 7-19 Normalized frequency of the threshold distance (the distance where the cantilever starts deflecting) measured in pentane/toluene = 0.43. This distribution show different height of deposited materials on the gold substrate (n = 30)

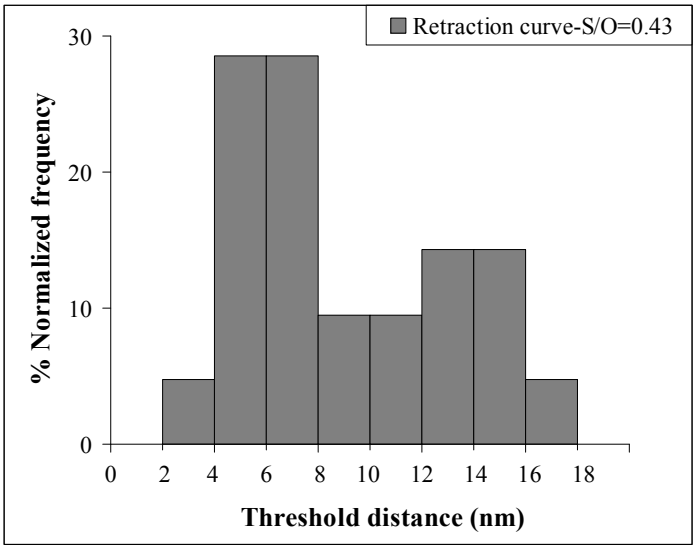

Figure 7-20 Normalized frequency of the threshold distance (returning of the cantilever to zero deflection) measured in pentane/toluene = 0.43. This distribution of the maximum distances for adhesive forces shows that the asphaltene material attached to the tip extends and breaks at different distances from the gold surface (n = 30)

Figure 7-19 and Figure 7-20 shows the threshold distances for the interactions of the AFM tip with the deposited asphaltenes on the approach and retraction curves, respectively. Both distributions show a mode at 6 - 8 nm, but the maximum distances for adhesion (16 - 18 nm) were larger than the maximum distances for repulsion (14 - 16 nm). This result suggests that the asphaltene aggregates elongate more due to the retraction of the AFM tip than they would normally extend into the solution.

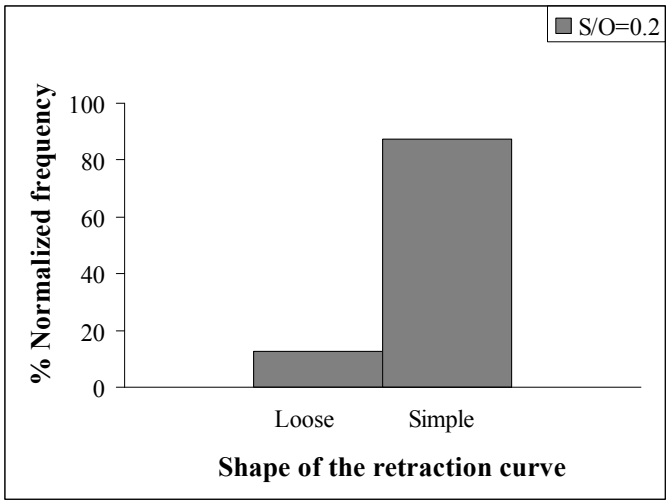

Figure 7-21 Distribution for the type of the adhesion in the retraction curves in pentane/toluene = 0.2 (n = 10)

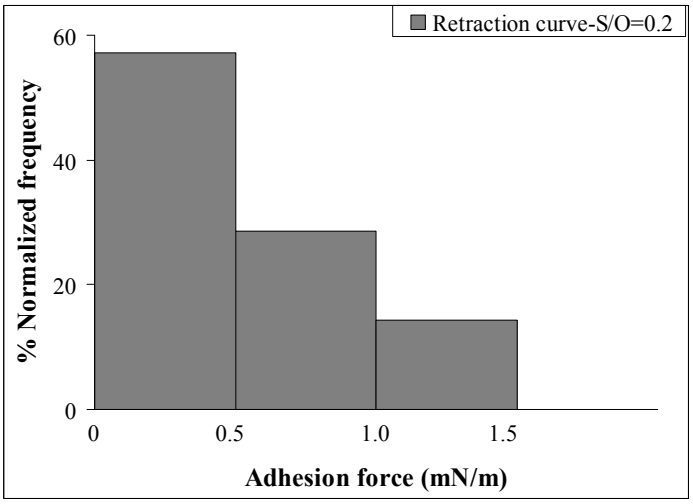

Figure 7-22 The normalized frequency for the adhesion forces in the retraction curve in pentane/toluene = 0.2 (n = 10)

Figure 7-21 shows the type of adhesion forces of the aggregates in the retraction curves at different positions on the gold substrate for S/O = 0.2. The

main observed pattern of the adhesion forces on the retraction curves were the simple structure and a few points showed loose structure.

The variety in the adhesion forces has decreased significantly compare to S/O = 0.43, and the strength of the aggregates at S/O = 0.2 (Figure 7-22) has a narrower distribution and is weaker (0 to 1.5 mN/m) compared to S/O = 0.43 (0.4 to 2.8 mN/m).

The threshold distances in the retraction curve (Figure 7-23) and the approach curves (Figure 7-24) has a narrower distribution for S/O = 0.2 (0 – 8 nm) in comparison to S/O = 0.43. The narrower distribution for the heights of the aggregates (threshold distance on the approach curves) showing a more uniform deposition of materials for S/O = 0.2. For S/O = 0.43, the threshold distances in the approach curves have a broad distribution (2 - 16 nm) which is an indication of higher heights of the patches of aggregates. The threshold distances for the retraction curve for S/O = 0.43 (2 - 18 nm) is higher than S/O = 0.2 (0 – 8 nm) as well, showing that the elongation of the aggregates in the retraction curves is more in the former S/O.

As illustrated in Figure 7-14, fewer types of adhesions curves were observed at S/O = 0.2; however, the height of asphaltene aggregates, the maximum separation for adhesive forces and the pattern of adhesion with separation distance were heterogeneous from point to point.

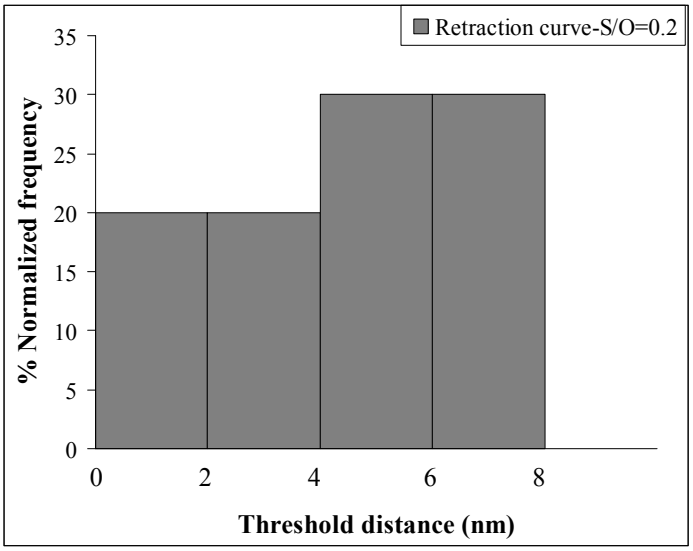

Figure 7-23 Normalized frequency for the distance of returning the cantilever to zero deflection during the retraction in pentane/toluene = 0.2 (n = 10)

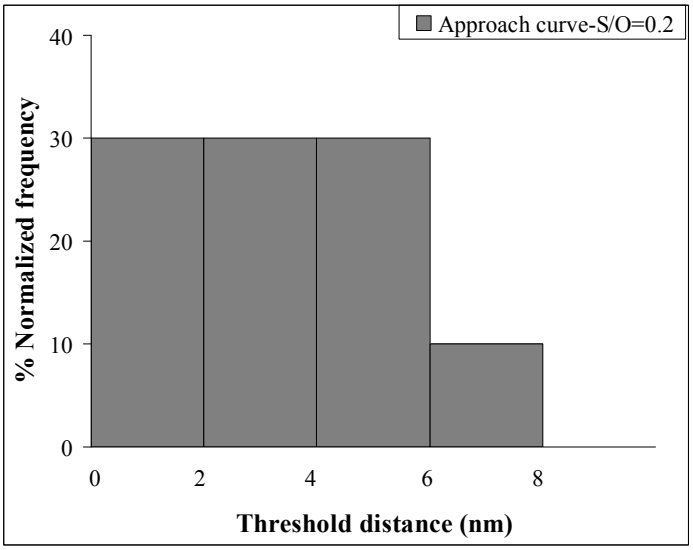

Figure 7-24 Normalized frequency for the distance where the cantilever starts deflecting in the approach curve in pentane/toluene = 0.2 (n = 10)

Broad distribution for the threshold distances on the approach curves (showing the height of the deposited materials) for S/O near the onset of

asphaltene precipitation shows that the topography of the deposited materials on the surface has changed at different position. For lower S/O, however, the narrower distribution of the threshold distances shows more uniform heights of materials on the substrate.

Summarizing the information above, we should say that for higher S/O especially above the onset of asphaltene precipitation the approach curves shows patches of aggregates with different heights and steric repulsion effect. The information that we obtained from the retraction curves showed different structure of deposited materials with a range of elasticity and lengths. The distribution of all the mentioned parameters for S/O below the onset point would decrease. Heterogeneous deposition of asphaltene on gold is observed for all the S/Os. However, by increasing S/O (more pentane in the solution) we observe more heterogeneous deposition of asphaltenes on surfaces.

It was mentioned in section 7. 4 that Amin *et al.* (2009) studied the heterogeneity of surfaces coated with precipitated asphaltene at different pressure. By increasing the pressure above the pressure of the onset point, surfaces with shorter and lower number of deposits i.e. less heterogeneous surfaces were observed at higher pressure. Higher pressure in Amin *et al.* work is similar to lower S/O in our work which leads to higher solubility of asphaltene in the solution. Similar to their work, we observed lower heterogeneity (i.e. shorter aggregates) on the gold substrate when asphaltene has a higher solubility in the solution i.e. lower S/O.

Asphaltene deposition similar to polymer brush structure on surfaces involves two stages. First, asphaltene aggregates directly adsorb on the surface of the substrate through several kinds of intermolecular interactions which form a single layer of adsorbed materials. Second, the aggregates interact with the pre-adsorbed aggregates monolayer leads to multilayer adsorption of the aggregates, the conformation of which is can be different by the interaction with the surface of materials.

Obtaining a structured polymer brush needs specific deposition method for site-selective immobilization of materials on the substrate. One of the methods for deposition of structured material on the substrate is LB coating method. Using LB method for coating surfaces with asphaltene leads to attachment of a monolayer of asphaltene to the surface. It is assumed that the polar functional group in the asphaltene structure would attach to the surface, leaving the side chains in the solution [9].

Some points should be noted in our method for coating the gold substrate:

1) In our work, the substrate was prepared by leaving the gold in the oil solution for 2 hours. In our method for coating the gold surface with asphaltenes, the aggregates were not forced to immobilize on specific sites on the gold surface Therefore, the groups in asphaltene structure that are attached to the surfaces and the ones that are left in the solution can vary from other methods.

2) We had various ratios of S/O leading to various amount and different structure of adsorbed materials on the surfaces especially below and above the onset of asphaltene precipitation.

3) We had multilayer adsorption of asphaltene on the substrate (shown by QCM results). Therefore, the structure and the side chains left in the solution in the multilayer deposits can be different than the monolayer ones.

Therefore, care should be taken in comparison our results with other literature work in this filed.

For all the S/Os no attraction was observed in the approach curves and the interaction between the tip and asphaltene coated surfaces were steric repulsion. The repulsion force in the solution shows that the deposited materials on the surface push away the tip. Similar observations were reported by Wang *et al.* (2009) for the approach curves [7, 9]. Therefore, when a bare surface approaches a coated surface with asphaltene, the main interaction between the surfaces is steric repulsion.

In the retraction curves, the tip was tangled by the side chains in the asphaltene structure and adhesion forces were observed. Different shapes for the adhesion forces and threshold distances were observed in the retraction curves due to different elongation length and rupture strength of the deposites attached to the tip. The variety in the retraction curves shows that the tip has attached to different types of deposited materials on the substrate.

The comparison between our work and Wang *et al.* work is presented in Table 7-4. The deposition mechanism of asphaltene on the substrate was different in the two studies. Wang et al. used LB method for deposition, whereas we soaked the gold substrate in the oil solution leading to adsorption of asphaltene materials on the surface. We added various ratios of pentane to the oil solution and had

different amounts and structure of adsorbed materials on the surface. However, they used similar materials to coat the surfaces for all the experiments and only change the medium where the force measurements were conducted.

Table 7-4 Comparison between our work and the literature on AFM in non-aqueous media

	Wang *et al*. (2010) [7]	**Wang *et al*. (2009) [9]**	**Our work**
Substrate	Silica wafer	Silica wafers	Gold plate
Method of coating the substrate	LB method	LB and dip coating method	Leaving the substrate in the solution for 2 hours
Concentration of asphalene in toluene (g/L)	2	2	27.3
Amount of deposited materials on the substrate	Constant	Constant	Changed due to addition of pentane to the solution
Media	HepTol	Toluene	PenTol
Ratio of solvent/toluene in the media (S/O)	1 - 0	0	0 - 0.5
Type of interaction forces in the approach curve	Steric repulsion for all the ratios expect for heptane	Steric repulsion	Steric repulsion
Type of adhesion forces in the retraction curve	Stretching in pure heptane	Repulsion	Different types of adhesion forces (simple, loose, and multiple) depending on the ratio of S/O
Threshold distance on the approach curve	4 (heptane) - 50 nm (toluene)	LB: 50 nm Dip coating: 50 nm	2.9 - 11.7 nm for S/O = 0 - 0.5
Threshold distance on the retraction curve	Not mentioned	LB: 50 nm Dip coating: 22 nm	2.6 - 9.5 nm for S/O = 0 - 0.5
Range of adhesion forces(mN/m)	0.12 - 0.33 for S/O = 0 - 0.7	LB: 1.25 Dip coating: 0.85	0.1 - 1.6 for S/O = 0 - 0.5

Steric repulsion was observed in all the approach curves in our work similar to their results. However, they observed an attractive force in pure heptane. The threshold distances in our work were smaller then their results in both the approach and retraction curves. This discrepancy can be due to the type of the materials that are adsorbed on the gold substrate. Comparing the adhesion forces for S/O = 0, which is in pure toluene, shows stronger aggregates attached to the tip in the case of their work. The aggregates that are attached to the tip in the retraction curves are the ones that are left in the solution. Therefore, we can assume that the asphaltene structures that are left in the solution may be weaker in our experiment comparing to Wang *et al.* (2009) work. However, increasing the amount of pentane in the model oil solution led to aggregates with longer length and stronger rupture strength in our work.

7.7 Summary

Asphaltene were adsorbed on the gold substrate at various S/O (0 - 0.5) and the force measurements were conducted for each substrate in toluene-pentane media with the same ratio as oil-toluene-pentane solution. The histograms based on AFM data (i.e. adhesion force, shape of the adhesion force, the distance before the cantilever goes to zero deflection on the approach curve and the distance before the cantilever become deflected on the approach curve) for S/O = 0.43 (onset of asphaltene precipitation) and 0.2 (far below the onset point) shows heterogeneous deposition of asphaltenes on the gold surface which increase significantly above S/O = 0.43. The types of the adhesion forces, especially above

the onset of asphaltene precipitation, show different structure for the deposited materials. More adhesion forces are observed for higher S/O.

For S/O = 0.43, aggregates have an elastic length in the range of 2 - 18 nm and adhesion forces of 0.4 to 2.8 mN/m. Both of these parameters were higher compared to the results at S/O = 0.2 which for the aggregates size is 2 - 8 nm and for the rupture strength is 0 to 1.5 mN/m. Different rupture strength for the aggregates with similar structure is possible as well. Broad distribution for the height of the materials (distances obtained when the cantilever starts deflecting) on the approach curves for S/O near the onset point shows that the topography of the deposited materials on the surface has altered at different position. The distance when the steric repulsion was observed on the approach curves varied as well for different positions on the substrate. Considering the results of both approach and retraction curves show that we had heterogeneous patches of aggregates on the gold substrate.

However, for lower S/O, the height of the adsorbed materials at different positions on the gold substrate is mostly similar indicating that the deposited materials have formed a more uniform layer on the gold substrate.

The purpose of measuring the forces at various S/Os was to determine the interaction forces between coated silica with different amounts and structures of adsorbed asphaltene on their surfaces. The objective was to have a clearer picture of destabilization of the silica suspension in the oil solution at various S/Os. Silica suspension in the oil solution is stabilized by means of steric repulsion due to the asphaltene materials adsorbed on particle surfaces. By adding pentane, more

asphaltene precipitate starts forming in the solution, which adsorb on the silica particles and co-precipitate suspended particles as well. Obtained AFM results indicate that at higher S/O asphaltene materials with a higher heterogeneous structure in length would form on solid surfaces. It was shown that the adhesive forces of these hairy structures increase for higher S/O. Above a certain S/O (i.e. 0.33), the interaction between the asphaltene with longer and more adhesive structure adsorbed on silica surfaces would lead to flocculation of the particles. The asphaltene bridges between silica particles are formed, leading to formation of large flocs that have faster settling rates compared to the original particles.

7.8 References

[1] Hodges, C. S., Cleaver, J. A. S., Ghadiri, M., 2002, "Forces between Polystyrene Particles in Water using the AFM: Pull-Off Force Vs Particle Size," Langmuir, 18(15) pp. 5741-5748.

[2] Cappella, B., and Dietler, G., 1999, "Force-Distance Curves by Atomic Force Microscopy," Surface Science Reports, 34(1-3) pp. 1-104.

[3] Dorobantu, L. S., Bhattacharjee, S., Foght, J. M., 2009, "Analysis of Force Interactions between AFM Tips and Hydrophobic Bacteria using DLVO Theory," Langmuir, 25(12) pp. 6968-6976.

[4] Duvigneau, J., Schonherr, H., and Vancso, G. J., 2010, "Nanoscale Thermal AFM of Polymers: Transient Heat Flow Effects," ACS Nano, 4(11) pp. 6932-6940.

[5] Benz, M., Gutsmann, T., Chen, N., 2004, "Correlation of AFM and SFA Measurements Concerning the Stability of Supported Lipid Bilayers," Biophysical Journal, 86(2).

[6] Long, J., Xu, Z., and Masliyah, J. H., 2007, "Single Molecule Force Spectroscopy of Asphaltene Aggregates," Langmuir, 23(11) pp. 6182-6190.

[7] Wang, S., Liu, J., Zhang, L., 2010, "Interaction Forces between Asphaltene Surfaces in Organic Solvents," Langmuir, 26(1) pp. 183-190.

[8] Wang, D., Fujinami, S., Nakajima, K., 2010, "Visualization of Nanomechanical Mapping on Polymer Nanocomposites by AFM Force Measurement," Polymer, 51(12) pp. 2455-2459.

[9] Shengqun, W., Jianjun, L., Liyan, Z., 2009, "Colloidal Interactions between Asphaltene Surfaces in Toluene," Energy and Fuels, 23(2) pp. 862-869.

[10] Elimelech, M., Gregory, J., Jia, X., 1995, "Particle deposition and aggregation : measurement, modelling and simulation,".

[11] Gregory, J., 1989, "Fundamentals of Flocculation," Critical Reviews in Environmental Control, 19(3) pp. 185-230.

[12] Masliyah, J.H., and Bhattacharjee, S., 2006, "Electrokinetic and colloid transport phenomena," Wiley-Interscience, Hoboken, N.J., .

[13] PH.C. Van Der Hoeven, and J.Lyklema, 1992, "Electrostatic Stabilization in Non-Aqueous Media," 42pp. 205-277.

[14] Suzuki, A., Ho, N. F. H., and Higuchi, W. I., 1969, "Predictions of Particle Size Distribution Changes in Emulsions and Suspensions by Digital Computation," Journal of Colloid and Interface Science, 29(3).

[15] Yang, C., Dabros, T., Li, D., 1998, "Kinetics of Particle Transport to a Solid Surface from an Impinging Jet Under Surface and External Force Fields," Journal of Colloid and Interface Science, 208(1) pp. 226-226.

[16] Briscoe, W. H., and Horn, R. G., 2002, "Direct Measurement of Surface Forces due to Charging of Solids Immersed in a Nonpolar Liquid," Langmuir, 18(10) pp. 3945-3956.

[17] Heinz, W. F., and Hoh, J. H., 1999, "Spatially Resolved Force Spectroscopy of Biological Surfaces using the Atomic Force Microscope," Trends in Biotechnology, 17(4) pp. 143-150.

8 Conclusion, implication and recommendation

8.1 Conclusion

The initial target of this thesis was to study the removal of micrometer sized particles (~ 1μm) from oil streams and vacuum residues by solvent treatment, aqueous treatment and the combination of the two methods. For this purpose, a model oil solution with various ratios of pitch material (thermally cracked vacuum residues from Cold Lake with 59.5 wt% asphaltene) and 1 μm silica particles representing the solid particles were prepared in toluene. Due to settling properties of the prepared oil solution, a mixture of 5 wt% pitch and 4 wt% silica in toluene was chosen as the model oil solution (O). Pentane (S) was chosen instead of heptane as the paraffinic solvent due to the faster settling properties of the precipitated flocs. The hypothesis was that by destabilizing the asphaltene in the oil solution due to the addition of pentane, silica particles would flocculate by means of the adsorbed asphaltene molecules or aggregates. Larger flocs would be formed; therefore, these flocs would settle faster than the original particles.

The onset of asphaltene precipitation was determined to occur at a pentane to oil ratio (S/O) of 0.43. Rapid settling of silica particles above the onset of asphaltene precipitation was observed; therefore, we wanted the lower limit of S/O for the removal of silica particles. The results for various S/Os below the onset point showed that until S/O = 0.33, destabilization and rapid settling of the silica suspension would still occur. The concentration of silica particles decreased to 0.035±0.010 wt % (as ash) in the supernatant for S/O = 0.43 after 1 hour. This reduction indicates more than 98% removal of the silica particles. For S/O = 0.33, the ash contents in the supernatant were 0.09 ± 0.01 wt %, which indicates more than 97.5±0.2% removal of silica particles.

Removal of solid particles by paraffinic treatment of the oil solution and oil emulsion was successful and the the remaining solid particles in the oil phase met the industrial threshold which is lower than 0.5 wt%. Removal of the particles below the onset of asphaltene precipitation is the novel finding of this thesis, which makes it possible to have less amount of precipitated asphaltene while removing the solids from the oil solution.

Due to the interesting results that we obtained from the paraffinic treatment of the oil solution to remove the silica particles, we decided to study the adsorption characteristics of asphaltene on solid surfaces (metallic and mineral surfaces) by using QCM (Quartz Crystal Microbalance) and FTIR (Fourier Transform Infra-Red) spectroscopy. In addition, AFM (Atomic Force Microscopy) was used to measure the forces between asphaltene coated surfaces to understand the mechanism of asphaltene adsorption better.

FTIR and QCM results showed that a significant amount of asphaltene adsorbed on the surfaces even below the onset of asphaltene precipitation (S/O = 0.43). The amount of adsorption, however, increased significantly after S/O = 0.43. For instance, the amount of adsorption by QCM at S/O = 0.33 is 2.82 mg/m^2, whereas at S/O=0.43 this amount increases to 15.35 mg/m^2. The amount of asphaltene adsorption was measured on silica particles with different hydrophobicity as well. The amount of adsorption on silica followed the same trend as on the gold surface; however, the amount of adsorption was lower for silica particles.

Self-association behavior of asphaltenes has been reported in the literature. Observation of adsorption by QCM method even at S/O = 0 in our study showed that asphaltene aggregation and adhesion occurs without the addition of pentane. Therefore, to study the adhesion of asphaltene aggregates, dilute solutions of asphaltene (0.05, 0.1, 0.5, and 1 g/L) in toluene were prepared and the amount of asphaltene adsorption on gold quartz crystal was measured. The diffusion coefficient of asphaltene onto the gold surface was estimated by using the Ward and Tordi (1946) equation. The size of the asphaltene aggregates was estimated using the Stokes-Einstein equation. The estimated size of the asphaltene aggregates in 0.05 g/L asphaltene solution was estimated to be around 18 nm by this method. The size of the asphaltene aggregates increased for higher concentrations of asphaltene in the toluene solution. Comparing the aggregate size and the diffusion coefficient in our study with the literature data shows that a smaller size and larger diffusion coefficient for asphaltene has been estimated by

other methods; this is likely due to limitations on the interpretation of the data obtained from QCM.

The objective of conducting the AFM experiments was to determine if the net interaction between the coated silica particles suspended in the oil solution would lead to flocculation of the particles. The interaction forces between asphaltene coated surfaces at various S/Os in organic solvents were measured by AFM. The substrate for the measurements was gold surfaces soaked in oil-toluene-pentane solutions at various ratio of S/O. Different amounts of added pentane led to different thicknesses and structures of deposited asphaltene on the gold substrates. Estimating the interaction on gold coated surfaces at different positions on the substrate showed some interesting results. At lower S/O (less amount of precipitates), the measured interaction forces were similar on different locations on the gold substrate. However, by increasing S/O, especially close to S/O = 0.43, a range of different interaction forces were measured at different positions on the substrate. This discrepancy shows that the AFM tip sampled different structures of deposited materials on the surface. Although the material deposited on the surface is asphaltene, the structure of the deposited materials can be different from point to point and was not homogeneous. It has been mentioned that asphaltene components can act as propagators, interacting from different active sites with the surface and with other asphaltene aggregates. Our AFM results show that the topography of the surface varies according to position. Therefore, it can be concluded that at different locations on the surface, asphaltene adsorption

on the gold substrate occurs between the active sites of the gold substrate with different active sites of the asphaltenes.

In addition to paraffinic treatment of the oil solution for removal of solid particles, we also studied the effect of adding small amounts of water on agglomeration of silica particles in the model oil solution. Addition of water (4 wt%) agglomerates the silica particles, causing faster settling of the solid particles. However, the sample should stand for mush longer time (more than 4 hours) compared to paraffinic treatment (1 hour) to have an efficient settling of silica particles. Emulsions of water in the oil solution were prepared as well and pentane was added at various ratios for both hydrophilic and hydrophobic silica particles. Comparing the results for paraffinic treatment of the oil emulsion and the oil solution showed that the removal of silica particles occurred at a lower S/O for the former solution. Therefore, paraffinic treatment of the oil solution in the presence of emulsified water leads to using less amounts of solvent for the removal of solid particles from the solution.

The idea of paraffinic treatment of the oil solution to remove the solid particles was that precipitated asphaltene would flocculate the solid particles; therefore, we would have larger flocs of the asphaltene - silica with faster settling rates. However, to eliminate the possibility of the settling of solid particles due to the dilution of the medium (changes in the viscosity and density), the oil solution was diluted with toluene and cyclopentane to determine the effect of viscosity and density. The results of dilution with both toluene and cyclopentane showed that the stability of the silica suspension in the oil solution did not change by diluting

the solution with the named solvents. Therefore, the main effect of the destabilizing and fast settling of the silica suspension upon addition of a paraffinic solvent is due to flocculation with precipitated asphaltene.

To generalize the work for other types of solids, kaolinite and silica particles with various hydrophobicities were used to represent the fine solid particles in the solution. Addition of pentane to these oil solutions with different types of solids showed that removal of these particles was also possible. Therefore, paraffinic treatment is a general method for the removal of solid particles regardless of their initial surface characteristics. Any type of solid in an oil solution would be coated with asphaltene materials, changing the wettability of the surface. Therefore, flocculation and fast settling of any type of solid is possible with this method.

8.2 Implication of the work

Removal of fine solid particles due to plugging and fouling problems is a challenging task in petroleum residues and heavy oil streams. As explained in earlier chapters, removal of fine particles (~1 μm) with a centrifuge or filtration is not feasible. Therefore, solvent treatment of the oil streams has been used for decades for the removal of fine particles and emulsified water. The solvents that have been used mainly in froth treatment plants, are paraffinic solvents such as pentane or heptane and also naphtha. By using either of these two solvents, the solid and water content of the oil streams would be less than 1 - 5 wt%.

In this research, flocculation and sedimentation of silica particles from a model oil solution was studied by adding pentane (non-aqueous treatment).

Destabilization of silica suspensions starts at S/O = 0.33 which was below the onset of asphaltene precipitation at S/O = 0.43. Addition of emulsified water improved the flocculation and destabilized the silica suspensions in the oil solution at lower S/O (S/O = 0.24) compared to non-aqueous treatment (S/O = 0.33). Use of this finding in industrial treatment would lead to consumption of less solvent for the removal of solid particles from the oil streams. In addition, any type of solid that exists in the oil solutions would be coated with asphaltenes; therefore paraffinic treatment is an efficient method for the removal of any solid. However, the efficiency of the method depends on the viscosity and density of the medium, size and concentration of the suspended particles, and the amount of added diluent.

The QCM results showed that more asphaltene adosption on solid surfaces occurs for higher S/O. Swollen behavior of asphaltene with solvent was observed and showed a more porous structure for asphaltene at higher S/O. The AFM results demonstrated that the adsorption of asphaltene on solid surfaces is heterogenous in height, adhesion to surfaces and elongation in the solvent. Therefore, a picture based on the results of QCM, AFM and flocculation of the silica particles can be drawn. The silica particles are dispersed in the oil solution and due to the adsorption of asphaltene materials on their surfaces, they form a stable suspension. When pentane is added to the solution, more asphaltene adsorb on the surface and the bridging effect of the asphaltene between the coated silica particles initiates. Above the specified ratio of pentane to oil solution (S/O > 0.33), longer asphaltene with higher adhesive forces would form on the surface of

the silica particles. These structures of asphaltene make a stronger bridge between the silica particles and flocculate the particles more. The porous structure of asphaltene can also trap some of the silica particles. Therefore, denser flocs of silica-asphaltene would form and sedimentation of these flocs at a higher rate compared to the original particles would occur.

The main implication of this research is that flocculation of silica particles by means of asphaltenes occurs even below the onset of precipitation. Therefore, with less solvent and less precipitated asphaltene, we were able to destabilize the silica suspensions in the oil solution and cause them to settle.

The sedimentation time for the asphaltene-silica flocs is shorter than the original suspended particles. However, from an industrial point of view this timing is not economical. Therefore, deep bed filters or inclined plate settlers can be used to accelerate the sedimentation of larger flocs.

8.3 Recommendations

8.3.1 AFM force measurement

The interacting force between asphaltene coated surfaces in non-aqueous medium by using AFM is attracting more attentions recently. In our AFM experiments, both the coating (deposited asphaltene on the surface of the gold) and the media (various S/O) was changing through the experiments. In our work the tip was not coated with asphaltene; therefore, we did not measure the interaction between the surfaces that both are coated with asphaltene due to the

limited time. There are numbers of works that have measured the interaction between coated substrate and coated tip; however, the deposited materials on the surface were the same and only the medium was changing. More interesting results can be governed by measuring the interaction between surfaces that have been coated at various S/Os (i.e. different types of adsorbed material on the surface) in non-aqueous media.

Measuring the interaction forces between surfaces in a real oil solution media (oil-pentane) was not possible because the media was not transparent. It would be interesting to find methods that the interaction between surfaces can be measured in the real oil solution medium while asphaltene is adsorbing on the surfaces.

In the case of our work, it was shown that in the presence of emulsified water, the removal of silica particles from the oil emulsions occurs at a lower S/O. However, the mechanism of how the precipitated asphaltene facilitates the removal of solid particles from the oil solution in the presence of emulsified water is not fully understood. The interaction between the emulsified water with the precipitated asphaltene and silica particles can be an important factor to understand the heteroflocculation mechanism better. This area can be studied using AFM.

8.3.2 Heteroflocculation in the presence of other types of solids

The results in chapter 5 showed that detabilizartion and sedimentation of silica suspensions would improve in the presence of water. This phenomenon was due to heteroflooculation of solid particles – emulsified water – precipited asphaltene

that led to denser flocs. It is interesting to determine if heteroflocculation of silica particles improves in the presence of other types of solids with different sizes and surface structure.

8.3.3 Using deep bed filters for removal of the asphaltene – silica flocs

Deep bed filters ususlly filter particles with sizes in the range of 10 - 20 μm. Therefore, they are not suitable for filtration of the suspended silica particles in the case of our study. However, by flocculation of the silica particles by means of asphaltene, the size of the flocs would increase. Therefore, deep bed filters can be used for faster separation of the asphaltene – silica flocs. However, the viscosity of the oil phase, the flow rate for the filtration, the concentration of the suspended flocs, the types of the materials that should be used in the filter median, and the reconditioning solvent should all be studied.

Appendix A Contact angle measurement of the silica particles

In the first stage of the work, we wanted to see if the contact angle of silica particles has any effect on the settling rate of asphaltene/silica flocs. Therefore, measuring the contact angles was the first step of the work. Various methods have been suggested on the literature to measure the contact angle of fine solid particles such as sessile drop, Washburn method, compressed disc, film trapping method, atomic force microscopy, and enthalpy of immersion.

The three methods that were used in this work are presented below:

A. 1 Washburn method

Measuring the contact angle by Washburn method is based on the penetration rate of a liquid through the particles. The packed bed of the particles is considered as bundles of capillaries. According to the Washburn equation (equation A.1), the rate of the liquid penetration is

$$h^2 = \frac{R\gamma_i \cos\theta}{2\mu} t \qquad \text{(A-1)}$$

where h is the penetration height, t is the penetration time, R is the effective pore radius, γ_i is the surface tension of the liquid, θ is the contact angle of liquid on the solids, and μ is the viscosity of the liquid.

For liquids that wet the particles, the contact angle is assumed to be zero ($\theta = 0$). For such a liquid, the height of the penetration can be recorded versus time. Plotting h^2 versus t would give a linear line that from the slope, the effective radius of the pores (R) can be estimated. Once R is known for the packed column, the contact angle of the particles can be determined for liquids with known viscosity and surface tension. There are several difficulties associated with this method; packing porosity of the particles affects the effective radius (R); each prepared column can be used for one set of experiments; and checking the repeatability of the results is difficult.

Hexane, heptane, octane, decane, and acetone were chosen as the wetting liquid in our experiments and the effective radius of the pores was calculated to be 3.58 ± 1.87 nm. The result for radius calculation for each solvent is shown in table A-1

Table A-1 Effective radius calculation for various solvent

Liquid	Slope (cm^2/s)	Surface tension (mN/m)	Viscosity (mPa·s)	R(nm)	Correlation
Hexane	0.0089	18.4	0.326	31.5	0.992
Heptane	0.0098	20.3	0.418	40.4	0.999
Octane	0.0076	21.6	0.542	38.1	0.999
Decane	0.0049	23.8	0.92	37.9	0.999
Acetone	0.0113	23.7	0.327	31.2	0.992

Silica particles with various hydrophobicities were prepared and the contact angle was measured by using water as the wicking solvent with surface tension 72.8 mN/m and viscosity 1.0 mPa·s. Dichlorodimethylesilane was used to make the silica particles hydrophobic.

Unfortunately, we were not able to get accurate results for measuring the contact angle of the silica particles by using this method. For hydrophilic silica particles, we treated them overnight with sulfuric acid (H_2SO_4) and expected to have low contact angle. However, many trials for measuring the contact angle of the hydrophilic particles showed values higher than 80° which can not be correct. The main problem with this method was preparation of the silica column which should be uniform. Even for the same particles the calculated slopes were not similar and the experiment was not repeatable [1, 2].

A. 2 Enthalpy of immersion

Calorimetry studies the material responses to temperature change and can be used to characterize the surface chemistry of solids and their interactions with solvents. Immersion calorimetry can be considered as an accurate method to investigate solid surface properties. When a clean solid is immersed into a liquid, energy is released or absorbed which is known as the enthalpy of immersion. The relationship between the contact angle and the enthalpy of immersion can be as follows:

$$h_i = -\gamma \cos\theta + T\frac{d(\gamma \cos\theta)}{dT} \tag{A-2}$$

where h_i is the enthalpy of immersion, T is the absolute temperature, γ is the interfacial tension, and θ is the contact angle. By using equation A. 2, the enthalpy of immersion can be calculated by knowing the information on contact angle but not vice versa. Therefore changes have been applied to equation A. 2 to estimate the contact angle by knowing the enthalpy of immersion information. Equation A. 2 gives the simple relation between contact angle and heat of immersion:

$$\cos\theta = \frac{-KT - h_i}{\gamma_{lv}} \tag{A-3}$$

If the solid/liquid surface tension is assumed to be independent of temperature, then the value of K is 7×10^{-5} J/m^2 K. The assumption for governing equation A. 3 can be found elsewhere [1].

The calorimeter used in the enthalpy of immersion study had two identical calorimetry chambers: one for holding the samples, and the other for reference. The particles at a certain amount are initially placed in a sample cell. The powder cell will be sealed, installed into the sample calorimetry cell, and about 5 mL of water injected in the wetting chamber. The same procedure is used to prepare the reference calorimetry cell except that no powders used in the powder cell. After installation the sample and the reference in the instrument, the temperature should reach 298 K and stays at this temperature for at least 3 hours. After the instrument reaches equilibrium, the membranes of the sample and the reference cells are broken at the same time by pushing the breaking rods. After breaking the membrane, the liquid penetrates into the powder cell and mixed with the particles and the released thermal energy is recorded.

The experiment was then repeated for silica particles for 5 times. The graph for heat rate versus time was not consistent and repeatable for similar samples. Therefore, the contact angle using this method was not a successful approach either.

A. 3 Sessile drop

In this method, a droplet of liquid is positioned on a solid surface. The three phase contact angle can then be estimated. In our work, we used FTA 200 (First Ten Angstroms, Inc., Virginia) for measuring the contact angle. FTA 200 is a flexible video system for measuring contact angle. The droplets on the surface can be observed live on the computer screen and images can be captured and kept for later image analysis.

The contact angle is measured on the surface of a compressed disc of particles; the assumption is that the packed disc has the same surface properties as those of the individual particles. The particles are compressed under large forces to form a disc with smooth and homogeneous surface. SEM images showed that the silica particles that we used are spherical so we were not able to make a compressed disc of silica particles. Therefore, solution of silica in toluene was sprayed on glass slides. The slides were then left till the solvent was evaporated. The sessile drop method was then applied on the coated glass slides with silica particles for measuring the contact angle.

A water droplet was positioned on the surface of the silica particles by means of an automatic syringe in the FTA 200 instrument. The droplet shape is

photographed by a CCD camera. The contact angle can easily be obtained by using the FTA 200 image analysis software.

Measuring the contact angle by this method has some technical issues such as: mechanical stress can change the surface characteristics of the fine particles; the disc particle size variation causes significant changes in disc surface roughness; the porous structure of the surfaces will result in contact angle hysteresis; liquid penetration in the porous surface of the disc leads to inaccurate and imprecise contact angle measurements. Although the result from this method for fine particles is not very accurate, we considered them as estimation for the contact angles of the silica particles with different hydrophobicities. The measured contact angle with this method is presented in chapter 4.

A. 4 References

[1] Yan, N. X., Maham, Y., Masliyah, J. H., 2000, "Measurement of Contact Angles for Fumed Silica Nanospheres using Enthalpy of Immersion Data," Journal of Colloid and Interface Science, 228(1) pp. 1-6.

[2] Ku, C., Henry, J. D.,Jr, Siriwardane, R., 1985, "Particle Transfer from a Continuous Oil to a Dispersed Water Phase: Model Particle Study," Journal of Colloid and Interface Science, 106(2) pp. 377-387.

Appendix B Size Distribution of Silica-Asphaltene flocs by Using Acoustic Spectroscopy

The other unsuccessful challenge of the work was to measure the size distribution of silica-asphaltene flocs at various S/O. It was expected that the size of flocs to be different at various ratio of pentane and increased for higher amount of pentane in the oil solution.

DT-1200 (Dispersion Technology, Inc. NY) was used to measure the size distribution of silica-asphaltene flocs in the model oil solution. The instrument yield a relationship between measured macroscopic acoustic properties, such as sound speed, attenuation, acoustic impedance, angular dependence of the scattered sound, etc., and the microscopic characteristics of the system, such as particle size distribution. The instrument results are more valid for dilute samples.

Measuring chamber of DT-1200 contains the acoustic sensors and the instrument measures the attenuation spectra for giving the particle size distribution. The chamber size was in the range of 20 - 110 ml.

The DT1200 software did not include the sound speed for all the liquids. Therefore, initially the attenuation for toluene and pentane and the pentol with various S/O was calibrated for the instrument. Six tests were run for each solvent and based on the average of the data the sound speed for each mixture and the pure solvents was defined in the software.

The model oil solution was prepared and pentane at various ratios was added to the model oil and the mixture was shaken for 25 minutes. The samples were then transferred to the instrument chamber. Each sample was being stirred during the experiment to keep the solution homogenous. The size distribution and bimodal and unimodal data were then reported by DT1200 software.

The size distribution of each solution without and with silica particles are shown in table B-1 and table B-2, respectively:

Table B-1 The size distribution of asphaltene flocs at various S/O

S/O	Size distribution 1 (µm)	Size distribution 2 (µm)	Size median (µm)	% Fitting error
0	0.0066	14.4	0.0087	6.1
0.28	0.023	5.6	0.0204	8.08
0.33	0.006	4.6	0.0106	8.59
0.4	0.032	9.3	0.0318	17.95
0.43	0.031	9.0	0.0306	16.39
0.5	0.031	8.6	0.0314	14.76

The results for the size distribution were not the results that we were expecting. Looking at the data in table B. 1 shows that the size distribution of asphaltene aggregates at S/O = 0 is higher than other S/O. What we expect is that the size distribution of the asphaltene flocs to be minimum at S/O = 0 and by

addition of pentane, this size distribution of the asphaltene flocs increases. However, the size distribution shown in table B. 1 does not follow any trend and the reported size is higher for S/O = 0.

Table B-2 The size distribution of silica-asphaltene flocs at various S/O

S/O	Size distribution 1 (µm)	Size distribution 2 (µm)	Size median (µm)	% Fitting error
0	1.79	1.79	9.73	2.83
0.28	0.49	6.46	2.70	9.30
0.33	0.98	4.76	2.14	3.68
0.4	0.18	7.62	0.07	24.13
0.43	0.28	6.43	2.97	16.63
0.5	0.18	5.71	0.05	23.53

The results in table B. 2 is another reason that the experiment for the model oil solution is not trustable. The size distribution of silica/asphaltene flocs does not follow any trend either. For instance, for S/O = 0.5 that we expect to see a big increase in the size of the flocs, the size distribution has decreased.

The fitting error for more dilute samples was high for the model oil solution and kept increasing for more dilute samples.

The reason that the method did not give any good results can be contributed to the complexity in the model oil solution and the structure of the asphaltene and silica/asphaltene flocs.

Appendix C AFM force plots for S/O = 0.5 and S/O = 0

Some of retraction-approach curve for S/O = 0.5 and S/O = 0 are shown in Figure C-1 and Figure C-2, respectively.

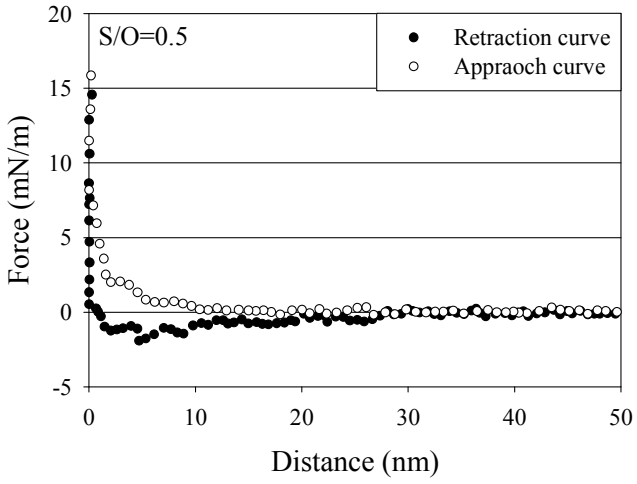

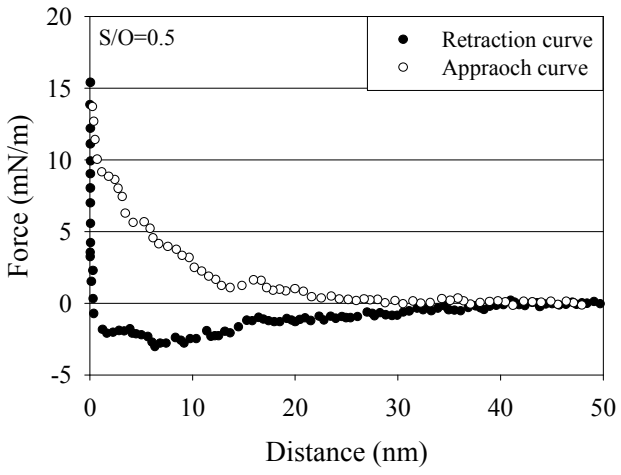

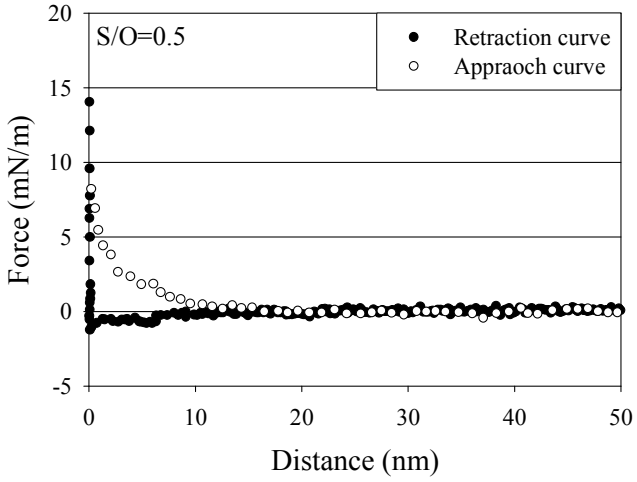
S/O=0.5
Retraction curve
Appraoch curve
Force (mN/m)
Distance (nm)
20
15
10
5
0
-5
0
10
20
30
40
50

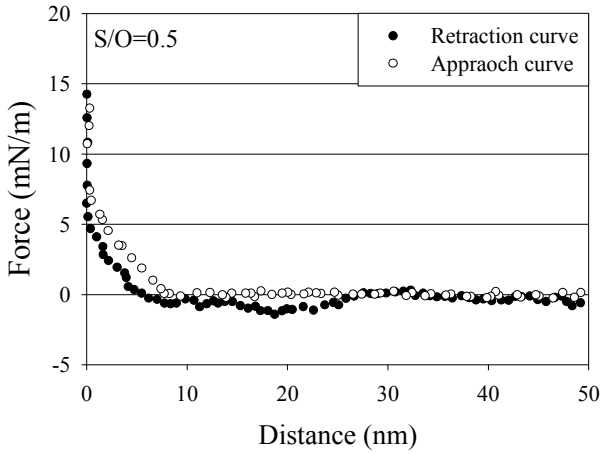
S/O=0.5
Retraction curve
Appraoch curve
Force (mN/m)
Distance (nm)
20
15
10
5
0
-5
0
10
20
30
40
50

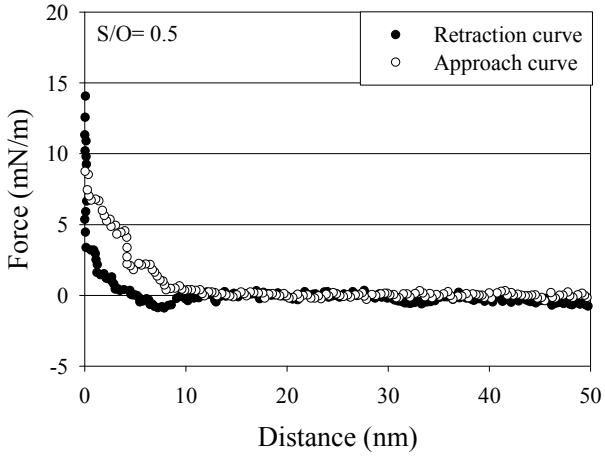
S/O= 0.5
Retraction curve
Approach curve
Force (mN/m)
Distance (nm)
20
15
10
5
0
-5
0
10
20
30
40
50

Figure C-1 Some of the representative force measurements between the AFM tip and asphaltene coated surfaces prepared in oil-toluene-pentane solution at S/O = 0.5. The medium was pentane/toluene = 0.5

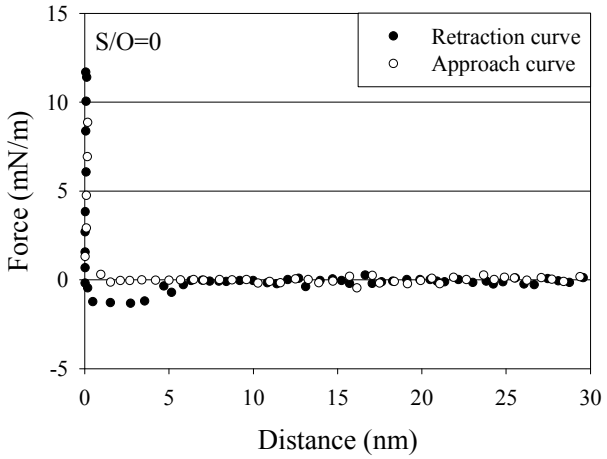

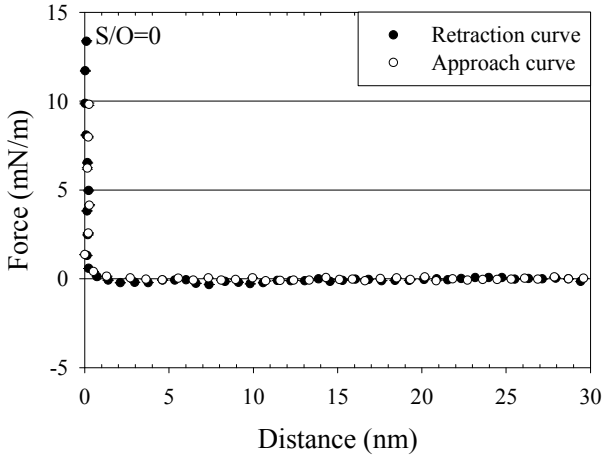

Figure C-2 Some of the representative force measurements between the AFM tip and asphaltene coated surfaces prepared in oil solution at S/O = 0. The medium was toluene